EXD2 governs germ stem cell homeostasis and lifespan by promoting mitoribosome integrity and translation

Article (Accepted Version)

EXD2 governs germ stem cell homeostasis and lifespan by promoting mitoribosome integrity and translation

Joana Silva[1], Suvi Aivio[1], Philip A. Knobel[1], Laura J. Bailey[2], Andreu Casali[1], Maria Vinaixa[3,4], Isabel Garcia-Cao[1], Étienne Coyaud[5,6], Alexis A. Jourdain[7,8,9], Pablo Perez-Ferreros[1], Ana M. Rojas[10], Albert Antolin-Fontes[1], Sara Samino-Gené[3,4], Brian Raught[5,6], Acaimo González-Reyes[11], Lluis Ribas de Pouplana[1,12], Aidan J. Doherty[2], Oscar Yanes[3,4] and Travis H. Stracker[1,*]

Affiliations

[1]Institute for Research in Biomedicine (IRB Barcelona), The Barcelona Institute of Science and Technology (BIST), C/ Baldiri Reixac 10, Barcelona 08028, Spain
[2]Genome Damage and Stability Centre, School of Life Sciences, University of Sussex, Brighton BN1 9RQ, UK
[3]Metabolomics Platform, Department of Electronic Engineering (DEEEA), Universitat Rovira i Virgili, Tarragona 43003, Spain
[4]Biomedical Research Centre in Diabetes and Associated Metabolic Disorders (CIBERDEM), 28029 Madrid, Spain
[5]Princess Margaret Cancer Centre, University Health Network, Canada
[6]Department of Medical Biophysics, University of Toronto, Toronto ON M5G 1L7, Canada
[7]Department of Molecular Biology, Howard Hughes Medical Institute, Massachusetts General Hospital, Boston, MA 02114, USA
[8]Department of Systems Biology, Harvard Medical School, Boston, MA 02115, USA
[9]Broad Institute of MIT and Harvard, Cambridge, MA 02142, USA
[10]Computational Biology and Bioinformatics Group, Institute of Biomedicine of Seville **(**IBIS/CSIC/US/HUVR**)**, Campus Hospital Universitario Virgen del Rocio, Seville 41013, Spain
[11]Centro Andaluz de Biología del Desarrollo, Universidad Pablo de Olavide/CSIC/JA, Carretera de Utrera km 1, Sevilla 41013, Spain
[12]Catalan Institution for Research and Advanced Studies (ICREA), Passeig Lluis Companys 23, Barcelona 08010, Spain

Short title: Metabolic regulation by EXD2

To whom correspondence should be addressed

*Travis H. Stracker, email: travis.stracker@irbbarcelona.org

Current affiliations:

Suvi Aivio: Department of Pathology, Brigham and Women's Hospital.

Pablo Pérez-Ferreros: EMBL Australia, UNSW, Lowy Cancer research Center, Single molecule Science Node, Sydney and Arc Center of Excellence in Advance Molecular Imaging

Philip A. Knobel: Department for Radiation Oncology, University Hospital Zurich, CH-8091 Zurich, Switzerland

Key words:

metabolism, respiration, EXD2, OXPHOS, stem cell, lifespan

Abstract

Mitochondria are subcellular organelles critical for meeting the bioenergetic and biosynthetic needs of the cell. Mitochondrial function relies on genes and RNA species encoded both in the nucleus and mitochondria, as well as their coordinated translation, import and respiratory complex assembly. Here we describe the characterization of exonuclease domain like 2 (EXD2), a nuclear encoded gene that we show is targeted to the mitochondria and prevents the aberrant association of mRNAs with the mitochondrial ribosome. The loss of EXD2 resulted in defective mitochondrial translation, impaired respiration, reduced ATP production, increased reactive oxygen species and widespread metabolic abnormalities. Depletion of EXD2/CG6744 in *D.melanogaster* caused developmental delays and premature female germline stem cell attrition, reduced fecundity and a dramatic extension of lifespan that could be reversed with an anti-oxidant diet. Our results define a conserved role for EXD2 in mitochondrial translation that influences development and aging.

Introduction

Mitochondria maintain a circular 16.6 kb DNA genome (mtDNA) encoding 2 rRNAs, 22 tRNAs and 13 open reading frames for electron transport chain (ETC) complex subunits and are the major source of ATP and the site of oxidative phosphorylation (OXPHOS) and the tricarboxylic acid (TCA) cycle that are essential for cellular respiration. In addition, mitochondria facilitate many metabolic reactions required for macromolecular synthesis, including production of lipids, dNTPs, heme, iron-sulfur clusters and amino acids[1].

The five complexes of the OXPHOS machinery carry out redox reactions from NADH and succinate to drive the majority of cellular ATP production through ATP synthase[1].

While most OXPHOS proteins are encoded in the nucleus, key components of all complexes, except Complex II (CII), are encoded by the mtDNA. The function and maintenance of the OXPHOS machinery is dependent on mtDNA integrity, transcription, precursor RNA processing, assembly of mitochondrial specific ribosomes and translation, the coordinated movement of nuclear encoded proteins into the mitochondria, and the ordered assembly and membrane insertion of mature OXPHOS complexes that is thought to take place in close proximity to the mtDNA and mitochondrial inner membrane[2]. Deficiencies in assembly or function of the OXPHOS machinery underlies many severe human diseases[3]. Paradoxically, some OXPHOS defects extend lifespan in both worms and flies, in some cases in a manner dependent on increased reactive oxygen species (ROS) production[4-6] that is classically associated with premature ageing[1].

The nuclear encoded Exonuclease 3'-5' domain containing 2 (EXD2) has previously been implicated in DNA repair through a role in DNA end-resection[7-10]. Here we report that EXD2 is a mitochondrial ribonuclease that is required for mitoribosome integrity and efficient mitochondrial translation. EXD2 depletion led to widespread metabolic defects, decreased respiration and increased ROS. At the organismal level, EXD2/CG6744 deficiency in *D.melanogaster* resulted in developmental delays, premature female germ stem cell attrition and a dramatically extended lifespan. Collectively, our results define a critical role for EXD2 in mitochondrial homeostasis.

EXD2 is a mitochondrial protein

EXD2 encodes a 3'-5' exonuclease (EXO) domain similar to *WRN*, mutated in Werner's Syndrome progeria (Supplementary Fig. 1a)[11]. Additionally, it has a highly conserved C-terminal HNH endonuclease-like domain, characterized by tandem CXXC motifs (Supplementary Fig. 1b-d). As previous reports suggested a role in

DNA repair[7-9], we examined EXD2 localization and found that EXD2 was predominantly cytoplasmic, regardless of treatment with Camptothecin (CPT) to induce DNA damage, and overlapped substantially with mitochondrial TOM20 (Fig. 1a). Comparative sequence analysis identified a putative, N-terminal mitochondrial targeting sequence (MTS) conserved in most EXD2 homologues identified (Supplementary Fig. 1e). Overexpression of a GFP tagged EXD2 (EXD2-GFP) or its MTS fused to GFP (MTS-GFP; aa 1-61) resulted in mitochondrial GFP signal, while the ΔMTS-GFP (aa 1-61 deleted) protein was diffusely nucleo-cytoplasmic and destabilized (Fig. 1b,c). Subcellular fractionation for endogenous EXD2 (Fig. 1d) and transmission electron microscopy (TEM) for stably expressed *EXD2-Strep-FLAG(SF)-WT* confirmed primarily mitochondrial localization (Fig. 1e and Supplementary Fig. 1f,g). In contrast to outer membrane (OM) proteins TOM20 or VDAC, that are accessible to proteinase-K (PK)-mediated digestion, EXD2 was resistant, similar to the inner membrane (IM) ATP5A subunit of ATP synthase (Fig. 1f). In addition, while treatment with carbonyl cyanide-4-(trifluoromethoxy)phenylhydrazone (FCCP) liberated TOM20 from the OM, EXD2 remained relatively resistant, similar to ETC components that localize to the IM or matrix (Supplementary Fig. 1h). Together, these results indicate that EXD2 is an intra-mitochondrial protein targeted by an N-terminal MTS.

EXD2 influences cellular metabolism

As mitochondria play a key role in metabolism, we examined the impact of EXD2 deficiency using complementary metabolomics approaches[12, 13]. EXD2 depletion (Fig. 2a,b) led to alterations in many metabolites, including those of the TCA cycle, antioxidants and glycolysis (Fig. 2c). Using the NMR based PEPA technique, we followed ^{13}C isotope incorporation from glucose or glutamine that are key precursors to many metabolites of central carbon metabolism[13, 14]. Pathway enrichment analysis

revealed significant alterations in several metabolite classes, including the glutathione cycle, amino acid and sugar metabolism, the pentose phosphate pathway (PPP) and the TCA cycle (Fig. 2d). Moreover, we observed marked defects in incorporation of glucose-derived carbon into many metabolites, while glutamine was relatively unaffected (Fig. 2e, 2f). These data indicated that EXD2 was required for glucose oxidation through the TCA cycle and glutathione synthesis, suggesting *EXD2*-deficient cells may have alterations in ROS or antioxidant capacity and rely on glutamine for the generation of key metabolites.

EXD2 prevents ROS and is required for OXPHOS activity and ATP production

To understand these effects, we generated *EXD2* knockout (KO) cell lines using CRISPR/CAS9 and complemented them with SF-tagged *EXD2* (*EXD2-SF-WT*) or mutants in the EXO domain (*NUC*) or the HNH-like domain (*C1* and *C2*) (Supplementary Fig. 1a,c and 2a)[15]**.** *EXD2*-deficient cells had reduced glutathione levels (Fig. 3a), consistent with metabolomics data (Fig. 2), and increased levels of ROS (Fig. 3b). Expression of *EXD2-SF-WT* or treatment with the anti-oxidant N-acetylcysteine (NAC), but not the *EXD2-SF-NUC* and *C2* mutants, rescued ROS levels to that of *WT* (Fig. 3b). EXD2-deficient cells also exhibited reduced levels of mtDNA (Fig. 3c and Supplementary Fig. 2c,d), a phenotype associated with increased ROS and defective respiration[16]. MtDNA reduction was independent of clear changes in mitochondrial mass (Fig. 3d,e and Supplementary Fig. 2e) or mtDNA replication (Supplementary Fig. 2f) and could be rescued with expression of *EXD2-SF-WT* and partially with NAC treatment (Fig. 3c and Supplementary Fig. 2d).

Growth of EXD2-deficient cell lines was indistinguishable from *wild type* (*WT*) parental U2OS cells in rich medium containing glucose and glutamine (Fig. 3f). However, we observed impaired growth of *EXD2-KO1* cells in media lacking

glutamine (Fig. 3g and Supplementary Fig. 2g) that was restored by *EXD2-SF-WT*, but not *EXD2-SF-NUC or C2* mutants (Fig. 3g). In contrast, NAC did not rescue, indicating that growth defects were not secondary to increased ROS production or sensitivity to hyperoxic culture conditions (Fig. 3h,i).

Mitochondrial ROS originates predominantly from CI and CIII of the ETC[17], so we addressed ETC function by measuring oxygen consumption rates (OCR) in both U2OS and MDA-MB-231 cells. Compared to parental or *EXD2-SF-WT* complemented cells, *EXD2-KO1* cells exhibited reduced OCR and ATP-linked respiration that could not be efficiently rescued by EXD2 mutants (Fig. 3j and Supplementary Fig. 2h). In addition, extracellular acidification rates (ECAR) were elevated in *EXD2-KO* or mutant cells, indicative of increased aerobic glycolysis and lactate production that can accompany defective OXPHOS (Fig. 3k and Supplementary Fig. 2i)[18]. NAC partially rescued overall OCRs but mitochondrial ATP-linked respiration remained impaired, suggesting reduced OXPHOS capacity could be one of the primary defects leading to increased ROS (Fig. 3l and Supplementary Fig. 2j).

Metabolomics data indicated that reduced OCR could reflect impaired glucose usage in *EXD2*-deficient cells (Fig. 2e,f). We tested this using specific media and observed an increase in OCR following glucose addition that was absent in cells lacking functional EXD2 (Fig. 3m). To more directly confirm a role for EXD2 in ATP production, we analyzed ATP levels using multiple methods and observed that *EXD2-KO1* cells had reduced levels of ATP that were rescued by *EXD2-SF-WT* expression (Fig. 3n and Supplementary Fig. 2k,l). Moreover, these defects were not rescued by NAC (Fig. 3n and Supplementary Fig. 2k). We therefore concluded that EXD2 deficiency results in impaired mitochondrial ATP production, ROS accumulation, reduced mtDNA levels and glutamine-dependent cell growth.

EXD2 associates with CI and the Mitoribosome

To determine how EXD2 influenced metabolism, we used BioID mass spectrometry (BioID-MS) to identify proximity interactors[19]. EXD2-WT and EXD2-C2 fused to a FLAG-tagged BirA* biotin ligase were overexpressed in the presence of biotin in human AD293 cells. While BirA* expression resulted in staining throughout the cell, streptavidin signal was only detected in the cytoplasm of biotin-supplemented cells expressing *EXD2-WT-BirA** or *EXD2-C2-BirA** and this co-localized extensively with TOM20 (Fig. 4a). BioID-MS revealed an EXD2 proximity interactome composed almost entirely of mitochondrial proteins (Fig. 4b and Supplementary Table 2) and highly enriched for components of CI and the small 28S subunit of the mitoribosome (Fig. 4c). This included almost all of the matrix exposed CI subunits[20], more than 10 subunits of the 28S mitoribosome, proteins involved in RNA processing or translation/assembly (ex. GRSF1, TACO1, ACAD9, LETM1), as well as enzymes implicated OXPHOS substrate generation (ex. MDH2, GLS) (Fig. 4c). Most interactions were also observed with *EXD2-C2* that fails to complement phenotypes of *EXD2-KO1* cells. However, the representation of 28S components was specifically reduced compared to *EXD2-WT* (Fig. 4c and Supplementary Table 2), suggesting the HNH-like domain influenced the frequency or affinity of this subset of interactors.

An interaction with the CI subunit NDUFA9 was observed in IP-westerns and *EXD2-KO1* cells showed a minor reduction in CI levels, as well as CI and CIII supercomplexes, and to a lesser extent, CV (ATP synthase), and CI dependent OCR was reduced (Supplementary Fig. 3a-d). As EXD2 did not appear to be present in fully assembled CI (Supplementary Fig. 3b), we analyzed the mitoribosome components and readily observed an interaction with DAP3 (28S subunit) that was impaired by the *EXD2-SF-C2* mutant (Fig. 4d). In contrast, we did not see an interaction with the large mitoribosome (39S) subunit MRPL3 or VDAC, an outer

mitochondrial membrane protein in IP-westerns (Fig. 4d). The mitoribosome association was further validated by confocal microscopy, where we observed extensive colocalization of endogenous EXD2 and MRPL12 (Fig. 4e). This further established the predominant mitochondrial localization of EXD2 and suggested that its primary functions could be linked to the OXPHOS machinery and the mitoribosome.

EXD2 prevents mitoribosomal mRNA accumulation and facilitates translation

We therefore examined mitoribosome integrity using sucrose gradient fractionation. EXD2 co-fractionated with the 28S and fully assembled 55S mitoribosome, but not with the free 39S subunit (Fig. 5a, top panels). As early 28S association of EXD2 suggested a potential role in or during assembly, we analyzed ribosome integrity in *EXD2-KO1* cells or those expressing *EXD2-SF-C2*. In either case, we observed a clear shift of the 28S DAP3 subunit into higher molecular weight complexes overlapping with 39S fractions (Fig. 5a, middle and bottom panels). Analysis of RNA revealed increased 12S rRNA and mtDNA encoded mRNAs in the aberrant fractions, suggesting premature mt-mRNA association with the 28S could yield the larger, aberrant complexes (Fig. 5b, compare top to middle and bottom panels). Consistent with this possibility, the profiles of RNAseA treated fractions were similar regardless of EXD2 status (Supplementary Fig. 4a). The *EXD2-C2* mutant protein did not visibly co-fractionate with the free 28S subunits, consistent with the HNH-like domain promoting the 28S association (Fig. 5a, bottom panel).

The appearance of aberrant 28S subunits suggested that mitochondrial translation could be impaired, so we analyzed this using metabolic pulse labeling[21]. A strong reduction in global mitochondrial translation rates was observed in U2OS and RPE1 cells lacking EXD2 (Fig. 5c-5f and Supplementary Fig. 4b-e) that was complemented

by *EXD2-SF-WT*, but not by *EXD2-SF-NUC* or *C2* mutants. Further, NAC did not influence the phenotype (Fig. 5f), suggesting it was likely a direct result of EXD2 loss. Together these data indicate that EXD2 prevents inappropriate mRNA association with mitoribosomes and facilitates efficient mitochondrial translation that requires both its EXO and HNH-like domains.

EXD2 is a ribonuclease that preferentially binds ssRNA

As EXD2 loss appeared to influence mRNA association with mitoribosomes, we considered that it may function as an RNAse. We examined the activity and specificity of bacterially purified EXD2, as well as WRN exonuclease domain (WRN-Exo) for comparison. The EXD2 MTS (aa 1-61) was removed for solubility, the EXD2-NUC mutant made to control for contaminating nucleases, and the EXD2-C2 mutant, that failed to complement *EXD2-KO1* cells, was also generated (Fig. 6a and Supplementary Fig. 5a). As previously reported[8], EXD2-WT, but not EXD2-NUC, exhibited 3'-5' exonuclease activity on ssDNA (Supplementary Fig. 5b). In addition, both EXD2-WT and the WRN-Exo exhibited activity on dsDNA, ssRNA, dsRNA, both strands of a DNA/RNA hybrid and several other DNA substrates (Fig. 6b-6d and Supplementary Fig. 5d-f). Similar activity was observed with EXD2-C2, although it was consistently lower, indicating that stability or selectivity of the enzyme-nucleic acid complex may be affected (Fig. 6e and Supplementary Fig. 5f-g). However, when $MgCl_2$ was used as a cofactor, both EXD2-WT and EXD2-C2, but not the closely related WRN-Exo, showed stronger substrate discrimination with exonuclease cleavage observed only on ssRNA or RNA/DNA hybrids (Fig. 6f-i and Supplementary Fig. 5h-k). Quantification of multiple experiments revealed that EXD2 had a roughly 3-fold increase in specific activity on ssRNA compared to ssDNA using $MnCl_2$ but in the presence of $MgCl_2$., EXD2 activity on ssDNA and dsDNA substrates was lost, reduced on hybrids, but similar on ssRNA (Fig. 6j and Supplementary Fig. 5l).

To determine if EXD2 had any binding preference, we performed electrophoretic mobility shift assays (EMSA) on fluorescently labeled substrates. We observed a clear supershift with ssRNA, but not with ssDNA or hybrid molecules when EXD2 was added (Fig. 6k). Similarly, EXD2-NUC and EXD2-C2 mutants bound preferentially to ssRNA, although the supershift was reduced with EXD2-C2 (Fig. 6l,m) and WRN-Exo domain did not exhibit any obvious substrate preference (Supplementary Fig. 5m). Together these data demonstrate that EXD2 and WRN have promiscuous $MnCl_2$-dependent activity on a variety of RNA and DNA substrates *in vitro*, but that EXD2 preferentially binds to ssRNA and can maintain its activity on ssRNA in the presence of $MgCl_2$, indicating that it is more likely to be the physiological substrate of its activity.

EXD2/CG6744 influences *Drosophila* metabolism and development

Given the influence of EXD2 on mitochondrial function, we examined the impact of depleting the *D.melanogaster* EXD2 ortholog *CG6744* (henceforth referred to as *dExd2*) (Supplementary Fig. 6a). Consistent with available data[22], two peaks of *dExd2* expression were observed in control *yellow white* flies in early embryos (0-4 hrs) and pupae (WPP) (Supplementary Fig. 6b,c), developmental phases associated with high metabolic activity[23]. We obtained flies with a transposon insertion and confirmed *dExd2* mRNA depletion in homozygous animals (Fig. 7a). Similar to human cells, mtDNA levels were lower in mutant animals and largely rescued by NAC (Fig. 7b) and mitochondrial translation rates were reduced in *dExd2*-deficient flies (Fig. 7c,d). Moreover, overexpressed dEXD2 localized extensively to the mitochondria of *Drosophila* S2 cells (Fig. 7e) and *dExd2*-deficient flies exhibited impaired respiration (Fig. 7f) and lower levels of ATP and glutathione (Fig. 7g). Embryos and pupae deficient for *dExd2* were smaller than controls but appeared morphologically normal, suggesting a developmental delay (Fig. 7h), and pupariation

times were extended, but could be normalized by NAC or further extended with paraquat (PQT), that elevates ROS levels (Fig. 7i). These effects were not due exclusively to maternal inheritance of defective mitochondria, as the expected ratio of normal to runted animals was observed following breedings from heterozygous females, that transmit intact mitochondria to all offspring, with homozygous males (Supplementary Fig. 6d).

EXD2 prevents germ stem cell attrition and regulates lifespan

As mitochondrial dysfunction and ROS extend or diminish lifespan in different experimental settings[4-6], we examined the lifespan of *dExd2*-deficient animals. We observed a slight but significant lifespan extension in males that was much more dramatic in females and normalized by NAC (Fig. 8a and Supplementary Table 1). In adult flies, expression of *dExd2* was higher in the ovary than the brain or gut (Fig. 8b) and mutants exhibited an accelerated reduction in fecundity that was largely rescued by NAC (Fig. 8c). To address the origin of this phenotype, we examined the pool of germ stem cells (GSCs) present in control and *dExd2*-deficient ovaries. As previously described, a progressive GSC decline in control flies was observed[24], a phenotype that was accelerated in *dExd2*-deficient animals and rescued by NAC (Fig. 8d,e). Cytological analysis of *dExd2*-deficient ovaries revealed a disorganized mitochondrial network with highly reduced levels of cytochrome-C, an essential component of the ETC, suggesting metabolic collapse in the germarium where the GSCs and somatic follicle stem cells reside (Fig. 8f). These results suggest that EXD2 is critical for mitochondrial homeostasis *in vivo* and that it prevents excess ROS production that retards normal development and causes the premature attrition of GSCs, reduced fecundity and extended lifespan (Supplementary Fig. 6e)[25].

Discussion

Our data connects the EXO and HNH-like domains of EXD2 to mitochondrial ribosome integrity, translation, OXPHOS activity, and *Drosophila* germline stem cell maintenance and lifespan. We propose that EXD2 acts as a ribonuclease that prevents precocious association of mitochondrial mRNAs with the free 28S mitoribosomal subunits prior to 55S assembly. This is consistent with the enrichment of 28S proteins in BioID-MS, the fractionation pattern of EXD2, its preference for ssRNA and the increased mRNA levels co-fractionating with aberrant 28S subunits in *EXD2*-deficient cells. Similar alterations in 28S subunit mobility were observed in cells lacking LRPPRC and SLIRP that influence stability and translation of mt-mRNA pools[26, 27]. While we cannot strictly rule out a role for EXD2 in mtRNA processing or stability, MitoString[28] analysis indicated that the profiles of *EXD2*-deficient cells were highly similar to parental or complemented cells and most known precursor RNA processing events occurred normally (Supplementary Fig. 7a,b), indicating that EXD2 is not likely required for global RNA precursor processing or mt-mRNA levels.

The EXO and HNH-like domains are both crucial for EXD2 function. Extending earlier reports[8], we identified additional EXD2 orthologs, defined by EXO and HNH domains (Supplementary Fig. 1a-c). *Arabidopsis* RRP6L3 is a likely EXD2 ortholog with a high degree of similarity in the HNH domain, although its EXO domain is more similar to RRP6 (exosomal RNAse) than WRN and it contains an additional HRDC domain absent in metazoan EXD2s. EXD2 also appears sporadically in some trypanosome lineages and in leishmania, EXD2 has an additional Z3H1 type zinc finger not present in other species. Thus, EXD2 is widely conserved and at least 3 major domain configurations exist, potentially reflecting specialization of function in those organisms.

Our data suggests the HNH-like motif influences stable binding of EXD2 to ssRNA and the 28S (Fig. 4,5), reflected by the absence of *EXD2-SF-C2* in 28S fractions (Fig.

5a) and its reduced RNA binding. The EXD2 HNH-like domain lacks conserved DH catalytic residues required for activity in other HNH-endonucleases (Supplementary Fig. 1d). Notably, in fold and function assignment searches (FFAS), several of the highest scoring HNH domains belong to proteins involved in chaperoning assembly and insertion of membrane complexes (DotN) or electron transport (NapB), suggesting a diverse repertoire of potential functions for this domain (Supplementary Fig. 1d).

Both human and *Drosophila* EXD2 were identified in a genome wide siRNA screen for host factors that support Dengue RNA virus replication but a specific role in the viral lifecycle has not been reported[29]. EXD2 was also implicated in DNA repair, reported to localize to nuclear chromatin and interact with the DNA resection machinery and identified on collapsed replication forks in an iPOND-MS screen[7-10, 30]. However, 11 mitochondrial proteins, including 5 mitoribosome proteins, were also identified in the iPOND-MS screen[30] with comparable scores, and using the reported fractionation methods[8], we readily identify EXD2 in chromatin fractions (Supplementary Fig. 7c) but they were highly contaminated with mitochondria, points that should be considered in light of the data reported here. We do not detect EXD2 in the nucleus (Fig. 1 and Supplementary Fig. 1h) and overexpressed human and fly EXD2 localizes primarily to mitochondria in IF with no clear nuclear staining (Figs. 1, 4 and 7), consistent also with the cytoplasmic localization reported for *Arabidopsis* RRP6L3[31]. Moreover, in an unbiased proteomics approach, we identified almost exclusively mitochondrial proteins, none of which have been implicated in DNA repair or replication, except for POLD4 (POLDIP2) and ATR, which also have mitochondrial roles (Fig. 4c and Supplementary Table 2)[32, 33].

Consistent with previous reports[8], we observed robust 3'-5' exonuclease activity but both EXD2 and WRN showed activity on all DNA and RNA substrates tested (Fig. 6

and Supplementary Fig. 5) when $MnCl_2$ was used in reactions. In contrast, EXD2 showed clear binding and activity on ssRNA in the presence of $MgCl_2$, suggesting its physiological substrate is RNA. Additionally, we did not observe defective RPA focus formation (Supplementary Fig. 7d,e) or DNA damage sensitivity in *EXD2*-deficient cells using several cell line backgrounds controlled with complementation (Supplementary Fig. 7f-h). We believe that our data strongly indicates that the primary role of EXD2 is to govern mitochondrial ribosome mRNA loading, translation and ATP production through its RNAse, and potentially other activities. However we cannot strictly rule out a DNA replication/repair role that we have not detected due to differences in technical conditions or cell line backgrounds. Notably, phenotypes associated with some translational regulators include defects in mitochondrial and nuclear genome maintenance[34], there are examples of DNA repair enzyme families with key roles in translational regulation[35] and numerous DNA repair nucleases (ex. FEN1 and DNA2) localize to both the nucleus and mitochondria[36, 37].

ROS levels, reproductive capacity, abundance and activity of OXPHOS components and global translation have all been shown to be major factors influencing lifespan in numerous organisms[4, 6, 38-40]. Depletion of mitochondrial translational regulators in *S.cerevisae* extends lifespan in a *Sir2* dependent manner[41] but we did not observe alterations in *Sir2* mRNA in *dExd2*-deficient flies and lifespan extension in females was independent of calorie restriction (CR), that is also *Sir2* dependent (Supplementary Fig. 7i,j)[42]. We propose that the dramatic lifespan extension in *dExd2*-deficient females is primarily the result of ROS-mediated, premature attrition of the GSC pool and loss of fecundity (Supplementary Fig. 6e), consistent with *dExd2* expression patterns, the rescue of GSC attrition, fecundity and lifespan with NAC treatment, the reduced respiration observed in *dExd2*-deficient flies and the close correlation between age of GSC loss and lifespan extension (Fig. 8). An inverse

relationship between lifespan and reproductive capacity was reported in several organisms, including *C.elegans* and *Drosophila*[25]. While multiple mechanisms have been proposed, including elevated ROS and antagonistic GSC to soma crosstalk, the precise nature of the signal that influences lifespan remains to be clarified[43].

While it remains unclear if EXD2 influences mammalian fertility or lifespan, analysis of mRNAs enriched in germ plasm of *Xenopus*, that is rich in mitochondria and RNA binding proteins, identified *xEXD2*[44], indicating that it could play a similar role in the vertebrate GSC niche. Patients with interstitial deletions in chromosome 14q24, that include *EXD2* and 18 neighboring genes, have been reported to have congenital heart defects, brachydactyly and intellectual disability[45], indicating that EXD2 loss may influence human development. However, the individual contribution of *EXD2* deficiency to these pathologies remains unclear. The precise control of mtDNA levels, RNA processing, ribosome assembly, translation and the dynamic composition and molecular regulation of OXPHOS complexes in mammals is critical for normal metabolism and healthy aging[1]. Our results, and those of others, suggest that many additional regulators of these processes have yet to be identified and their characterization will further enhance our understanding of mitochondrial regulation and its role in ageing.

Figures legends

Figure 1: EXD2 is a mitochondrial protein. (**a**) Immunofluorescence of endogenous EXD2 in U2OS cells revealed extensive co-localization with the mitochondrial TOM20 protein. EXD2 localization was unaltered by treatment with 1μM camptothecin (CPT) to induce DNA damage (lower panels). Scale bar = 20μm. (**b**) EXD2 contains a mitochondrial-targeting signal (MTS) that is necessary and sufficient for mitochondrial localization. Amino acids 1-61 of EXD2 are sufficient to localize GFP to mitochondria (bottom panel). Deletion of EXD2 aa 1-61 leads to diffuse nuclear-cytoplasmic localization (middle panels). Scale bar = 15μm. Panels in a, b represent 1 out of 5 experiments. (**c**) Western blot of GFP fusion proteins with expected sizes indicated. Note poor expression/destabilization of ΔMTS-GFP. Arrowheads indicate the protein of the corresponding label color. (**d**) Subcellular fractionation of EXD2 (hatched boxes) in the presence or absence of 1μM CPT indicated exclusively mitochondrial localization. Data represent 1 out of 3 experiments (**e**) Transmission electron microscopy (TEM) indicated mitochondrial (dashed outlines) localization of EXD2-SF-WT. Scale bar = 200nm. See Supplementary Fig. 1f,g for additional examples. (**f**) Western blot of mitochondria isolated from U2OS cells treated with 50μg/ml proteinase-K (PK) in the presence or absence of Triton X-100 shows that EXD2 is resistant, similar to OXPHOS subunit ATP5A, indicating IM and/or matrix localization Data in e, f represent 1 out of 2 experiments. Uncropped blots shown in Supplementary Fig. 9.

Figure 2: EXD2 is required for metabolic homeostasis. (**a**) Quantitative real time PCR (qRT-PCR) confirmed reduction of *EXD2* mRNA following expression of stable shRNAs against *EXD2*. Averages from 7 independent experiments in triplicate are plotted (n=7). (**b**) Confirmation of reduced EXD2 protein levels in cells expressing shRNAs against *EXD2*. Actin serves as a loading control. Data represent 1 out of 5

experiments. (**c**) Heatmap representation of metabolite fold changes (FC) significantly altered by EXD2 (shEXD2-22) depletion compared to control (shCont) cells is shown. Values represent mean of n=5 independent samples. Depicted metabolites have a FC >1.3 with an adjusted p-value of <0.01 (t-test). (**d**) Pathway enrichment analysis of metabolite differences from MS-data and ^{1}H-NMR metabolite profiling. X-axis represents Pathway Impact calculated from topological analysis based on the centrality measures of individual metabolites in a given metabolic network and the y-axis represents FDR p-values from a hypergeometric test. Overrepresented pathways with higher impact are highlighted with darker color and size. (**e**) Metabolic summary chart showing active pathways in U2OS cell lines, as revealed by ^{1}H-NMR positional enrichment by proton analysis (PEPA)[13]. Metabolic structures are depicted with red and blue dots indicating fates of [U-^{13}C]glucose or [U-^{13}C]glutamine respectively. FC of metabolites identified from both approaches are indicated in red (up) or green (down) text in accordance with the heatmap. (**f**) *EXD2* depletion impairs glucose usage. Examples of ^{1}H-NMR metabolite profiling predicted significant fractional enrichments. Red and blue dots represent individual F values calculated using [U-^{13}C]glucose or [U-^{13}C]glutamine, respectively. Results from n=3 independent cultures plotted as mean(SD) with individual values shown. Source data for the figure is provided in Supplementary Table 1 and unprocessed scans for 2b in Supplementary Fig. 9.

Figure 3: Characterization of EXD2 deficient cells. (**a**) Glutathione (GSH or GSSG) levels in MDA-MB-231 cells measured by liquid chromatography-mass spectrometry (LC-MS) -/+ NAC or treatment with CAP or FCCP. Values of n=3 (*WT*) or n=4 (all others) independent cultures with mean(SD) (**p<0.01, unpaired t-test, two-tailed). Color key applies to all panels in figure. (**b**) ROS levels in MDA-MB-231 cells measured with MitoSOX red. Controls and gating examples in Supplementary

Fig. 8. Averages of n=3 independent experiments with mean(SD) (**p<0.01, ***p<0.001, unpaired t-test, two-tailed). (**c**) MtDNA levels determined using qRT-PCR in U2OS cells in presence or absence of NAC. Averages of n=3 independent experiments with mean(SD). Similar results obtained in multiple cell lines (Supplementary Figs. 2c and 2d). Statistical analysis of 3b-c: one-way ANOVA with Dunnet's test (***p<0.001, **p<0.01, *p<0.05). (**d**) Mitochondrial mass measured by MitoTracker Green FM staining of U2OS cells. Averages from n=3 independent experiments with mean(SD) plotted. (**e**) Mitochondrial mass measured by western for VDAC1 levels Data represent 1 out of 3 experiments. (**f-i**) *EXD2*-deficient cells grow normally in rich media (**f**) but glutamine removal severely impaired growth (**g**). NAC did not rescue growth in absence of glutamine (**h**) but slightly reduced growth in all lines (**i**). Mean(SD) of n=3 independent experiments shown. (**j-k**) OCR analysis (mitochondrial stress test: Oligomycin, FCCP and Antimycin+Rotenone) revealed decreased basal, ATP-linked and maximal respiration in *EXD2*-deficient cells and increased ECAR (glycolysis stress test: Glucose, Oligomycin and 2-DG) that was rescued by *EXD2-SF-WT* but not *NUC* or *C2* mutants in U2OS cells. Red arrows indicate treatment between category measurements. All time course values from quadruplicate cultures of 2 independent experiments with mean are shown for j-k. (**l**) Influence of NAC on OCR. Values from quadruplicate cultures of 2 independent experiments with mean are shown. Similar results in MDA-MB-231 shown in Supplementary Fig. 3h-j. (**m**) U2OS cells treated with glucose to distinguish OCR from glutaminolysis or glycolysis. All time course values from quadruplicate cultures of n=2 independent experiments with mean are shown. (**n**) Lower ATP levels in *EXD2-KO1* U2OS cells than *WT* or complemented cells. Averages from n=3 independent cultures shown with mean(SD) (**p<0.0070 and 0.0029, unpaired t-test,

two-tailed). Source data for figure and statistical information in Supplementary Table 1 and uncropped western blots in Supplementary Figure 9.

Figure 4: EXD2 interacts with Complex I and the mitoribosome. (**a**) Expression of FLAG-tagged BirA*, EXD2-C2-BirA* or EXD2-WT-BirA* fusion proteins with or without 24 hours of biotin labeling. BirA* expressing control cells showed diffuse nucleo-cytoplasmic streptavidin signal while Streptavidin staining was predominantly cytoplasmic for EXD2-C2-BirA* or EXD2-WT-BirA* and overlapped extensively with the mitochondrial marker TOM20. Scale bar = 10μm. (**b**) Graphical representation of the subcellular localization of proximity interactors in EXD2-WT-BirA* or EXD2-C2-BirA* expressing cells. Summarized results provided in Supplementary Table 2. (**c**) EXD2 associates with primarily mitochondrial proteins and interactors are enriched for Complex I and the mitoribosome. Proteins are color-coded based on the statistical analysis (see legend and Supplementary Table 2) and those involved in human hereditary diseases are circled in yellow. (**d**) EXD2 interacts with DAP3 in IP-western, but not with VDAC or MRPL3, and the interaction is severely reduced in cells expressing the EXD2-C2 mutant. Results from immunoprecipitation-western blotting of U2OS cell extracts are shown. Data represent 1 out of 3 experiments. Uncropped western blots shown in Supplementary Figure 9. (**e**) Immunofluorescence analysis of endogenous human EXD2 in U2OS cells using confocal microscopy revealed extensive co-localization with the mitoribosome protein MRPL12. Scale bar = 10μm. Images in a and e represent more than 25 cells analyzed in two experiments.

Figure 5: EXD2 prevents aberrant mRNA association with the mitoribosome and facilitates translation. (**a**). Sucrose gradient fractionation shows distribution of markers of the 28S (DAP3) and 39S (MRPL12) mitoribosome. EXD2 co-sediments with the 28S and assembled 55S mitoribosome. *EXD2-KO1* and *EXD2-SF-C2* cells show differences in 28S distribution (compare red boxes). Quantification shown for

WT and *EXD2-KO1* (right panel) with individual values of n=3 independent experiments shown with mean(SD). Quantification of *EXD2-SF-C2* with individual values of n=2 independent experiments shown with mean. Graphical representation of detected components shown below each plot. (**b**) QRT-PCR analysis of the sedimentation profile of the indicated mitochondrial transcripts in *WT*, *EXD2-KO1* and *EXD2-SF-C2* cells. The abundance of transcripts in each fraction is shown as a percentage of the total levels. The distribution of fractions containing the 28S, 39S and 55S detected by western blot shown for reference. Quantification of n=3 independent experiments is shown for *WT* and *EXD2-KO1* with all values and the mean(SD) indicated. Quantification of n=2 independent experiments is shown for *EXD2-C2* with individual values and mean indicated. (**c**) EXD2 is required for efficient mitochondrial translation. Phosphorimager scans of ^{35}S-Methionine labeled mitochondrial translation products separated by SDS-PAGE and blotted to PVDF membranes shown for the indicated cell lines. Subsequent western blotting for GAPDH was performed to ensure equal loading. Approximate size of mitochondrial translation products is indicated to right of gel. (**d**) Quantification of n=7 independent experiments compared to the WT sample is plotted with mean(SD). ***p<0.0001, unpaired t-test, two-tailed. (**e**) The WT but not the NUC and C2 mutant forms of EXD2 can rescue the translation defect of cells lacking EXD2. (**f**) The mitochondrial translation defect is not rescued by the administration of NAC to the culture medium. Data in e, f represent one out of 3 experiments. Controls treated with CAP, to block mitochondrial translation, or CAP without emetine, to allow only cytoplasmic translation, are shown. Additional examples used for quantification in Supplementary Fig. 4, source data and statistics in Supplementary Table 1 and uncropped blots in Supplementary Fig. 9.

Figure 6: EXD2 preferentially targets ssRNA. (**a**) Schematic of proteins used in biochemical analysis. (**b**) EXD2-WT (5-80 nM) or EXD2-NUC (40-80 nM) were incubated with 20nM fluorescently labelled ssDNA or dsDNA or (**c**) 20nM RNA/DNA (FAM/Cy5) hybrid in the presence of 10mM $MnCl_2$. Bold font indicates molecule visualized and sepia panel is the same gel scanned with a second laser for Cy5 labeled DNA. (**d**) EXD2-WT (5-80nM) was incubated with a dsRNA FAM substrate (forward) in the presence of 10mM $MnCl_2$. (**e**) EXD2-C1/2 (5-80 nM) was incubated with 20nM fluorescently labelled ssRNA or RNA/DNA hybrid in the presence of 10mM $MnCl_2$. (**f**) EXD2-WT (5-80nM) or EXD2-NUC (40-80nM) was incubated with 20nM fluorescently labelled ssDNA or dsDNA or (**g**) 20nM RNA/DNA (FAM/Cy5) hybrid in the presence of 10mM $MgCl_2$. (**h**) EXD2-WT (5-80nM) was incubated with a dsRNA FAM substrate (forward) in the presence of 10mM $MgCl_2$. (**i**) EXD2-C1/2 (5-80 nM) was incubated with 20nM fluorescently labelled ssRNA or RNA/DNA hybrid in the presence of 10mM $MgCl_2$. All reactions in (b-i) were carried out for 30 min at 37°C before being separated on an 18% polyacrylamide urea TBE gel and 30 bp indicated with black arrowhead (b-i). (**j**) Quantification of specific activity (nM substrate cleavage/nM protein per minute) of EXD2-WT on indicated substrates in the presence of $MgCl_2$ or $MnCl_2$. Data compiled from n=3 independent experiments and all values with mean(SD) are shown. (**k**) EXD2-WT (20-310 nM), (**l**) EXD2-NUC (20-310 nM), (**m**) EXD2-C1/2 (20-310 nM) were incubated with 20nM fluorescently labelled ssDNA, ssRNA, RNA/DNA hybrid or dsDNA, 30 min on ice. Red arrow indicates the protein/nucleic acid complex formed with ssRNA and reduced with the EXD2-C1/2 mutant and black arrowhead = 40 bp (k-m). Data in b-c, e-g, i, k-l, are representative of three experiments; 6d, 6h, 6m, are representative of two experiments. Source data in Supplementary Table 1 and additional analysis and uncropped gels in Supplementary Figs. 5 and 9, respectively.

Figure 7: Metabolic and developmental defects in *dExd2* deficient flies. (**a**) Reduced *dExd2* expression in *dExd2*^{EY03872} flies compared with control *(yellow white, yw)* measured by qRT-PCR. Averages from n=3 independent experiments plotted with mean(SD) (***p=0.0002 and 0.0003, unpaired t-test, two-tailed). (**b**) mtDNA levels analyzed using qRT-PCR in flies reared in food +/- NAC. Averages from n=3 experiments plotted with mean (SD). **p=0.0083 female, **p=0.0013 male, unpaired t-test, two-tailed. (**c**) Phosphorimager scan of mitochondrial translation products. Western blotting for VDAC shows equal loading. (**d**) Quantification of n=3 independent experiments compared to WT sample with mean(SD) shown with individual values. **p=0.0024, unpaired t-test, two-tailed. (**e**) Confocal immunofluorescence of exogenously expressed dEXD2-BirA*-FLAG or BirA*-FLAG in Drosophila S2 cells. Extensive co-localization of EXD2-BirA*-FLAG but not BirA*-FLAG is observed with the mitochondrial protein ATP5A. Scale bar=0.2 μm. Data represent 30 cells from 2 experiments. (**f**) Reduced oxygen consumption in *dExd2*-deficient flies is not rescued with NAC treatment. Measurements from n=4 or n=3 (NAC samples) independent experiments are plotted with mean(SD). *p<0.05, ***p<0.001, one way ANOVA with Dunnet's test. (**g**) LC-MS analysis of the indicated metabolites in 1 week old flies reared on normal food or food containing NAC. n=4 independent biological replicates plotted with the mean(SD). (**h**) *dExd2*^{EY03872} embryos and pupae are smaller than controls. Individual values and mean(SD) from n=100 embryos and n=31 pupae are shown (***p<0.0001, t-test two-tailed). A representative example of pupae of each genotype is shown, scale bar=500μm. (**i**) Delayed pupariation in *dExd2*^{EY03872} flies is rescued by NAC and enhanced by PQT at doses that do not strongly affect controls. Mean(SD) compiled from n=3 independent experiments with 40 flies per point is plotted. Source data for figure and additional

statistical information in Supplementary Table 1 and uncropped blots in Supplementary Figure 9.

Figure 8: Germline stem cell attrition and increased lifespan in *dExd2* deficient flies. (**a**) Significantly increased lifespan in *dExd2*^{EY03872} flies compared to controls, particularly for females. NAC normalizes lifespan of *dExd2*-deficient females. Mean(SD) was compiled from n=3 independent experiments, each using 60 flies. ***p<4.03x10^{-10} for males and ***p<2.22x10^{-16} for females, proportional hazard-Cox model. (**b**) QRT-PCR analysis of different *Drosophila* tissues shows high *dExd2* mRNA levels in the ovaries of control flies compared to other tissues. Values from n=3 independent experiments are plotted with mean(SD). (**c**) Fecundity was reduced in *dExd2*^{EY03872} flies and partially rescued by NAC. A total of 60 flies were used for each group and mean(SD) shown. (**d**) Age dependent attrition of GSCs in *dExd2*^{EY03872} flies was rescued by NAC. GSCs were identified by Hts staining and indicated by white arrows. Scale bar = 20μm. (**e**) Quantification of GSCs of each genotype for the indicated ages +/- NAC treatment. Mean was compiled from n=15 independent germaria at each time point and mean(SD) shown. Statistical analysis performed using the proportional odds cumulative link model (***p=1.38E-08 for week 7). (**f**) Immunofluorescence analysis revealed a strong decrease in Cytochrome-C (Cyt-C) levels and disorganized ATP synthase patterns (ATP5A) in *dExd2*^{EY03872} mutant germaria. Scale bar=20 μm. Source data and additional statistical analysis in Supplementary Table 1.

Acknowledgements

We are grateful to A. Zorzano, A. Vaquero, E. Hidalgo, W.M. Keyes, M. Milan, J. Casanova, M. Solà, V. Mootha, J. Guinovart and the Stracker lab for helpful input and

discussions, N. Gallisa for help generating BioID constructs, J.J.P. Perry and J.A. Tainer for the WRN-Exo expression construct, A. Bratic and N.G. Larsson for sharing advice and protocols, the Advanced Digital Microscopy and Biostatistics/Bioinformatics IRB core facilities, to the Ministerio de Economía y Competitividad (MINECO) for funding to THS, LRdP and OY (THS: BFU2012-39521;BFU2015-68354, Ayudas para incentivar la incorporación estable de doctores (IED) 2015, LRdP: BIO2015-64572, THS and LRdP: institutional funding through the Centres of Excellence Severo Ochoa award and from the CERCA Programme of the Catalan Government, and OY: SAF2011-30578 and BFU2014-57466), the Spanish Biomedical Research Centre in Diabetes and Associated Metabolic Disorders (CIBERDEM), an initiative of Instituto de Investigacion Carlos III (ISCIII) for funding to OY, and the Biotechnology and Biological Sciences Research Council [BBSRC: BB/H019723/1 and BB/M008800/1], for funding to AJD and LB. SA was supported by a Finnish Cultural Society Fellowship, JS by a fellowship from *Fundação para a Ciência e a Tecnologia* (SFRH/BD/87025/2012), PAK by an Advanced Postdoc Mobility fellowship from the Swiss National Science Foundation (SNF), IGC by an Asociación Española Contra el Cáncer (AECC) fellowship, AAF by a Severo Ochoa FPI fellowship (MINECO; SVP2014068398) and AAJ by an EMBO long-term fellowship (ALTF 554-2015).

Contributions

JS and SA performed the majority of experiments characterizing cell lines and effects of EXD2 deficiency; JS performed sucrose gradient fractionations; LB and AJD purified and characterized bacterial EXD2 and WRN, performed mtDNA replication assays and analyzed data; JS, SA, AC and AGR characterized *Drosophila*; PAK and PP performed BioID assays; MV, SSG and OY carried out metabolomics and mass spectrometry, analyzed data and prepared figures; EC and BR purified biotinylated

peptides, performed MS and analyzed data; AAJ performed the MitoString assay; IGC, JS, SA and THS performed survival assays and analyzed DNA damage responses; THS and JS performed mitochondrial translation assays; PAK and AAF performed IF analysis in *Drosophila* S2 cells; AMR performed computational and evolutionary analysis; LRdP provided critical technical expertise and advice; THS analyzed data, prepared figures, supervised experiments and wrote the manuscript with editorial contributions from all authors.

Competing financial interests

The authors declare no competing interests

Corresponding author

Travis H. Stracker: travis.stracker@irbbarcelona.org

References

1. Kauppila, T.E., Kauppila, J.H. & Larsson, N.G. Mammalian Mitochondria and Aging: An Update. *Cell Metab* **25**, 57-71 (2017).
2. Jourdain, A.A., Boehm, E., Maundrell, K. & Martinou, J.C. Mitochondrial RNA granules: Compartmentalizing mitochondrial gene expression. *J Cell Biol* **212**, 611-614 (2016).
3. Chinnery, P.F. Mitochondrial disease in adults: what's old and what's new? *EMBO molecular medicine* **7**, 1503-1512 (2015).
4. Yang, W. & Hekimi, S. Two modes of mitochondrial dysfunction lead independently to lifespan extension in Caenorhabditis elegans. *Aging Cell* **9**, 433-447 (2010).
5. Schmeisser, S. *et al.* Neuronal ROS signaling rather than AMPK/sirtuin-mediated energy sensing links dietary restriction to lifespan extension. *Molecular metabolism* **2**, 92-102 (2013).
6. Dillin, A. *et al.* Rates of behavior and aging specified by mitochondrial function during development. *Science* **298**, 2398-2401 (2002).
7. Smogorzewska, A. *et al.* A genetic screen identifies FAN1, a Fanconi anemia-associated nuclease necessary for DNA interstrand crosslink repair. *Mol Cell* **39**, 36-47 (2010).
8. Broderick, R. *et al.* EXD2 promotes homologous recombination by facilitating DNA end resection. *Nat Cell Biol* **18**, 271-280 (2016).
9. Cox, L.S., Clancy, D.J., Boubriak, I. & Saunders, R.D. Modeling Werner Syndrome in Drosophila melanogaster: hyper-recombination in flies lacking WRN-like exonuclease. *Ann N Y Acad Sci* **1119**, 274-288 (2007).
10. Biehs, R. *et al.* DNA Double-Strand Break Resection Occurs during Non-homologous End Joining in G1 but Is Distinct from Resection during Homologous Recombination. *Mol Cell* **65**, 671-684 e675 (2017).
11. Kudlow, B.A., Kennedy, B.K. & Monnat, R.J., Jr. Werner and Hutchinson-Gilford progeria syndromes: mechanistic basis of human progeroid diseases. *Nat Rev Mol Cell Biol* **8**, 394-404 (2007).
12. Evans, A.M., DeHaven, C.D., Barrett, T., Mitchell, M. & Milgram, E. Integrated, nontargeted ultrahigh performance liquid chromatography/electrospray ionization tandem mass spectrometry platform for the identification and relative quantification of the small-molecule complement of biological systems. *Anal Chem* **81**, 6656-6667 (2009).
13. Vinaixa, M. *et al.* Positional Enrichment by Proton Analysis (PEPA): A One-Dimensional 1 H-NMR Approach for 13 C Stable Isotope Tracer Studies in Metabolomics. *Angew Chem Int Ed Engl* **56**, 3531-3535 (2017).
14. Deberardinis, R.J., Sayed, N., Ditsworth, D. & Thompson, C.B. Brick by brick: metabolism and tumor cell growth. *Curr Opin Genet Dev* **18**, 54-61 (2008).
15. Cong, L. *et al.* Multiplex Genome Engineering Using CRISPR/Cas Systems. *Science* (2013).
16. Fukuoh, A. *et al.* Screen for mitochondrial DNA copy number maintenance genes reveals essential role for ATP synthase. *Mol Syst Biol* **10**, 734 (2014).
17. West, A.P., Shadel, G.S. & Ghosh, S. Mitochondria in innate immune responses. *Nat Rev Immunol* **11**, 389-402 (2011).
18. Smeitink, J.A., Zeviani, M., Turnbull, D.M. & Jacobs, H.T. Mitochondrial medicine: a metabolic perspective on the pathology of oxidative phosphorylation disorders. *Cell Metab* **3**, 9-13 (2006).

19. Roux, K.J., Kim, D.I. & Burke, B. BioID: a screen for protein-protein interactions. *Current protocols in protein science / editorial board, John E. Coligan ... [et al.]* **74**, Unit 19 23 (2013).
20. Sanchez-Caballero, L., Guerrero-Castillo, S. & Nijtmans, L. Unraveling the complexity of mitochondrial complex I assembly: A dynamic process. *Biochim Biophys Acta* **1857**, 980-990 (2016).
21. Sasarman, F. & Shoubridge, E.A. Radioactive labeling of mitochondrial translation products in cultured cells. *Methods Mol Biol* **837**, 207-217 (2012).
22. Attrill, H. *et al.* FlyBase: establishing a Gene Group resource for Drosophila melanogaster. *Nucleic Acids Res* **44**, D786-792 (2016).
23. Merkey, A.B., Wong, C.K., Hoshizaki, D.K. & Gibbs, A.G. Energetics of metamorphosis in Drosophila melanogaster. *Journal of insect physiology* **57**, 1437-1445 (2011).
24. Hsu, H.J. & Drummond-Barbosa, D. Insulin levels control female germline stem cell maintenance via the niche in Drosophila. *Proc Natl Acad Sci U S A* **106**, 1117-1121 (2009).
25. Hansen, M., Flatt, T. & Aguilaniu, H. Reproduction, fat metabolism, and life span: what is the connection? *Cell Metab* **17**, 10-19 (2013).
26. Ruzzenente, B. *et al.* LRPPRC is necessary for polyadenylation and coordination of translation of mitochondrial mRNAs. *EMBO J* **31**, 443-456 (2012).
27. Bratic, A. *et al.* The bicoid stability factor controls polyadenylation and expression of specific mitochondrial mRNAs in Drosophila melanogaster. *PLoS Genet* **7**, e1002324 (2011).
28. Wolf, A.R. & Mootha, V.K. Functional genomic analysis of human mitochondrial RNA processing. *Cell Rep* **7**, 918-931 (2014).
29. Sessions, O.M. *et al.* Discovery of insect and human dengue virus host factors. *Nature* **458**, 1047-1050 (2009).
30. Sirbu, B.M. *et al.* Identification of proteins at active, stalled, and collapsed replication forks using isolation of proteins on nascent DNA (iPOND) coupled with mass spectrometry. *J Biol Chem* **288**, 31458-31467 (2013).
31. Lange, H. *et al.* Degradation of a polyadenylated rRNA maturation by-product involves one of the three RRP6-like proteins in Arabidopsis thaliana. *Mol Cell Biol* **28**, 3038-3044 (2008).
32. Xie, B. *et al.* Further characterization of human DNA polymerase delta interacting protein 38. *J Biol Chem* **280**, 22375-22384 (2005).
33. Hilton, B.A. *et al.* ATR Plays a Direct Antiapoptotic Role at Mitochondria, which Is Regulated by Prolyl Isomerase Pin1. *Mol Cell* **60**, 35-46 (2015).
34. Oberto, J. *et al.* Qri7/OSGEPL, the mitochondrial version of the universal Kae1/YgjD protein, is essential for mitochondrial genome maintenance. *Nucleic Acids Res* **37**, 5343-5352 (2009).
35. Ougland, R., Rognes, T., Klungland, A. & Larsen, E. Non-homologous functions of the AlkB homologs. *J Mol Cell Biol* **7**, 494-504 (2015).
36. Liu, P. *et al.* Removal of oxidative DNA damage via FEN1-dependent long-patch base excision repair in human cell mitochondria. *Mol Cell Biol* **28**, 4975-4987 (2008).
37. Zheng, L. *et al.* Human DNA2 is a mitochondrial nuclease/helicase for efficient processing of DNA replication and repair intermediates. *Mol Cell* **32**, 325-336 (2008).
38. Copeland, J.M. *et al.* Extension of Drosophila life span by RNAi of the mitochondrial respiratory chain. *Curr Biol* **19**, 1591-1598 (2009).

39. Miwa, S. *et al.* Low abundance of the matrix arm of complex I in mitochondria predicts longevity in mice. *Nature communications* **5**, 3837 (2014).
40. Scialo, F. *et al.* Mitochondrial ROS Produced via Reverse Electron Transport Extend Animal Lifespan. *Cell Metab* **23**, 725-734 (2016).
41. Caballero, A. *et al.* Absence of mitochondrial translation control proteins extends life span by activating sirtuin-dependent silencing. *Mol Cell* **42**, 390-400 (2011).
42. Guarente, L. & Picard, F. Calorie restriction--the SIR2 connection. *Cell* **120**, 473-482 (2005).
43. Quiros, P.M., Mottis, A. & Auwerx, J. Mitonuclear communication in homeostasis and stress. *Nat Rev Mol Cell Biol* **17**, 213-226 (2016).
44. Cuykendall, T.N. & Houston, D.W. Identification of germ plasm-associated transcripts by microarray analysis of Xenopus vegetal cortex RNA. *Dev Dyn* **239**, 1838-1848 (2010).
45. Oehl-Jaschkowitz, B. *et al.* Deletions in 14q24.1q24.3 are associated with congenital heart defects, brachydactyly, and mild intellectual disability. *Am J Med Genet A* **164A**, 620-626 (2014).

Methods

Generation of expression constructs

Human *EXD2* was amplified from U2OS cell cDNA, sequenced and cloned into pENTR/D-TOPO (Invitrogen) following manufacturer's protocol. *EXD2* was subcloned using LR clonase into the retroviral vector pLPC-C-SF-TAP (SF=Strep-FLAG) generated by subcloning the C-SF-TAP cassette (a kind gift from C.J. Gloeckner[46]) into the pLPC-N-Myc plasmid (a kind gift from T. de Lange, Addgene plasmid #12540). *EXD2* mutants were generated using the QuikChange Lightning Site-Directed Mutagenesis Kit (Agilent Technologies 210518-5) according to manufacturer's instructions. Clones were purified using the PureLink® Quick Plasmid Miniprep Kit (Invitrogen) and the sequence of constructs confirmed. Large-scale plasmid purification was performed using the PureYield™ Plasmid Maxiprep System (Promega). Primers sequences are provided in Supplementary Table 3.

Human cell culture

Human cell lines (U2OS, HEK293T, AD293, MDA-MB-231 and RPE1) were cultured in Dulbecco's modified Eagle Medium (DMEM, Invitrogen 41966) supplemented with 10% (v/v) fetal bovine serum (FBS; Sigma F7524-500ML) and 100U/ml penicillin/streptomycin (P/S; Reactiva, 01030311B000) in 5% CO_2. In some experiments cells were treated with 100µg/ml Chloramphenicol (CAP) (Sigma, C3175), 25μM carbonyl cyanide-4-(trifluoromethoxy)phenylhydrazone (FCCP) (Sigma, C2920) or 5 mM N-acetylcysteine (NAC) (Sigma, A9165).

Generation of retrovirus/lentivirus and stable cell lines

For viral production, HEK293T cells were seeded in 10cm plates 24 h prior to transfection with polyethyleneimide (PEI; Polysciences Euro GMBH). For lentivirus, a mixture of 10µg lentivirus-shRNA, 2µg REV, 6µg RSV-RRE and 2µg VSV-G plasmids[47] with 78µl PEI and 900µl 150mM NaCl was added to the cell culture media

and for retrovirus, a mixture of 10μg retroviral vector DNA, 9μg GAG-Pol (pCL-Eco)[48] and 1μg VSV-G plasmids with 78μl PEI and 900μl 150mM NaCl was added to the cell culture media. In both cases, 16 h later, cells were washed in PBS and the media replaced. 48 h later the viral supernatant was removed, cleared with a 0.45μM filter, and incubated with target cells. 3 days after infection, cells were selected with Puromycin (Sigma, P8833-25MG) for 5 days and maintained subsequently in the normal growth medium. Lentivirus shRNA constructs were purchased from the Sigma MISSION lentiviral library against *EXD2* (sh31: TRCN0000051631 (NM_018199.1-155s1c1), sh22: TRCN0000327822 (NM_018199.2-1001s21c1) and shRNA against GFP (SCH005) and sh-non-targeter (shNT, SHC016) were used as controls.

Generation of *EXD2* knockout cells with CRISPR/CAS9

Forward and reverse oligonucleotides containing the guide sequence were annealed and cloned into the pX330-U6-Chimeric_BB-CBh-hSpCas9 (a gift from Feng Zhang, Addgene plasmid #42230)[15] modified to coexpresses EGFP (a gift from C.Cortina and E.Batlle) and this was transfected into U2OS and MDA-MB-231 cells using Lipofectamine® 2000 Transfection Reagent (ThermoFisher). GFP-positive cells were sorted 24 h after transfection (BD FACSAria III SORP) and expanded from single cells. Screening for *EXD2-KO* cells was carried out by western blotting. Two clones each of U2OS and MDA-MB-231 showing complete loss of EXD2 protein were selected for further phenotypic analysis.

Isolation of DNA, RNA and cDNA preparation

For DNA isolation of human cancer cell lines, 1,000,000 cells were plated on 10 cm plates and collected 24 h later in 515μl of lysis buffer (75mM NaCl, 50mM EDTA, 0.02% SDS, 0.4mg/ml Proteinase-K (PK)). Lysate was transferred to 1.5ml Eppendorf tubes and incubated at 50°C for 2 h. 1 volume of isopropanol was added and mixed and incubated at 4°C O/N. Tubes were centrifuged at 8,500g for 30min at

4°C and pellets washed with 70% EtOH and air-dried. DNA was resuspended in TE and diluted to 100ng/ml for qPCR. *Drosophila melanogaster* DNA was obtained from adult flies that were snap frozen in liquid nitrogen and the abdomens homogenized with a pestle in grinding buffer (0.2M sucrose, 0.1M Tris pH 9.2, 50mM EDTA and 0.5% SDS) and incubated at 65°C for 10 min. KAc was added to a final concentration of 5M and the samples were incubated on ice for 20min. DNA was precipitated with Phenol/Chloroform/Ethanol. Total RNA was isolated using the PureLink RNA mini kit (Ambion) according to manufacturers instructions. 1µg of total RNA was used as a template for cDNA synthesis using a High Capacity RNA-to-cDNA Kit (ThermoFisher).

Quantitative real time PCR (qRT-PCR)

Real-time quantitative PCR was performed using a Step-One-Plus real-time PCR (Applied Biosystems) Instrument and quantified with the comparative CT method. Amplification was performed using Power SYBR Green PCR Master Mix (Applied Biosystems, 4309155). Analysis of EXD2 mRNA levels was done using Taqman probes from Applied Biosystems (*EXD2* Hs00217045_m1, *ACTB* 4352935E) together with Taqman master mix (Applied Biosystems). Primers used are provided in Supplementary Table 3.

Flow cytometry based assays for mitochondrial function

For the analysis of mitochondrial mass, 150,000 cells were seeded in 6-well plates in duplicate 24h prior to analysis. Cells were incubated for 30min with 250nM MitoTracker Green FM or Deep Red probes (ThermoFisher) in normal growth medium at 37°C. Cells were trypsinized and washed with warm PBS once, stained with 500 nM 4',6-Diamidino-2-Phenylindole, Dihydrochloride (DAPI) and analyzed by flow cytometry immediately. To detect intracellular and mitochondrial ROS production, 150,000 cells were seeded in 6-well plates in duplicate 24 h prior to analysis. Cells were incubated at 37°C for 30 min in 5µM MitoSox (Molecular Probes, M36008) and

then trypsinized and washed with warm PBS once and analyzed immediately by flow cytometry. Data was collected with a Gallios using Kaluza for Gallios software (Beckman Coulter) and analyzed using FlowJo v9.9.6 (FlowJo LLC). Data was plotted and statistically analyzed in Prism7 and examples provided in Supplementary Fig. 8.

Immunofluorescence

For immunofluorescence, cells were fixed with 4% formaldehyde for 10 min at room temperature (RT). After two washes with PBS, cells were permeabilized with PBS containing 2% Triton X-100 for 10 min at RT. Cell were washed twice with PBS and incubated with first antibody (1:500) in PBS-T containing 10% FBS for 1 h at RT. After two washes with PBS-T, cells were incubated with secondary antibody (1:500) in PBS-T containing 10% FBS and DAPI for 1 h at RT. Slides were rinsed in PBS-T, washed twice for 5 min in PBS-T and mounted with Vectashield (Vector Laboratories, H-1000). *Drosophila* embryos (0-15h) were collected, dechorionated with bleach for 90s and rinsed with 0.1% Triton X-100. Embryos were incubated in a solution containing 4% formaldehyde and heptane (1:1) for 20 min in a rotator at RT. Formaldehyde was replaced with methanol, samples were vortexed for 20 sec and the embryos were transferred to new vials and washed extensively with PBS-T containing 0.3% bovine serum albumin (BSA). Samples were incubated with primary antibody for 4 h at RT and after two washes with PBS-T they were incubated with secondary antibody for 2 h at RT, followed by an incubation with DAPI for 15 min at RT. Embryos were rinsed in PBS-T, washed twice for 5 min in PBS-T containing 0.3% BSA and mounted with Fluoromount (Sigma, F4680). Adult ovaries from *Drosophila* were dissected in Schneider medium and fixed in 4% formaldehyde in PBS for 20 min at RT. After washing with PBS, they were permeabilized with 1% Triton X-100 in PBS for 2 h and then incubated in PBS-T (1% (w/v) BSA, 0.2% Triton

X-100, PBS) for 1 h. Ovaries were then incubated with primary antibodies diluted in PBS-T O/N at 4°C. The next day, they were washed with PBS, incubated in the dark with secondary antibodies diluted in PBS-T for 3 h at RT and further stained with rhodamine-phalloidin (Biotium, #00027) and Hoechst (Sigma) for 20 min. After final washes with PBS, ovaries were mounted in Vectashield (Vector Laboratories, H-1000) Images were acquired with a Leica SPE confocal microscope and cropped in ImageJ[49]. Depth (z) thresholds were set accordingly in order to apprehend the entire architecture. In some cases, brightness and contrast were adjusted in ImageJ (v1.49b). Any changes were applied to all images equally for direct comparison. Antibodies used are provided in Supplementary Table 4.

Protein lysates, fractionation and Western blotting

Cells were rinsed with PBS and collected in lysis buffer (50mM HEPES, 16mM NaCl, 1% NP-40, 0.5% DOC, 0.1% SDS, 1x protease inhibitor cocktail (Roche, 04693132001) and phosphatase inhibitor cocktail (Sigma, P5726). Samples were sonicated (15s-15s) for 30 min, spun down at 4°C for 20 min at 12,000xg and quantified with the DC Protein assay (Biorad, 500-0114). 50µg of total protein was boiled 10 min with loading dye (50mM Tris-Cl (pH 6.8), 0.3% SDS, 0.1% bromophenol blue, 10% glycerol, 0.4% ß-mercaptoethanol) and separated by SDS-PAGE followed by electrophoretic transfer to PVDF membrane (Millipore). Membranes were blocked for 20 min in PBS-T with 5% dry milk and primary antibody (in PBS-T with 5% dry milk) was added for either 1 hour at RT or O/N at 4°C. Membranes were washed 3X in PBS-T and incubated with secondary antibody (in PBS-T with 5% dry milk) 1 h at RT. After 3X PBS-T washes, ECL-reagent (Amersham, RPN2132) and X-ray film (Fujifilm, 47410 19236) were used to detect signal. Antibodies used are listed in Supplementary Table 4. Separation of cellular compartments was performed according to manufacturers instructions with Standard

Cell Fractionation Kit (Abcam, ab109719). Further HCl treatment of the nuclear fractions was used for chromatin extraction. Alternative chromatin fractionation (Supplementary Fig. 7c) was performed as described previously[8]. U2OS cells were resuspended in buffer A (10mM HEPES-KOH pH=7.9, 10mM KCl, 1.5mM $MgCl_2$, 340mM sucrose, 10% glycerol, 1mM DTT, 1x protease inhibitor cocktail (Roche, 04693132001) and phosphatase inhibitor cocktail (Sigma, P5726)) and Triton-X100 was added to a final concentration of 0.1%. After incubation on ice for 5 min, samples were centrifuged at 1300xg for 4 min. Pelleted nuclei were washed with buffer A, resuspended in buffer B (3mM EDTA, 0.2mM EGTA, 1mM DTT, 1x protease inhibitor cocktail (Roche, 04693132001) and phosphatase inhibitor cocktail (Sigma, P5726)) and lysed for 20 min on ice. After centrifugation at 1,700xg for 5 min, the supernatant (nuclear soluble fraction) was collected, and the pellet (chromatin fraction) was washed with buffer B, resuspended in urea buffer (9M urea, 50mM Tris-HCl pH=7.3) and sonicated.

Submitochondrial fractionation

PK treatment of mitochondria was performed as previously described[50]. Briefly, U2OS cells were homogenized in ice-cold MB buffer (210mM mannitol, 70mM sucrose, 10mM HEPES-KOH pH 7.4 and 1mM EDTA) with a glass dounce homogenizer (40 tight strokes) and mitochondria were obtained by differential centrifugation. To test protease accessibility, 100µg of mitochondria were resuspended in 200µl of MB buffer, swelling buffer (10mM HEPES-KOH pH7.4), or MB + 0.2% (v/v) Triton X-100. PK was added to a final concentration of 50µg/ml and the samples were incubated on ice for 30 min. Proteolysis was stopped by adding 2mM phenylmethylsulphonyl fluoride. Samples were precipitated with trichloro-acetic acid (TCA; Sigma, T6399) and analyzed by SDS-PAGE. Analysis of differential protein retention after FCCP treatment was performed by treating U2OS cells with

25μM FCCP for 24 hours. Separation of cellular compartments was performed according to manufacturers instructions with Standard Cell Fractionation Kit (Abcam, ab109719). Further HCl treatment of the nuclear fractions was used for chromatin extraction.

Metabolomic analysis of human cell lines

A combination of LC-MS and GC-MS analysis performed by Metabolon (www.metabolon.com)[12] was used for the detection of a total of 253 metabolites in cell extracts. Analysis was performed using 5 independent cultures of control U2OS cells selected with a stable shRNA against *GFP* (shCont) or *EXD2* (shEXD2-22). Cells were collected, snap frozen and metabolites were extracted using a proprietary series of organic and aqueous extractions and divided into two fractions for analysis using liquid chromatography/mass spectrometry (LC/MS, LC/MS2) and gas chromatography/mass spectrometry (GC/MS). LC/MS was based on a Waters ACQUITY UPLC and a Thermo-Finnigan LTQ mass spectrometer, which consisted of an electrospray ionization (ESI) source and linear ion-trap (LIT) mass analyzer. Samples for GC/MS were re-dried under vacuum desiccation for a minimum of 24 h prior and derivatized under dried nitrogen using bistrimethyl-silyl-triflouroacetamide (BSTFA; Sigma, 33024). The GC column was 5% phenyl and the temperature ramp from 40°C to 300°C in a 16 min period. Samples were analyzed on a Thermo-Finnigan Trace DSQ fast-scanning single-quadrupole mass spectrometer using electron impact ionization.

For ^{13}C stable isotope tracer analysis, $6xE^6$ U2OS cells stably expressing the indicated shRNA constructs were seeded on 15cm tissue culture plates in triplicate. The following day, cells were rinsed 2X in PBS and 20ml media (DMEM w/o glucose, w/o glutamine, 10% FBS, 1x P/S) containing 5mM glucose (unlabeled or [U^{13}C6]-D-Glucose, Cambridge Isotope Laboratories, CLM-1396-1) or 2mM glutamine

(unlabeled or [U-^{13}C5]-Glutamine, Cambridge Isotope Laboratories, CLM-1822-H-0.1) was added to the cells for 6 h. Cells were collected by trypsinization and 10xE^6 cells were pelleted and snap-frozen, after which the metabolites were extracted into solvent by adding 2ml of ice-cold chloroform/methanol (2:1 v/v). The suspension was bath-sonicated for 3 min, and 2ml of cold water was added and then, 1ml of chloroform/methanol (2:1 v/v) was added to the samples followed by bath-sonication for 3 min. Cell lysates were centrifuged (5,000xg for 15 min at 4°C) and the aqueous phase transferred into a new tube. Samples were frozen until analysis using Positional Enrichment by Proton Analysis (PEPA)[13]. PEPA detects the position of carbon label in isotopically enriched metabolites and quantifies fractional enrichment by indirect determination of ^{13}C-satellite peaks using 1D-^{1}H-NMR spectra.

Liquid chromatography-mass spectrometry (LC-MS) analyses

Metabolites were extracted from snap frozen cell pellets by adding 200μL of cold acetonitrile (ACN)/H_2O (1:1) with 1% meta-phosphoric acid (MPA) and 0.1% formic acid (previously filtered, 1:1 v/v). Samples were vortexed for 30 sec and immersed in liquid N_2 to disrupt cell membranes followed by 30 sec of bath-sonication and these two steps were repeated 3 times. Then, samples were incubated at -20ºC for 2 h. Finally, samples were centrifuged at 17,000xg for 15 min and the supernatant was collected into a LC-MS vial. Samples were injected in a UHPLC system (1290 Agilent) coupled to a triple quadrupole (QqQ) MS (6490 Agilent Technologies) operated in multiple reaction monitoring (MRM) and positive (POS) or negative (NEG) electrospray ionization (ESI) mode. Metabolites were separated using C18-RP (ACQUITY UPLC BEH C18 1.7 uM, Waters) chromatography at a flow rate of 0.3mL/min. The solvent system was A= 20mM ammonium acetate + 15mM NH3 in water, and B=acetonitrile:water (95:5). The linear gradient elution started at 100% A (time 0-2 min), 65% A (time 2-5 min) and finished at 100% B (time 5.5 min). MRM

transitions were: GSH (NEG, 306 → 143.2, 128), GSSG (NEG, 611.1→ 306.2, 143), ATP (POS, 508→ 136, 410), ADP (POS 428 → 136, 348). Cellular ATP content was determined using a luminescence assay (ThermoFisher) according to manufacturer's instructions and the relative ATP levels were normalized by the protein content of each sample.

Seahorse bioanalyzer analysis

Cellular respiration was measured using a Seahorse XF24 bioanalyzer (Seahorse Biosciences). U2OS or MDA-MB-231 cells were seeded at 50,000-75,000 cells/well respectively on XF24 V7 PS cell culture microplates (Seahorse Biosciences, 100777-004) and cultured for 16 h prior to the analysis. The analysis was performed according to the manufacturer's instructions in DMEM (Seahorse Bioscience 102353-100) supplemented with 5.5mM D-glucose and 2mM L-glutamine for the OCR experiments. For OCR measurement (Mito Stress Test), the following reagents were added: oligomycin (1μM), FCCP (0.4μM), and rotenone (1μM) + antimycin A (1μM). For the ECAR analysis (Glycolysis Stress Test) the following reagents were added: glucose (10mM), oligomycin (1μm) and 2-DG (50mM). For the OCR analysis of individual complexes, digitonin (25μg/mL) was added to the media to allow cells to permeabilize for approximately one hour, followed by sequential injections of malate (2.5mM) + pyruvate (5mM), rotenone (1μM), succinate (10mM) and antimycin (5μM). Results were normalized to protein content using the DC Protein assay (Biorad, 500-0114).

BioID analysis of proximity interactions

EXD2 and *EXD2-C2* were PCR amplified from previously described clones and *dExd2* (*CG6744*) was amplified from sequence verified cDNA clones purchased from Gene Synthesis (Life Technologies) with primers containing 5' AscI or 3' NotI restriction sites (see Supplementary Table 3 for primers) using KOD Hot Start DNA

Polymerase (Millipore) and cycling conditions recommended from the manufacturer (Polymerase activation at 95°C for 2 min, denaturation at 95°C for 20 sec, annealing at 55°C for 10 sec and extension at 70°C for 50 sec, repeated for 40 cycles). PCR products were purified using the PureLink Quick Gel Extraction Kit (Invitrogen) and cloned into pCR2.1-TOPO vector (Invitrogen). Top10 competent *E. coli* cells (Invitrogen) were transformed with pCR2.1-TOPO clones and colonies were selected in carbenicillin. Constructs were verified by restriction digestion and sequencing (Macrogen) with primers for the TOPO vector (T7 Promoter-F and M13-R). Afterwards, *EXD2*, *EXD2-C2* and *dExd2* were cut from the pCR2.1-TOPO vector by restriction digestion with AscI (NEB) and NotI-HF (NEB), purified using the PureLink Quick Gel Extraction Kit (Invitrogen) and ligated into pcDNA5/FRT/TO-C-FLAG-hBirA* (kind gift from Dr. Brian Raught) using Quick Ligation Kit (BioLabs). Top10 competent *E. coli* cells (Invitrogen) were transformed and carbenicillin selected and the constructs were confirmed by restriction digestion and sequencing (Macrogen). For expression in *Drosophila* Schneider 2 (S2) cells, dEXD2-BirA*-FLAG was PCR amplified and subcloned into the pMK33-C-TAP-FLAG-HA-BD plasmid backbone (Flybase: FBmc0003027).

AD293 cells were seeded and transfected the next day with BirA* vectors using PEI (Polysciences Euro GMBH) +/- 50μM biotin (IBIAN Biotechnology 2-1016-002). For mass spectrometry, 5x15cm plates per condition were harvested 24h post-transfection by trypsinization, washing 2X in PBS and snap freezing on dry ice. Cell pellets were lysed in 5ml modified RIPA buffer (150mM Tris-HCl pH 7.5, 150mM NaCl, 1mM EDTA, 1mM EGTA, 1% Triton X-100, 0.1% SDS, 1:500 protease inhibitor cocktail (Sigma-Aldrich), 1:1000 benzonase (Novagen)) on ice and biotinylated proteins were isolated using streptavidin-sepharose beads (GE). Proteins were

washed in Ammonium bicarbonate and digested with trypsin. Mass spectrometry was performed as previously described[51].

Sucrose gradient analysis of mitochondrial ribosomes

U2OS cells were treated with 100µg/ml CAP and incubated at 37°C for 10 min. Cells were then washed and homogenized in ice-cold STE buffer (250mM sucrose, 5mM TrisHCl pH 7.5 and 1mM EGTA, 2mM DTT, 100µg/ml CAP, 20U/ml RNase inhibitors and 1X complete protease inhibitor) with a glass Dounce homogenizer (40 tight strokes). Mitochondria were obtained by differential centrifugation and loaded (0.9mg) on a 5ml linear sucrose gradient (10-30% [vol/vol]) in a gradient forming buffer (20mM Tris-HCl pH 7.5, 10mM $MgCl_2$, 100mM KCl, 2mM DTT, 100µg/ml chloramphenicol, 20U/ml RNase inhibitors and 1X complete protease inhibitor). The gradients were centrifuged for 2 h at 39,000rpm at 4°C and fractions of 350µl were collected from the top and precipitated with TCA. Samples were then analyzed by SDS-PAGE and qRT-PCR.

Analysis of mitochondrial translation

To analyze the rate of mitochondrial translation, experiments were performed essentially as described[21] with minor modifications. 400,000 cells were plated on 6 cm plates the day prior to the experiment. Media was replaced with 2ml DMEM lacking methionine or cysteine (Life Technologies) with 10% dialyzed FBS (Hyclone) for 20 min. 100µl of 6 mg/ml sterile filtered emetine (Sigma) in PBS was added to the media for 10 min followed by the addition of 200µCi/ml of ^{35}S EasyTag (Perkin Elmer) for 1 h. For some experiments, CAP (Sigma) was added at 40 µg/ml to inhibit mitochondrial translation or the anti-oxidant NAC (Sigma) was added at 5 mM. Labeling media was removed and cells washed 2X in PBS followed by a 10 min incubation in DMEM with 10% FBS and P/S. Cells were washed 3X in PBS and scraped into 1ml PBS. Following gentle centrifugation at 1,000g, cell pellets were

resuspended in RIPA buffer (50mM Tris–HCl pH 7.5, 150mM NaCl, 1% NP-40, 1mM $MgCl_2$, 1X EDTA-free protease inhibitor cocktail (Roche)), nuclei pelleted by centrifugation at 2,000xg for 10 min and the protein concentration determined by a modified BCA assay (Biorad). 20-40µg of lysate was run on a 14% SDS-PAGE gel and transferred to PVDF membrane by western blotting. Dried membranes were exposed to a Storage Phosphor Screen (Molecular Dynamics) for 3 to 8 days and imaged using a Typhoon 8600 Variable Mode Imager (Molecular Dynamics). Contrast was adjusted and band intensity was quantified using ImageJ[49]. *In organello Drosophila* translation assays were performed as previously described[27]. Briefly, mitochondria were isolated from third-instar larvae and treated with 200µg/ml emetine and 100µg/ml cyclohexamide to inhibit cytoplasmic translation. 0.4mg of isolated mitochondria were incubated with 178 µCi ^{35}S EasyTag (Perkin Elmer) for 1 h at 30°C and equal amounts of mitochondrial protein were loaded on a 14% SDS-PAGE gel and transferred to PVDF membrane by western blotting at 100V for 1 h. Labeled proteins were visualized by autoradiography as previously described.

Protein purification and enzymatic assays

Recombinant EXD2 (61-621) was used for protein expression due to its improved solubility and yield. It was PCR amplified and cloned into pet28a with an N-terminal His-SUMO tag using BsmBI and XbaI and protein was expressed in *E.coli* Bl21(DE3)pLysSRARE by the addition of 1mM IPTG at 25°C for 3 h. Soluble proteins were purified using Nickel affinity resin in 50mM Tris Ph7.5, 500mM NaCl, 10% glycerol and eluted with increasing imidazole concentrations (up to 300mM). The resulting protein was then further purified by gel filtration using a Superdex 200 10/300 GL column (GE Healthcare) in 50mM Tris pH 7.5, 500mM NaCl, 10% glycerol. To confirm the activity was that of EXD2 rather than potential contaminants, mutations D108A and E110A (EXD2-NUC) were generated in the active site by site-

directed mutagenesis. In addition, an EXD2-C1/2 mutant was generated (420CxxC to SxxS and 460CxxC to SxxS) using a QuikChange Lightning Site-Directed Mutagenesis Kit (Agilent Technologies, 210518-5). These proteins were then expressed and purified as described for the WT.

WRN exo (1-333) was purified as described previously[52]. Briefly, the protein was expressed in *E.coli* Bl21(DE3)pLysSRARE by the addition of 1mM IPTG at 25°C for 4 h. Protein was purified on nickel affinity resin in 50mM Tris Ph7.5, 500mM Nacl, 10% glycerol, Q ion exchange chromatography in 50mM Tris Ph7.5, 10% glycerol followed by gel filtration using an S200 column in 50mM Tris Ph7.5, 500mM Nacl, 10% glycerol.

For enzymatic activity assays, 5-80nM protein was incubated with 20nM 5' FAM or Cy5 labeled DNA/RNA in 50mM Tris pH7.5, 0.5µg/ml BSA and 10% glycerol with the addition of 10nM $MnCl_2$ or $MgCl_2$. Reactions were incubated at 37°C for 30 min before DNA was denatured by boiling in 35% formamide. Where substrates contained RNA, 50% formamide was added and no boiling step was used. DNA was separated on an 18% polyacrylamide urea TBE gel (21W, 2 h) and products were visualized using a Fujifilm FLA-5100 image reader. For the blocked 5' end oligo assay, 0.5 units ExoI (NEB) was used as a positive control and the reaction was carried out in the supplied reaction buffer. Oligos were annealed to form double stranded (ds) substrates in 10mM Tris pH 7.5 by boiling followed by slow cooling.

Electrophoretic mobility shift assays (EMSA)

For electrophoretic mobility shift assays (EMSA), 20-310nM protein was incubated with 20nM 5' FAM or Cy5 labelled DNA/RNA in 50mM Tris pH 7.5, 0.5µg/ml BSA and 10% glycerol and incubated on ice for 30 min. Complexes were then separated on an 8% polyacrylamide gel in 0.5x TBE (75V for 80 min) and products were visualized

using a Fujifilm FLA-5100 image reader. All primers used are listed in Supplementary Table 3.

Drosophila stocks and maintenance

Drosophila melanogaster with a transposon insertion mapped to *CG6744/dExd2* (y^1 w^{67c23}; P{EPgy2}$CG6744^{EY03872}$; stock #16578) were obtained from the Bloomington Drosophila Stock Center at Indiana University (http://flystocks.bio.indiana.edu/) and reduced transcript level was confirmed by qRT-PCR as described. Flies were maintained at 25 °C on a 12 h:12 h light:dark cycle at constant humidity. Flies were back-crossed to our control *yellow white* flies for 8 generations prior to performing the analyses reported here.

Drosophila food preparation

For lifespan analysis, different fly-food formulations were prepared. Normal food (100g yeast, 100g sugar, 20g agar, 30ml nipagen and 3ml propionic acid per liter of food); Low Sugar food (100g yeast, 50g sugar, 20g agar, 30ml nipagen and 3ml propionic acid per liter of food); Low Yeast food (50g yeast, 100g sugar, 20g agar, 30ml nipagen and 3ml propionic acid per liter of food); Antioxidant food (100g yeast, 100g sugar, 20g agar, 30ml nipagen, 3ml propionic acid and 10mg/ml NAC per liter of food); and Paraquat (PQT) food (100g yeast, 100g sugar, 20g agar, 30ml nipagen, 3ml propionic acid and 5mM PQT). To prepare each diet, yeast, sucrose and agar were first dissolved in water and boiled for 10 min. After cooling, propionic acid and nipagen were added, and the food was distributed into the glass vials and allowed to solidify. Finally, NAC or PQT were added to the specific diets.

Analysis of *Drosophila* lifespan, fecundity and development

To assess lifespan, newly hatched flies from each genotype were allowed to mate for 48 h, after which females and males were separated and grouped into 30 flies per vial. Food vials were changed every 3 days and deaths were scored until all flies

were dead. To determine fecundity, age- and diet-specific flies from each genotype were allowed to mate for 4 h and fecundity was estimated from 6 independent egg-counts. The mean number eggs/fly was calculated. For the analysis of development, 0-4 h embryos were collected on grape-juice agar plates. To assess pupariation, 40 newly hatched larvae were transferred to specific-food vials. Once the L3 stage was reached, larvae were monitored and new pupae were counted every 2 h. For size measurements, 0-4 hours embryos and pupae were mounted for imaging and processed with ImageJ[49]. Expression data shown in Supplementary Fig. 6c was obtained from ModENCODE/FlyBase[53, 54]

Culture and transfection of *Drosophila* S2 cells

Drosophila Schneider 2 cells (S2) were maintained at 25ºC in Schneider's *Drosophila* medium (Lonza) supplemented with 10% (v/v) FBS (Gibco, 10270-500ML) and 50µg/ml P/S (Gibco, 15140-122). S2 cells were transfected using Effectene (Qiagen, 301425) following the manufacturer's protocol.

Oxygen consumption measurement

Oxygen consumption was measured in inverted and permeabilized larval tissues using an Oxygraph-2k (Oroboros) as previously described[55]. Mitochondrial-dependent respiration was measured by supplying ETC substrates: 10mM glutamate, 2mM malate, 2.5mM ADP and 10mM succinate. Larvae were then stressed with 0.5µM of FCCP to measure maximal respiration and the ETC was inhibited by adding 0.5µM rotenone and 2.5µM antimycin. Final values were normalized to the protein content of each sample.

Transmission electron microscopy (TEM)

HEK293T-cells stably overexpressing *EXD2-WT-SF* or empty control SF-vector (*Cont-SF*) were grown to 80% confluency, washed 3X in PBS and fixed in 2.5% glutaraldehyde for 1 h. Cells were detached by scraping and pelleted (4°C, 2,500rpm

for 10 min). Pellets were washed in 0.1M PB 4X for 10 min, stained with 1% OsO_4 for 1 h and washed again for 10 min in 0.1M PB. Cells were dehydrated at 4°C (series of acetone concentrations: 50, 70, 90, 96, 100%) prior to embedding. Sections were cut with a UCT ultramicrotome (Leica Microsystems) and incubated with blocking buffer (5% and 1% BSA) in 0.01M PBS solutions for 10 and 1 min, respectively). Grids were incubated 30 min at RT with polyclonal FLAG antibody (Sigma) diluted 1 to 10 in blocking buffer (1% BSA in 0.01M PBS). After four washes (0.25% Tween 20 in 0.01M PBS for 4 min and 1% BSA in 0.01M PBS for 1 min), sections were incubated with IgM anti-rabbit coupled colloidal gold particles (Jackson, West Grove, USA) diluted in blocking buffer for 15 min, rinsed with water, rinsed in 0.01M PBS, fixed in 1% GA in 0.01M PBS, and rinsed abundantly in ddH_2O. Sections were stained with 1% potassium permanganate and 1% UA in water for 15 min. Controls for non-specific binding of the colloidal gold-conjugated antibody were performed by omitting the primary antibody. Electron micrographs were obtained with a Jeol JEM 1010 MT electron microscope (Japan) operating at 80kV in the Electron Microscopy core unit of the Parc Cientific de Barcelona.

Alamar Blue survival assays

Measurements were made according to manufacturer´s instructions (Invitrogen, DAL1025). Briefly, cells were seeded at a density of 300 cells per well in 96-well plates and allowed to attach overnight. After completion of drug treatments (7 days), a dilution 1:10 of Alamar Blue reagent in medium was added to each well. After 2-4 h incubation at 37ºC, fluorescence was measured in a FL600 Microplate Fluorescence Reader (BIOTEK).

Colony formation assays

For colony formation assays, cells were seeded at a density of 300 cells per well in 6-well plates and allowed to attach overnight. After completion of drug treatments (12 days), cells were stained with 0.1% crystal violet in 20% methanol. The number of

colonies was analyzed using ImageJ[49]. Cells were treated with the indicated doses of CPT-11 (Sigma, I1406), mitomycin-C (MMC; Sigma, M4287) or Olaparib (Selleckchem, AZD2281).

Blue Native Page electrophoresis

Blue native PAGE (BN-PAGE) analysis was performed according to a previously published protocol[56]. Briefly, 200µg of mitochondria were isolated from U2OS cells, solubilized with 8g/g digitonin and loaded into a gradient gel. Coomassie staining allowed for the identification of mitochondrial complexes.

MitoString assay

Total RNA was isolated according to manufacturers instructions (PureLink RNA mini kit, Ambion). The MitoString assay was performed as described[28].

2D-agarose gel electrophoresis of mitochondrial replication intermediates

2D agarose gel electrophoresis (2D-AGE) was carried out as described previously[57]. Briefly, total DNA was extracted from $4x10^6$ cells using Phenol chloroform and proteinase K. 30μg total DNA was digested with HinCII (NEB) and DNA was then separated in the first dimension on a 0.4% TBE agarose gel without ethidium bromide (EtBr) for 18 h at 1.1 V/cm. The lane was then cut from the gel and rotated 90° and the DNA was further separated in a 1 % TBE agarose gel containing 500 ng/ml EtBr for 6 h at 260 mA, 4°C. The gel was Southern blotted and DNA was identified using a radioactive probe made using Ready-To-Go™ dCTP DNA labeling beads (GE healthcare). The probe was specific to region 16341-151 and was generated by PCR (primer sequences in Supplementary Table 3)[58]. Labeled membranes were exposed to a phosphor screen that was scanned using a Fujifilm FLA-5100 image reader.

Computational and phylogenetic analysis

Human EXD2 was used as a query in phmmer searches (20718988) in a database of reference proteomes focusing on the UNIPROT reference proteomes having

complete genomes. We extracted the EXO domain multiple sequence alignment from the PFAM database (PFAM name is DNA_pol_A_exo1), built a hidden Markov profile from the seed alignment using HMMER(http://hmmer.org/) and searched in our database of Reference proteomes with this profile. Then we collected all the sequences having and EXO domain (~300 sequences). The HNH domain was extracted from PFAM (PFAM name HNH) and we built a hidden Markov profile for searching our database. EXD2_HUMAN was recovered at a significant e-value above threshold. We next scanned all of the sequences for additional domains using hmmscan (from HMMER suite) to annotate the sequences. Multiple sequence alignments of proteins were conducted using MAFFT in its slow and accurate version (L-IN-SI)[59]. Alignments were visualized in Belvu[60] and Jalview[61]. Sequence alignments shown in Supplementary Fig. 1a, c-e performed using the T-Coffee webserver[62], the output formatted in Jalview[61] and modified in Adobe Illustrator. Mitochondrial targeting probability was predicted using MitoProt II[62].

For the phylogenetic analysis, we conducted two different phylogenies, using only the EXO domain; a large tree of ~290 sequences, including a large number of bacterial sequences (available upon request), and a refined tree including representative sequences exhibiting different domain arrangements (Supplementary Fig 1b). We conducted probabilistic-based phylogenies using MrBayes[63]. A total of 4 independent chains with 4 runs were run under a mixed model of evolution over 5 million generations. 25% percent of initial trees were discarded and a total of 1,500,004 trees were sampled. Specific parameters to run the search were: prset aamodelpr=mixed; lset rates=gamma; relburnin=yes burningfrac=0.5. The tree was annotated using in-house scripts to show the domain distributions associated with the EXO domains in these sequences and visualized using iTOL[64]. Additional analyses

were run using alternative ML–base methods, in particular RAxML, giving the same topologies.

For the structural bioinformatics analysis of the EXD2 HNH domain (aa 408-470), The EXD2 HNH-like domain was modeled using SCWRL[65] and superimposed on the PDB structures with the best Fold and Function Assignment (FFAS03)[66] scores (5X42: Legionella pneumophila DotN: score -15, 5H0M: deep-sea thermophilic bacteriophage GVE2 HNH endonuclease[67]: score -12.0, 5MKW: Human ZRANB3 HNH domain[68]: score -11.7 and 1OGY: heterodimeric nitrate reductase NAPB from Rhodobacter sphaeroides[69]: score -11.1). Several structures were obtained as reliable templates (between -9 and -16) and the best scoring template in terms of alignment length, %identity and %of gaps (5H0M) was used to generate the model in Supplementary Fig. 1d.

Statistics and reproducibility

Statistical analysis was performed using Prism 7 and R. An unpaired two-tailed t-test was performed when comparing two groups except when stated otherwise. An ANOVA test was used when comparing more than two groups, followed by Dunnett's multiple comparison test. For metabolomics data, raw data was median-centered, and metabolite levels compared between shCont and shEXD2-22 groups using a two-tailed t-test. False discovery rate was controlled using the Benjamini & Hochberg procedure (p-adjusted < 0.1 and FC above 1.3 in absolute value was used for statistical significance). Data analysis was performed using R version 3.2.0. MetPa[70] was used to perform pathway enrichment and topological analysis. Survival or cumulative hazard functions were estimated using the Turnbull method for interval censored data using Kaplan-Meier estimates as a baseline and comparisons performed by proportional-hazard Cox models with interval censored data implemented in Rpackage (https://cran.r-

project.org/web/packages/icenReg/index.html). GSC attrition was analyzed with a proportional odds cumulative link model (ordinal regression) implemented in Rpackage (https://cran.r-project.org/web/packages/ordinal/index.html). P-values were adjusted for multiple testing using the Benjimini and Hochberg method and Hazard Ratios (HR) and their corresponding 95% confidence intervals were computed as a measure of association for data in Fig. 7i, 8a and 8e. Experiments were generally performed 2-3 times except for Supplementary figure 1f, 1h-j and 4a, which were performed once.

Data availability

Metabolomics data and statistics used for Figs. 2c and 2f are provided in Supplementary Table 1. Raw data for Fig. 2 is available in the Metabolights repository (ID: MTBLS247 (http://www.ebi.ac.uk/metabolights/MTBLS247)) and an annotated summary of BioID-MS data from Fig. 4 is provided in Supplementary Table 2 and raw data available in the MassIVE repository (ID: MSV000081337). Additional source data and statistical information for all plotted figures is provided in Supplementary Table 1 and uncropped blots and gels in Supplementary Figure 9. All other data are available from the corresponding author upon reasonable request.

References

46. Gloeckner, C.J., Boldt, K., Schumacher, A., Roepman, R. & Ueffing, M. A novel tandem affinity purification strategy for the efficient isolation and characterisation of native protein complexes. *Proteomics* **7**, 4228-4234 (2007).
47. Naldini, L. *et al.* In vivo gene delivery and stable transduction of nondividing cells by a lentiviral vector. *Science* **272**, 263-267 (1996).
48. Naviaux, R.K., Costanzi, E., Haas, M. & Verma, I.M. The pCL vector system: rapid production of helper-free, high-titer, recombinant retroviruses. *J Virol* **70**, 5701-5705 (1996).
49. Schindelin, J. *et al.* Fiji: an open-source platform for biological-image analysis. *Nat Methods* **9**, 676-682 (2012).
50. Jourdain, A.A. *et al.* GRSF1 regulates RNA processing in mitochondrial RNA granules. *Cell Metab* **17**, 399-410 (2013).
51. Gupta, G.D. *et al.* A Dynamic Protein Interaction Landscape of the Human Centrosome-Cilium Interface. *Cell* **163**, 1484-1499 (2015).

52. Perry, J.J. *et al.* WRN exonuclease structure and molecular mechanism imply an editing role in DNA end processing. *Nat Struct Mol Biol* **13**, 414-422 (2006).
53. Graveley, B.R. *et al.* The developmental transcriptome of Drosophila melanogaster. *Nature* **471**, 473-479 (2011).
54. Gelbart, W.M. & Emmert, D.B. (2013).
55. Guitart, T. *et al.* New aminoacyl-tRNA synthetase-like protein in insecta with an essential mitochondrial function. *J Biol Chem* **285**, 38157-38166 (2010).
56. Wittig, I., Braun, H.P. & Schagger, H. Blue native PAGE. *Nat Protoc* **1**, 418-428 (2006).
57. Reyes, A., Yasukawa, T., Cluett, T.J. & Holt, I.J. Analysis of mitochondrial DNA by two-dimensional agarose gel electrophoresis. *Methods Mol Biol* **554**, 15-35 (2009).
58. Yasukawa, T., Yang, M.Y., Jacobs, H.T. & Holt, I.J. A bidirectional origin of replication maps to the major noncoding region of human mitochondrial DNA. *Mol Cell* **18**, 651-662 (2005).
59. Katoh, K. & Standley, D.M. MAFFT multiple sequence alignment software version 7: improvements in performance and usability. *Molecular biology and evolution* **30**, 772-780 (2013).
60. Sonnhammer, E.L. & Hollich, V. Scoredist: a simple and robust protein sequence distance estimator. *BMC bioinformatics* **6**, 108 (2005).
61. Waterhouse, A.M., Procter, J.B., Martin, D.M., Clamp, M. & Barton, G.J. Jalview Version 2--a multiple sequence alignment editor and analysis workbench. *Bioinformatics* **25**, 1189-1191 (2009).
62. Claros, M.G. & Vincens, P. Computational method to predict mitochondrially imported proteins and their targeting sequences. *Eur J Biochem* **241**, 779-786 (1996).
63. Ronquist, F. *et al.* MrBayes 3.2: efficient Bayesian phylogenetic inference and model choice across a large model space. *Syst Biol* **61**, 539-542 (2012).
64. Letunic, I. & Bork, P. Interactive tree of life (iTOL) v3: an online tool for the display and annotation of phylogenetic and other trees. *Nucleic Acids Res* **44**, W242-245 (2016).
65. Krivov, G.G., Shapovalov, M.V. & Dunbrack, R.L., Jr. Improved prediction of protein side-chain conformations with SCWRL4. *Proteins* **77**, 778-795 (2009).
66. Xu, D., Jaroszewski, L., Li, Z. & Godzik, A. FFAS-3D: improving fold recognition by including optimized structural features and template re-ranking. *Bioinformatics* **30**, 660-667 (2014).
67. Zhang, L. *et al.* Structural and functional characterization of deep-sea thermophilic bacteriophage GVE2 HNH endonuclease. *Scientific reports* **7**, 42542 (2017).
68. Sebesta, M., Cooper, C.D.O., Ariza, A., Carnie, C.J. & Ahel, D. Structural insights into the function of ZRANB3 in replication stress response. *Nature communications* **8**, 15847 (2017).
69. Arnoux, P. *et al.* Structural and redox plasticity in the heterodimeric periplasmic nitrate reductase. *Nat Struct Biol* **10**, 928-934 (2003).
70. Xia, J. & Wishart, D.S. MetPA: a web-based metabolomics tool for pathway analysis and visualization. *Bioinformatics* **26**, 2342-2344 (2010).

Figure 1

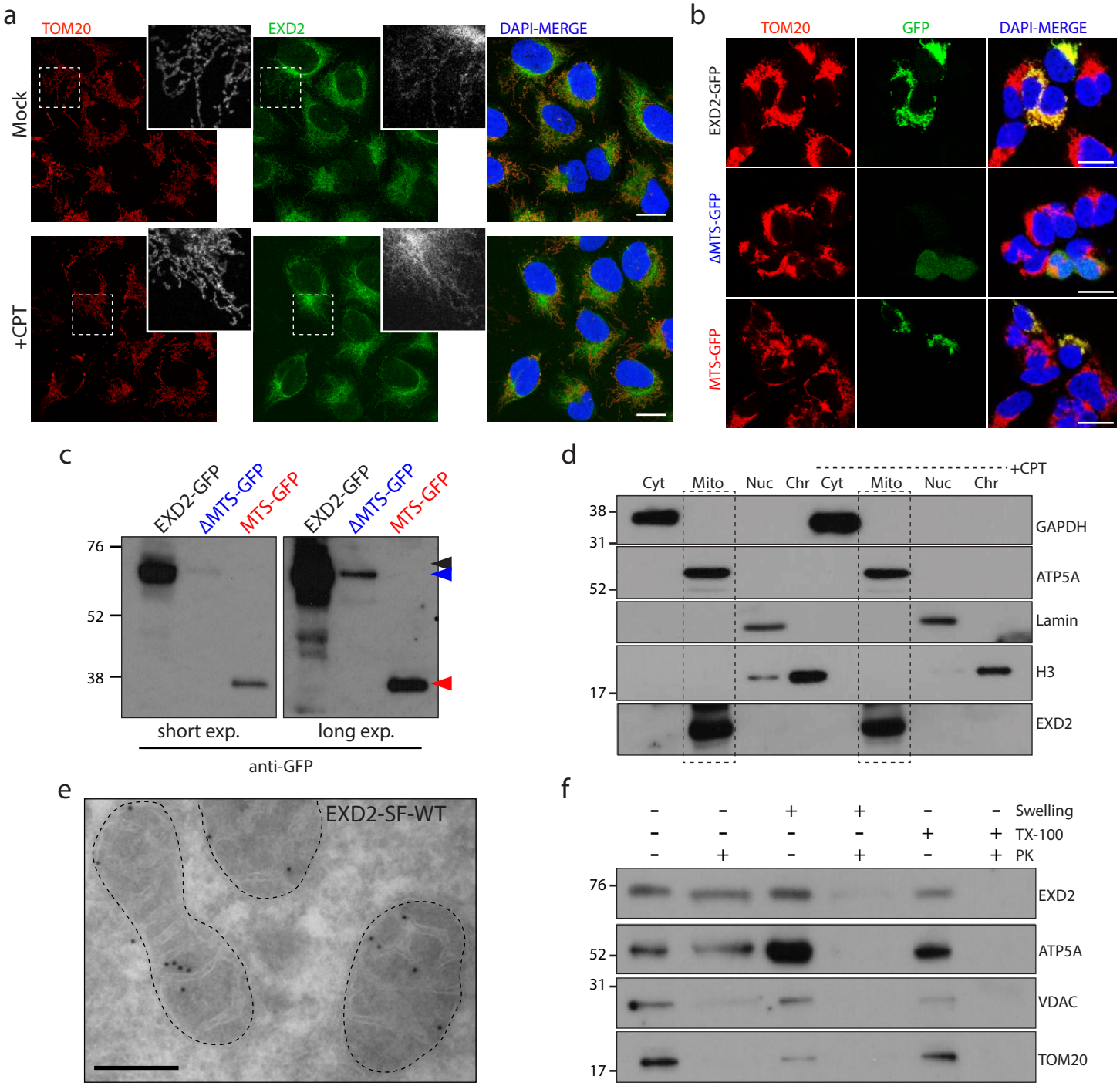
a
TOM20
EXD2
DAPI-MERGE
Mock
+CPT
b
TOM20
GFP
DAPI-MERGE
EXD2-GFP
ΔMTS-GFP
MTS-GFP
c
EXD2-GFP
ΔMTS-GFP
MTS-GFP
EXD2-GFP
ΔMTS-GFP
MTS-GFP
76
52
38
short exp.
long exp.
anti-GFP
d
+CPT
Cyt
Mito
Nuc
Chr
Cyt
Mito
Nuc
Chr
38
31
52
17
GAPDH
ATP5A
Lamin
H3
EXD2
e
EXD2-SF-WT
f
Swelling
TX-100
PK
76
52
31
17
EXD2
ATP5A
VDAC
TOM20

Figure 2

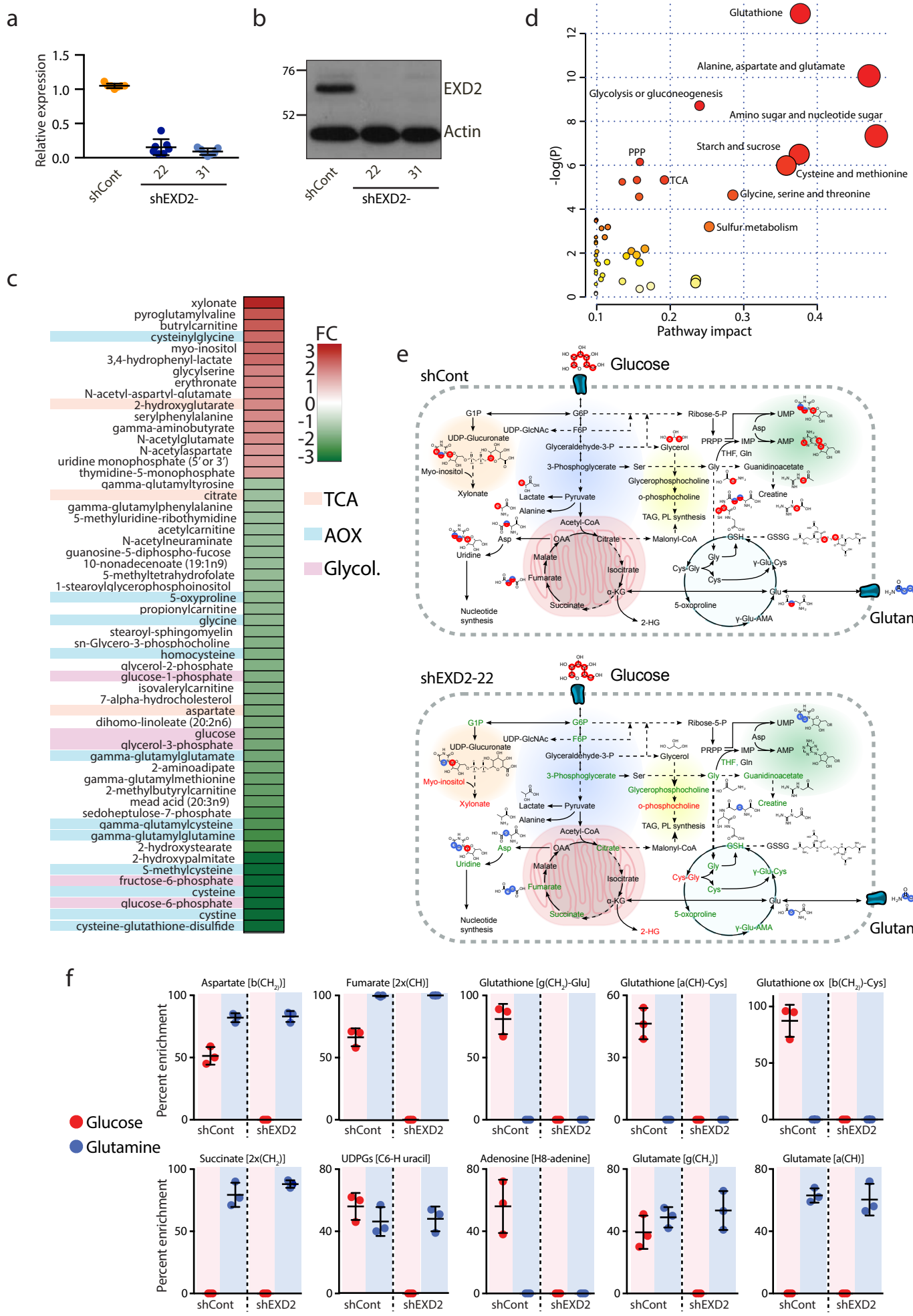
a
Relative expression
1.5
1.0
0.5
0.0
shCont
22
31
shEXD2-
b
76
52
EXD2
Actin
shCont
22
31
shEXD2-
d
Glutathione
Alanine, aspartate and glutamate
Glycolysis or gluconeogenesis
Amino sugar and nucleotide sugar
Starch and sucrose
PPP
TCA
Cysteine and methionine
Glycine, serine and threonine
Sulfur metabolism
-log(P)
Pathway impact
c
xylonate
pyroglutamylvaline
butrylcarnitine
cysteinylglycine
myo-inositol
3,4-hydrophenyl-lactate
glycylserine
erythronate
N-acetyl-aspartyl-glutamate
2-hydroxyglutarate
serylphenylalanine
gamma-aminobutyrate
N-acetylglutamate
N-acetylaspartate
uridine monophosphate (5' or 3')
thymidine-5-monophosphate
gamma-glutamyltyrosine
citrate
gamma-glutamylphenylalanine
5-methyluridine-ribothymidine
acetylcarnitine
N-acetylneuraminate
guanosine-5-diphospho-fucose
10-nonadecenoate (19:1n9)
5-methyltetrahydrofolate
1-stearoylglycerophosphoinositol
5-oxyproline
propionylcarnitine
glycine
stearoyl-sphingomyelin
sn-Glycero-3-phosphocholine
homocysteine
glycerol-2-phosphate
glucose-1-phosphate
isovalerylcarnitine
7-alpha-hydrocholesterol
aspartate
dihomo-linoleate (20:2n6)
glucose
glycerol-3-phosphate
gamma-glutamylglutamate
2-aminoadipate
gamma-glutamylmethionine
2-methylbutyrylcarnitine
mead acid (20:3n9)
sedoheptulose-7-phosphate
gamma-glutamylcysteine
gamma-glutamylglutamine
2-hydroxystearate
2-hydroxypalmitate
S-methylcysteine
fructose-6-phosphate
cysteine
glucose-6-phosphate
cystine
cysteine-glutathione-disulfide
FC
3
2
1
0
-1
-2
-3
TCA
AOX
Glycol.
e
shCont
Glucose
G1P
G6P
Ribose-5-P
UMP
Asp
AMP
IMP
PRPP
THF, Gln
UDP-Glucuronate
UDP-GlcNAc
F6P
Glyceraldehyde-3-P
Glycerol
Myo-inositol
3-Phosphoglycerate
Ser
Gly
Guanidinoacetate
Glycerophosphocholine
Xylonate
Lactate
Pyruvate
o-phosphocholine
Creatine
Alanine
TAG, PL synthesis
Acetyl-CoA
OAA
Citrate
Malonyl-CoA
GSH
GSSG
Asp
Uridine
Malate
Isocitrate
Fumarate
α-KG
Cys-Gly
Gly
γ-Glu-Cys
Cys
Glu
Succinate
5-oxoproline
Nucleotide synthesis
2-HG
γ-Glu-AMA
Glutamine
shEXD2-22
Glucose
Glutamine
f
Glucose
Glutamine
Percent enrichment
Aspartate [b(CH2)]
Fumarate [2x(CH)]
Glutathione [g(CH2)-Glu]
Glutathione [a(CH)-Cys]
Glutathione ox [b(CH2)-Cys]
Succinate [2x(CH2)]
UDPGs [C6-H uracil]
Adenosine [H8-adenine]
Glutamate [g(CH2)]
Glutamate [a(CH)]
shCont
shEXD2

Figure 3

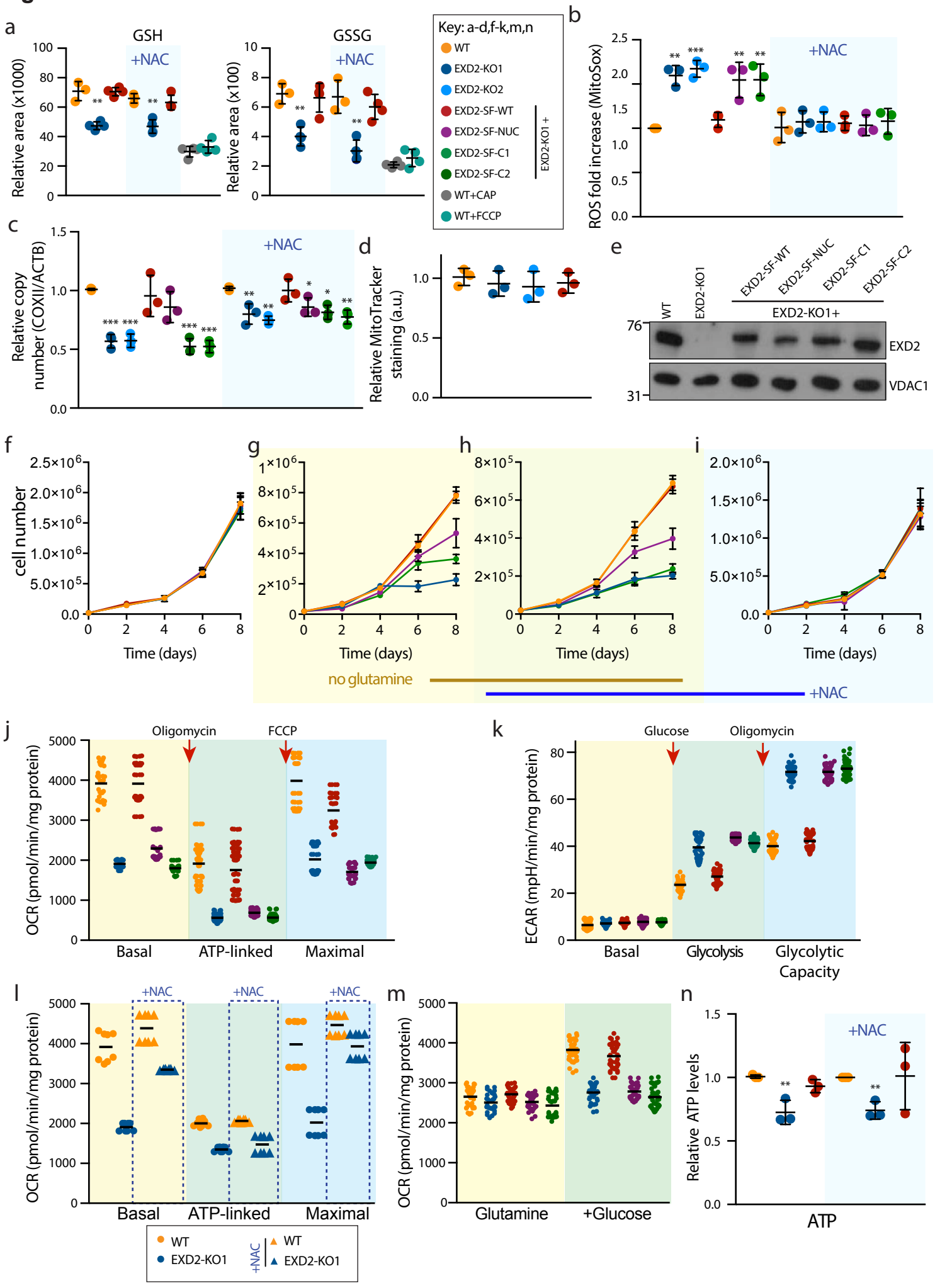
a
GSH
GSSG
+NAC
Relative area (x1000)
Relative area (x100)
Key: a-d,f-k,m,n
WT
EXD2-KO1
EXD2-KO2
EXD2-SF-WT
EXD2-SF-NUC
EXD2-SF-C1
EXD2-SF-C2
WT+CAP
WT+FCCP
EXD2-KO1 +
b
ROS fold increase (MitoSox)
c
Relative copy number (COXII/ACTB)
d
Relative MitoTracker staining (a.u.)
e
WT
EXD2-KO1
EXD2-SF-WT
EXD2-SF-NUC
EXD2-SF-C1
EXD2-SF-C2
EXD2-KO1+
76
31
EXD2
VDAC1
f
cell number
Time (days)
g
h
i
no glutamine
+NAC
j
Oligomycin
FCCP
OCR (pmol/min/mg protein)
Basal
ATP-linked
Maximal
k
Glucose
Oligomycin
ECAR (mpH/min/mg protein)
Basal
Glycolysis
Glycolytic Capacity
l
+NAC
+NAC
+NAC
OCR (pmol/min/mg protein)
Basal
ATP-linked
Maximal
WT
EXD2-KO1
+NAC
WT
EXD2-KO1
m
OCR (pmol/min/mg protein)
Glutamine
+Glucose
n
+NAC
Relative ATP levels
ATP

Figure 4

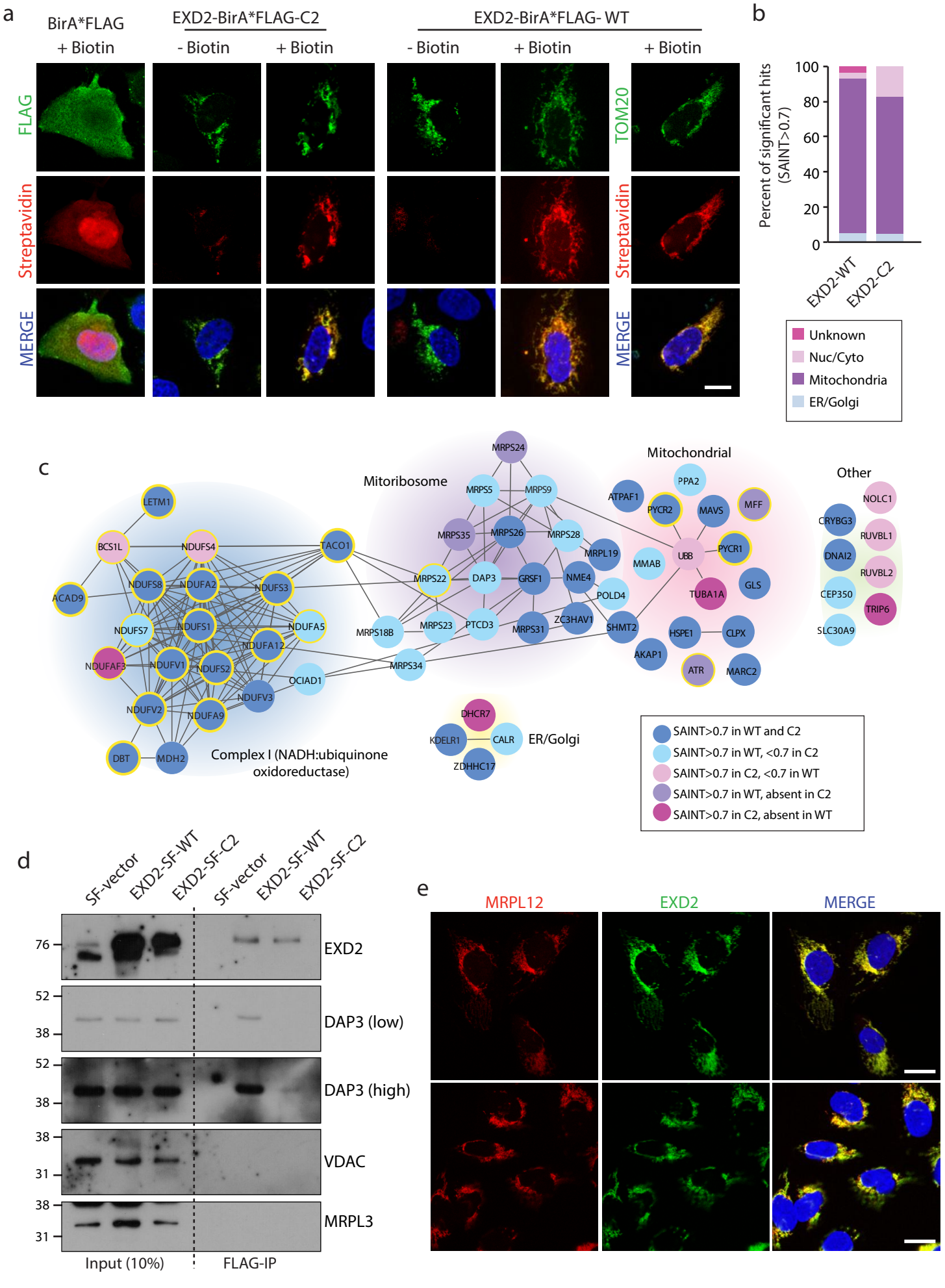
a
BirA*FLAG
+ Biotin
EXD2-BirA*FLAG-C2
- Biotin
+ Biotin
EXD2-BirA*FLAG- WT
- Biotin
+ Biotin
+ Biotin
FLAG
Streptavidin
MERGE
TOM20
Streptavidin
MERGE
b
Percent of significant hits (SAINT>0.7)
100
80
60
40
20
0
EXD2-WT
EXD2-C2
Unknown
Nuc/Cyto
Mitochondria
ER/Golgi
c
Mitoribosome
Mitochondrial
Other
Complex I (NADH:ubiquinone oxidoreductase)
ER/Golgi
SAINT>0.7 in WT and C2
SAINT>0.7 in WT, <0.7 in C2
SAINT>0.7 in C2, <0.7 in WT
SAINT>0.7 in WT, absent in C2
SAINT>0.7 in C2, absent in WT
d
SF-vector
EXD2-SF-WT
EXD2-SF-C2
SF-vector
EXD2-SF-WT
EXD2-SF-C2
76
EXD2
52
38
DAP3 (low)
52
38
DAP3 (high)
38
31
VDAC
38
31
MRPL3
Input (10%)
FLAG-IP
e
MRPL12
EXD2
MERGE

Figure 5

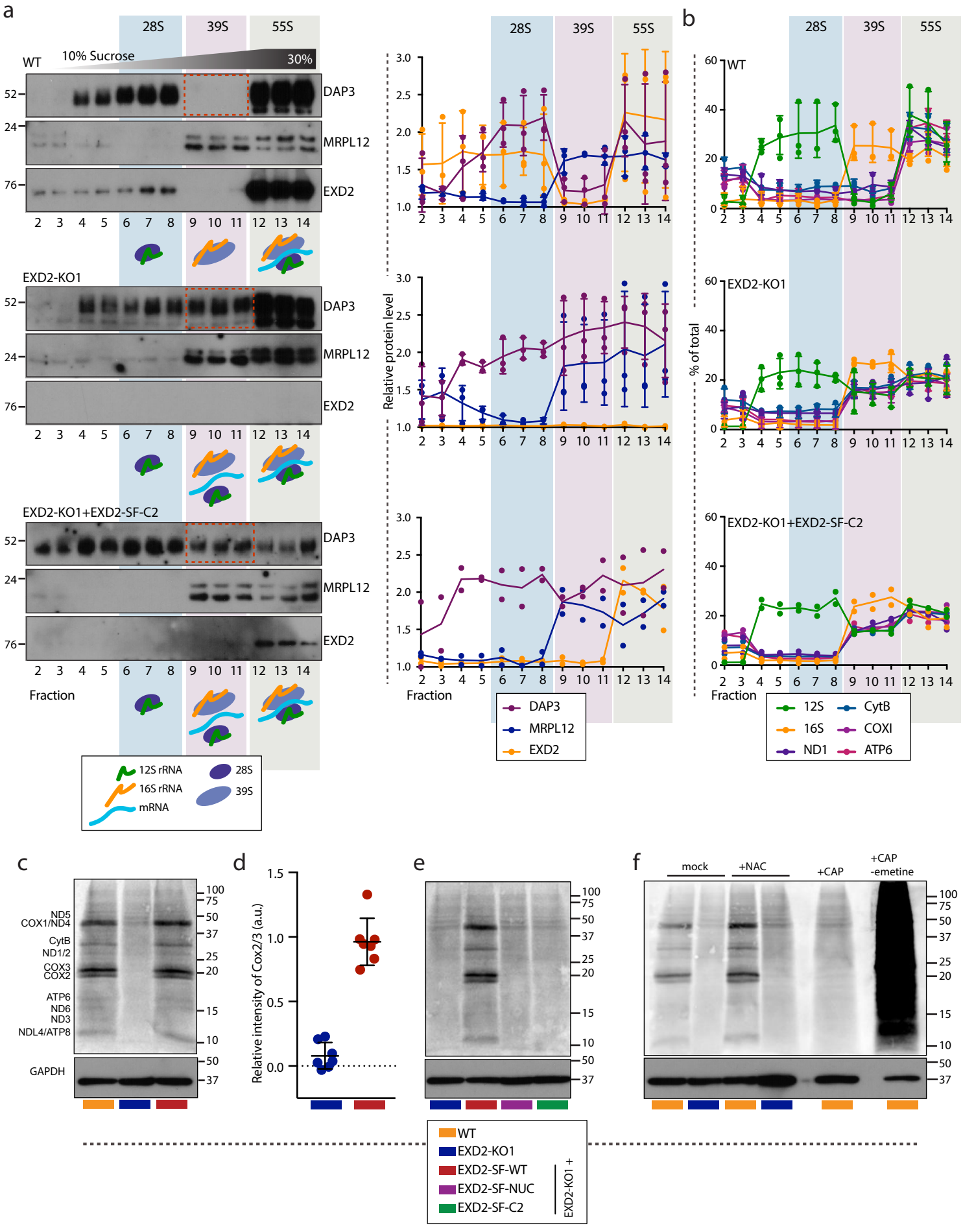
a
28S
39S
55S
WT
10% Sucrose
30%
52
24
76
DAP3
MRPL12
EXD2
2 3 4 5 6 7 8 9 10 11 12 13 14
EXD2-KO1
EXD2-KO1+EXD2-SF-C2
Fraction
12S rRNA
16S rRNA
mRNA
28S
39S
Relative protein level
DAP3
MRPL12
EXD2
b
% of total
12S
16S
ND1
CytB
COXI
ATP6
c
ND5
COX1/ND4
CytB
ND1/2
COX3
COX2
ATP6
ND6
ND3
NDL4/ATP8
GAPDH
d
Relative intensity of Cox2/3 (a.u.)
e
f
mock
+NAC
+CAP
+CAP
-emetine
WT
EXD2-KO1
EXD2-SF-WT
EXD2-SF-NUC
EXD2-SF-C2
EXD2-KO1 +

Figure 6

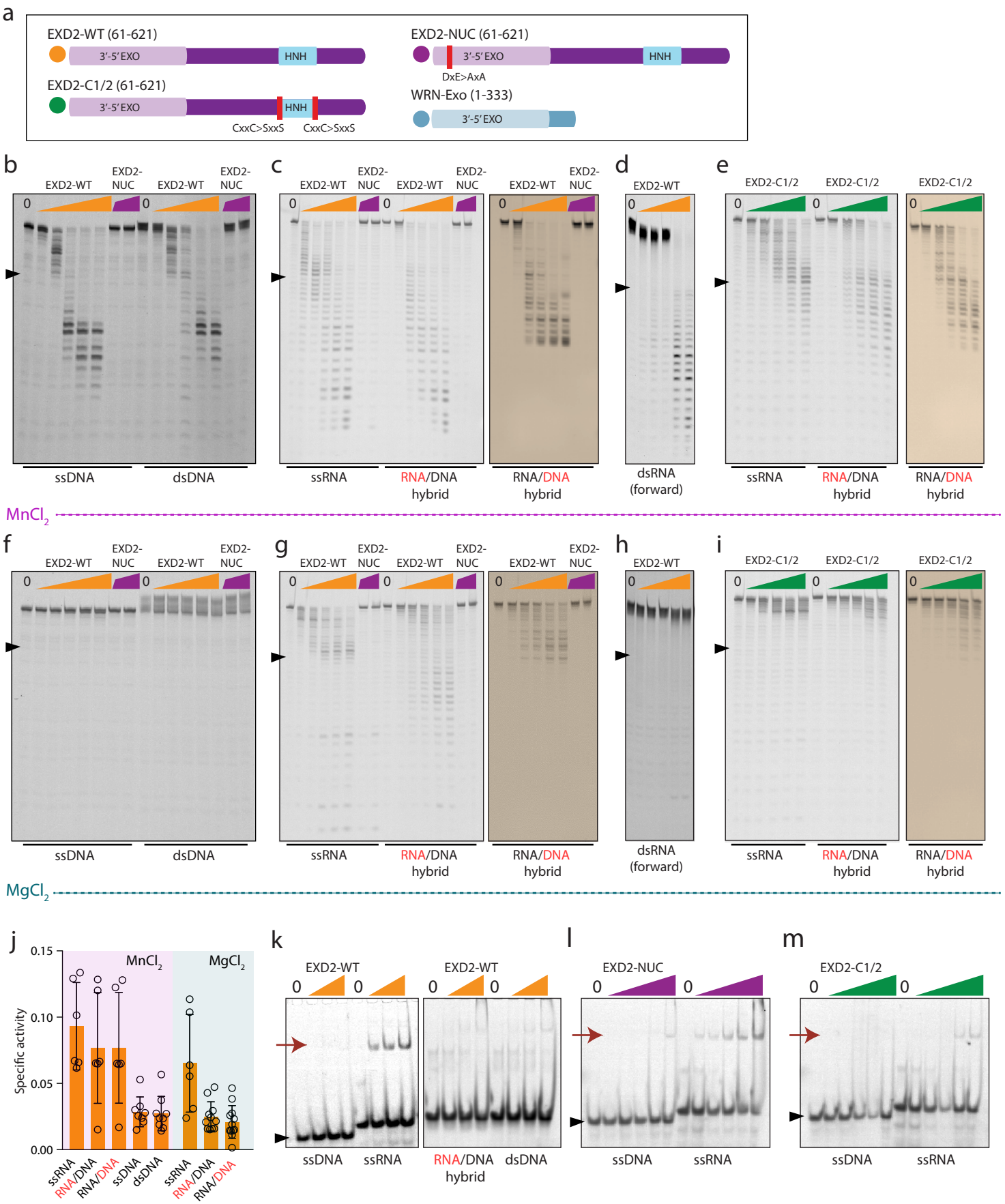
a
EXD2-WT (61-621)
3′-5′ EXO
HNH
EXD2-C1/2 (61-621)
CxxC>SxxS
CxxC>SxxS
EXD2-NUC (61-621)
DxE>AxA
WRN-Exo (1-333)
b
EXD2-WT
EXD2-NUC
ssDNA
dsDNA
c
ssRNA
RNA/DNA hybrid
d
dsRNA (forward)
e
EXD2-C1/2
MnCl2
f
g
h
i
MgCl2
j
Specific activity
0.15
0.10
0.05
0.00
k
l
m

Figure 7

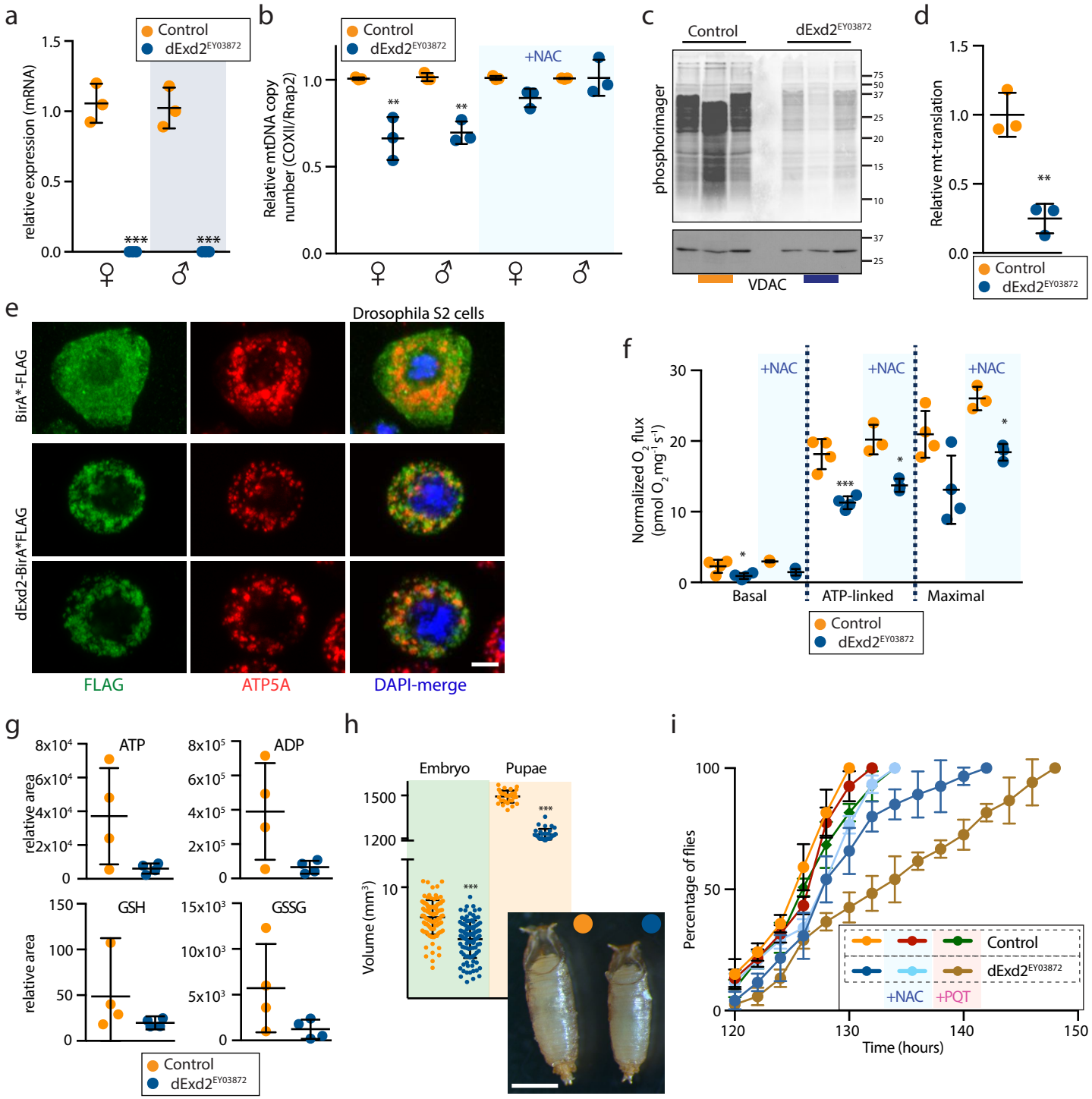
a
Control
dExd2EY03872
relative expression (mRNA)
1.5
1.0
0.5
0.0
***
***
♀
♂
b
Control
dExd2EY03872
+NAC
Relative mtDNA copy number (COXII/Rnap2)
1.0
0.5
0.0
**
**
♀
♂
♀
♂
c
Control
dExd2EY03872
phosphorimager
75
50
37
25
20
15
10
37
25
VDAC
d
Relative mt-translation
1.5
1.0
0.5
0.0
**
Control
dExd2EY03872
e
Drosophila S2 cells
BirA*-FLAG
dExd2-BirA*FLAG
FLAG
ATP5A
DAPI-merge
f
Normalized O2 flux (pmol O2 mg-1 s-1)
30
20
10
0
+NAC
+NAC
+NAC
*
***
*
*
Basal
ATP-linked
Maximal
Control
dExd2EY03872
g
ATP
ADP
GSH
GSSG
relative area
8x10⁴
6x10⁴
4x10⁴
2x10⁴
0
8x10⁵
6x10⁵
4x10⁵
2x10⁵
0
150
100
50
0
15x10³
10x10³
5x10³
0
Control
dExd2EY03872
h
Embryo
Pupae
Volume (mm³)
1500
1200
10
***
***
i
Percentage of flies
100
50
0
120
130
140
150
Time (hours)
Control
dExd2EY03872
+NAC
+PQT

Figure 8

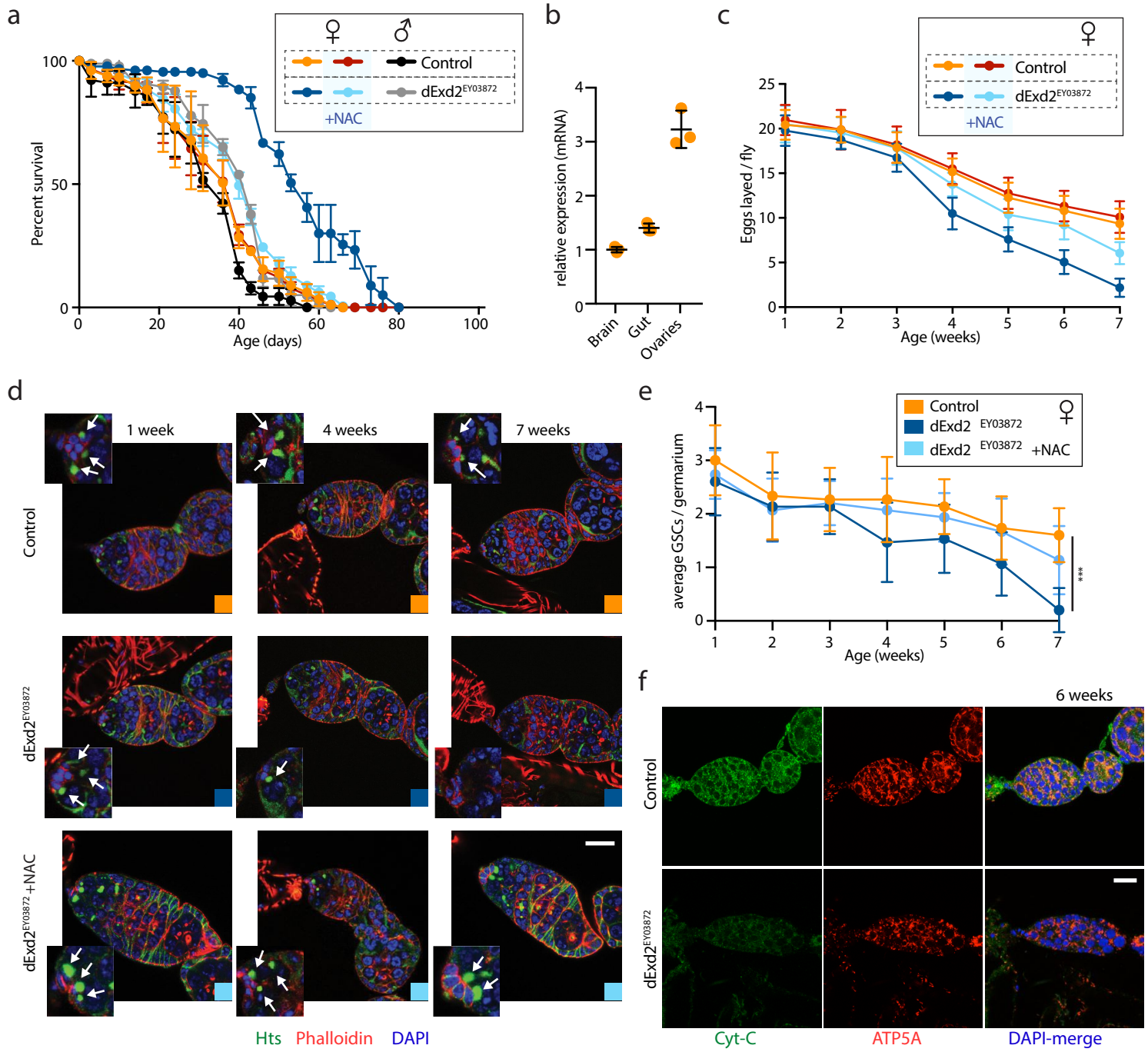
a
♀
♂
Control
dExd2EY03872
+NAC
Percent survival
Age (days)
b
relative expression (mRNA)
Brain
Gut
Ovaries
c
♀
Control
dExd2EY03872
+NAC
Eggs layed / fly
Age (weeks)
d
1 week
4 weeks
7 weeks
Control
dExd2EY03872
dExd2EY03872+NAC
Hts
Phalloidin
DAPI
e
Control
dExd2 EY03872
dExd2 EY03872 +NAC
♀
average GSCs / germarium
***
Age (weeks)
f
6 weeks
Control
dExd2EY03872
Cyt-C
ATP5A
DAPI-merge

Supplementary Figure 1

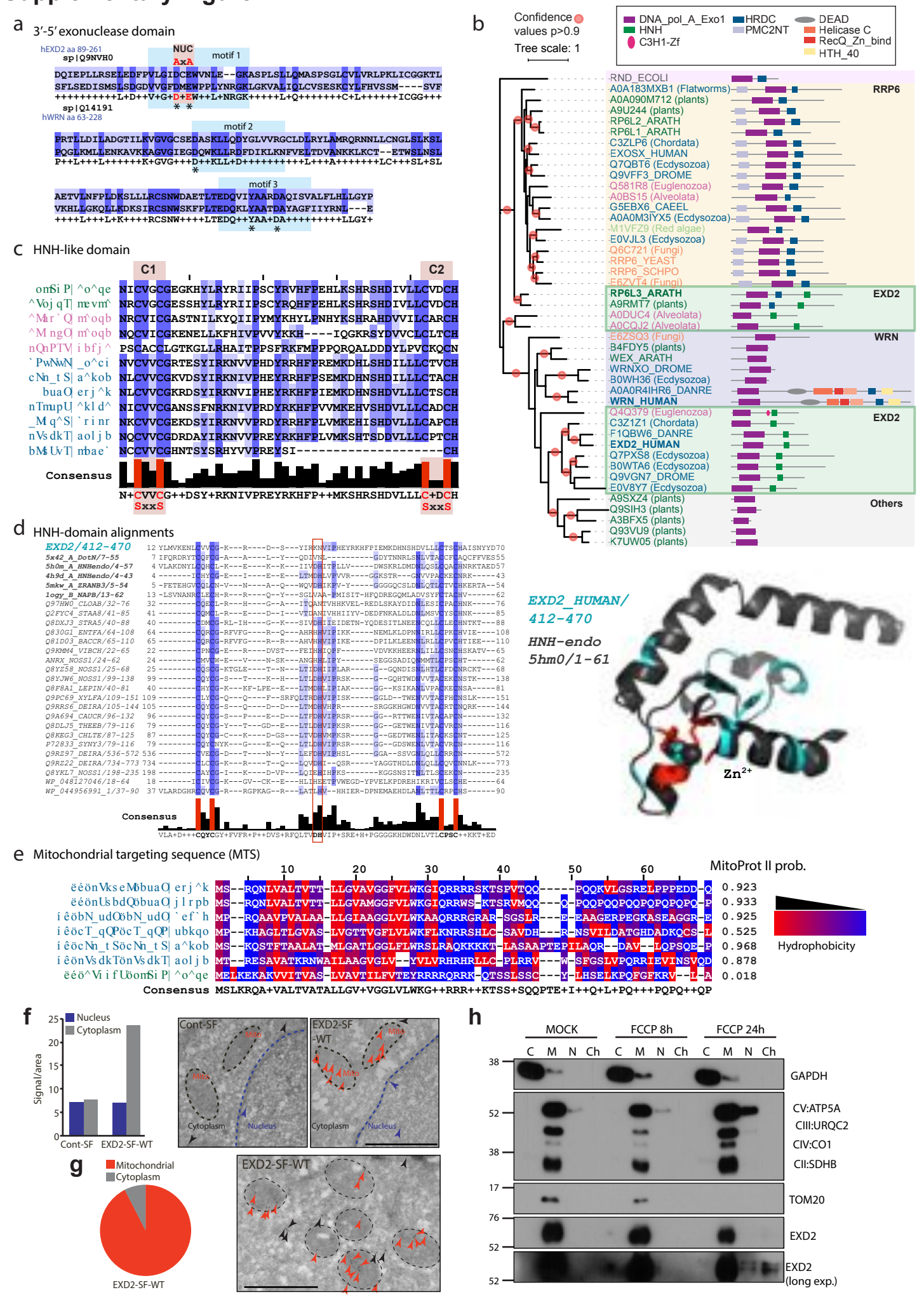

EXD2_HUMAN/ 412-470

HNH-endo 5hm0/1-61

Zn^{2+}

Supplementary Figure 2

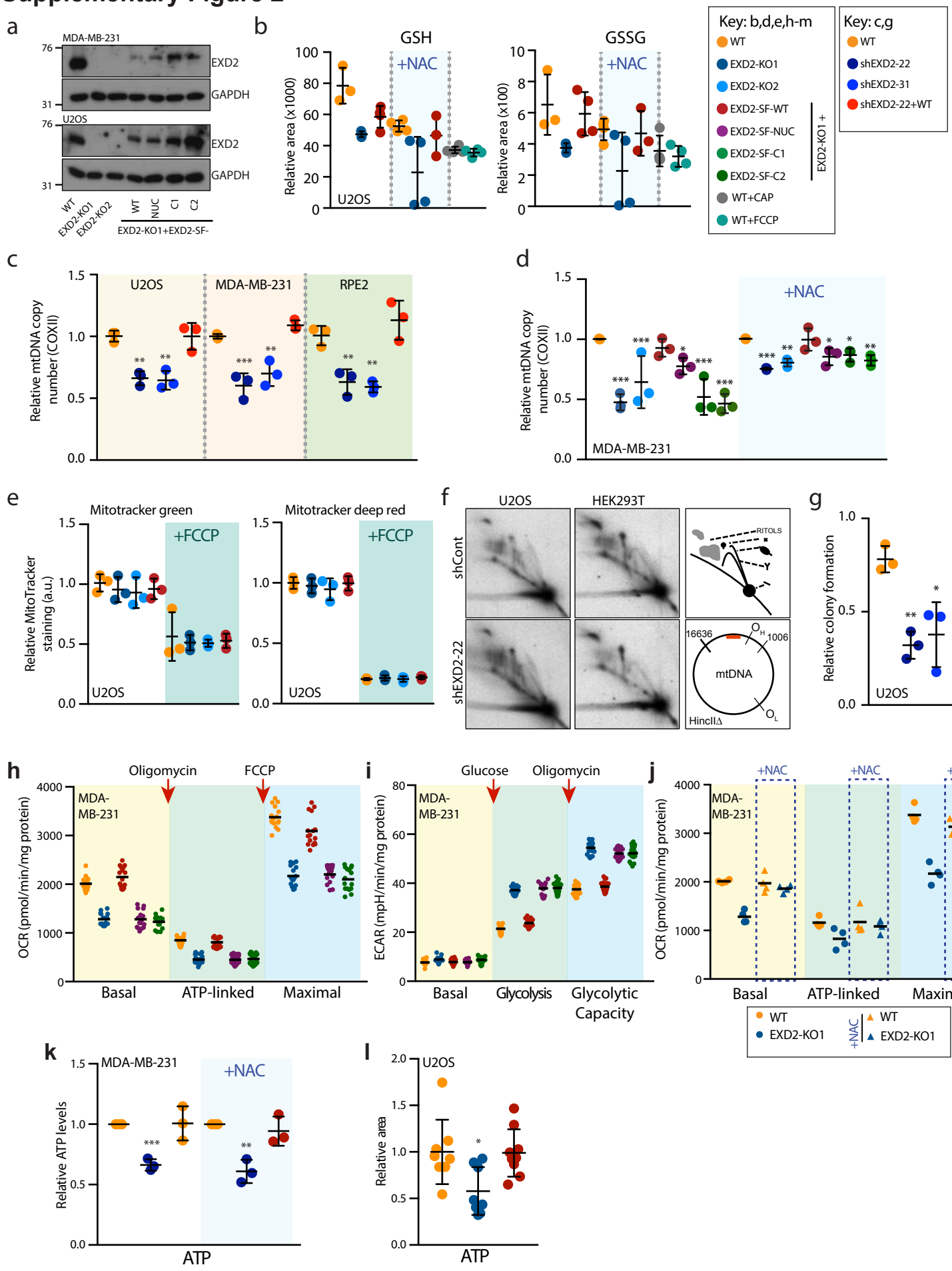

Supplementary Figure 3

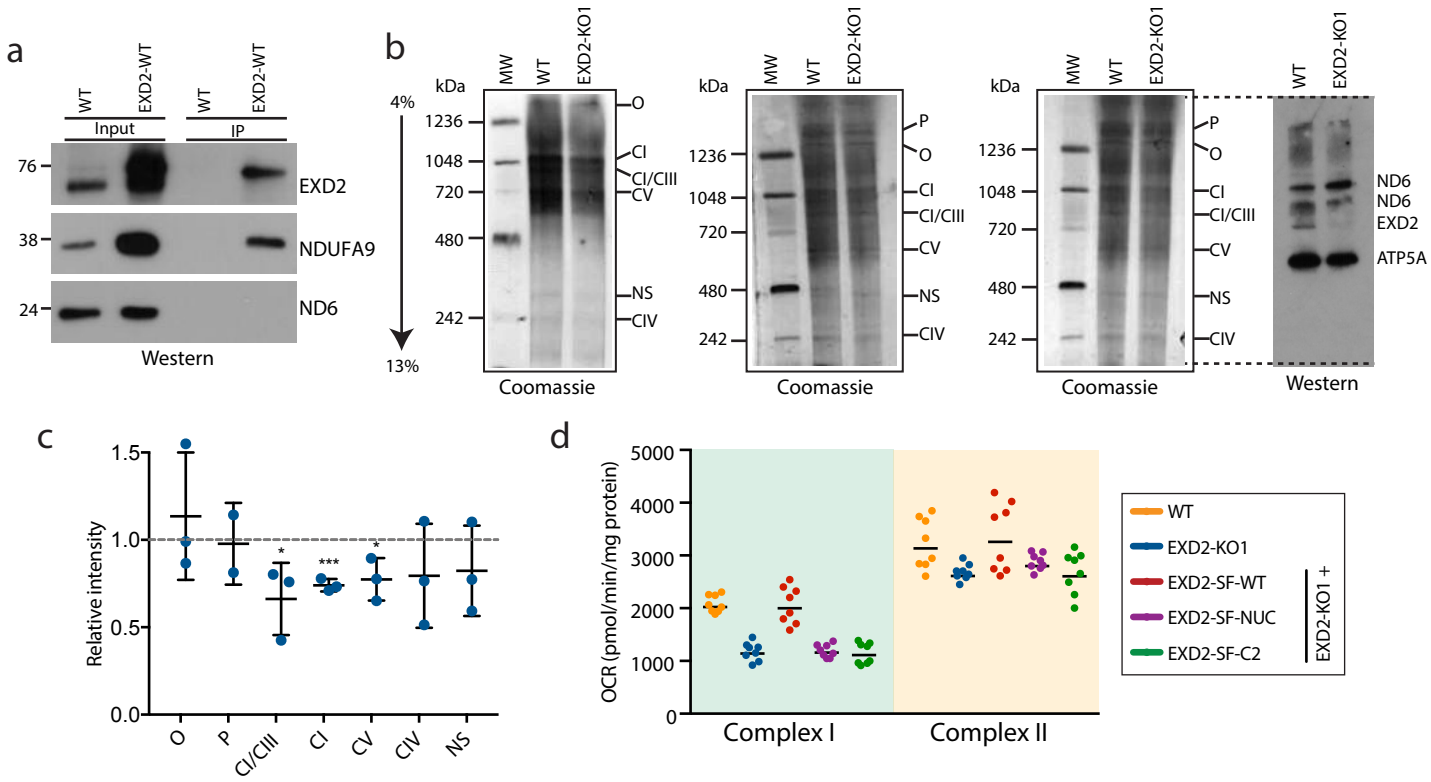

Supplementary Figure 4

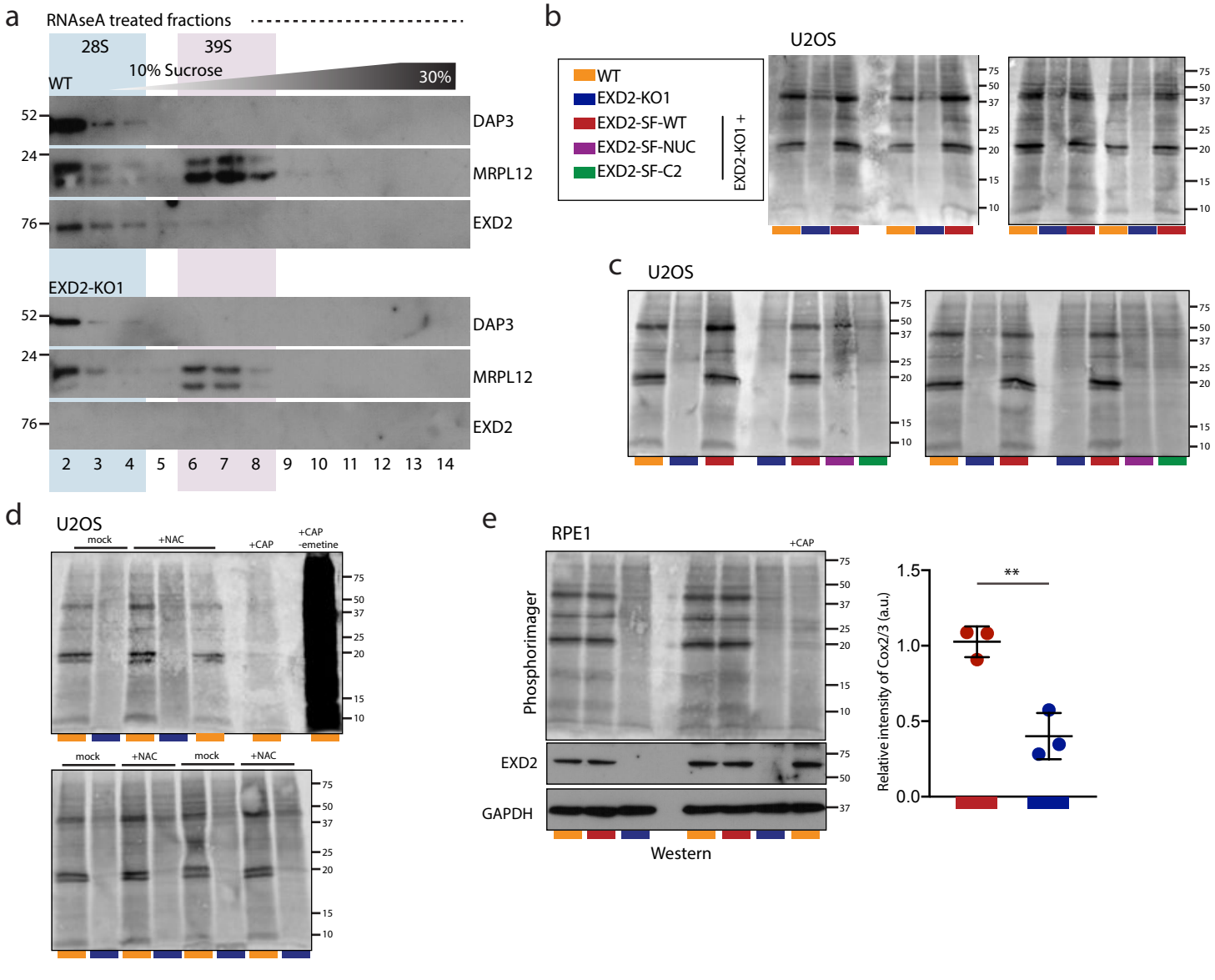

Supplementary Figure 5

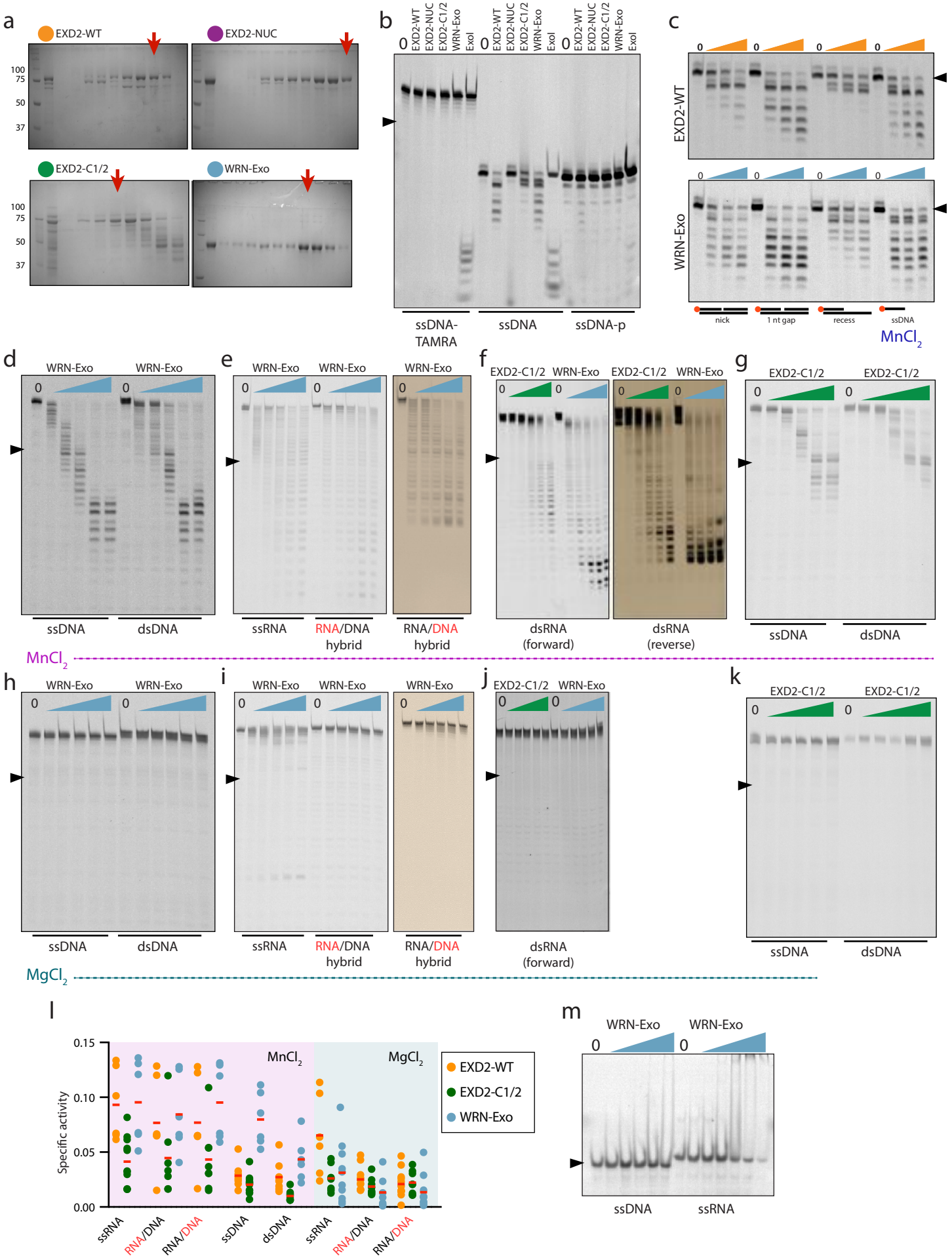

Supplementary Figure 6

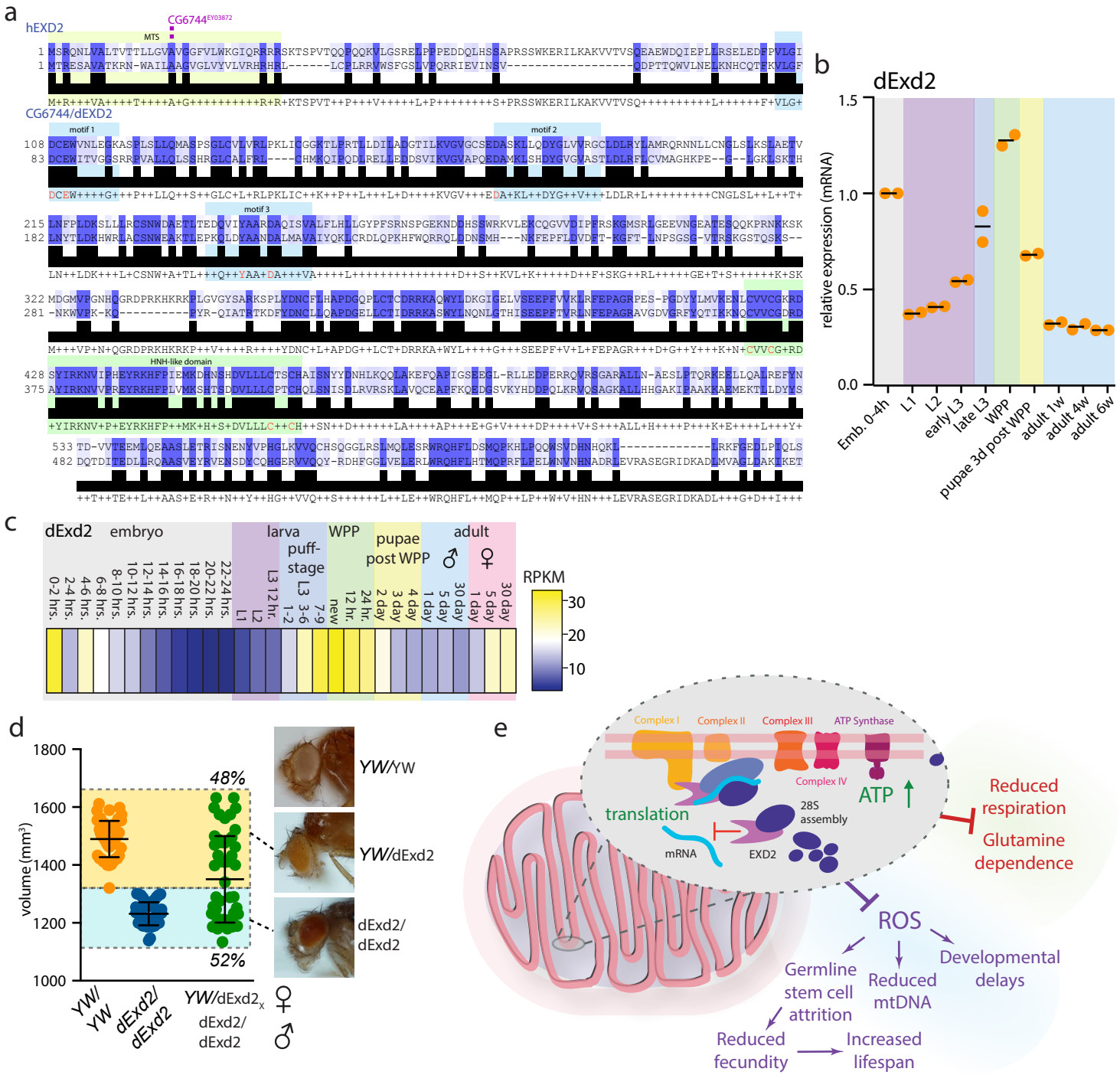

Supplementary Figure 7

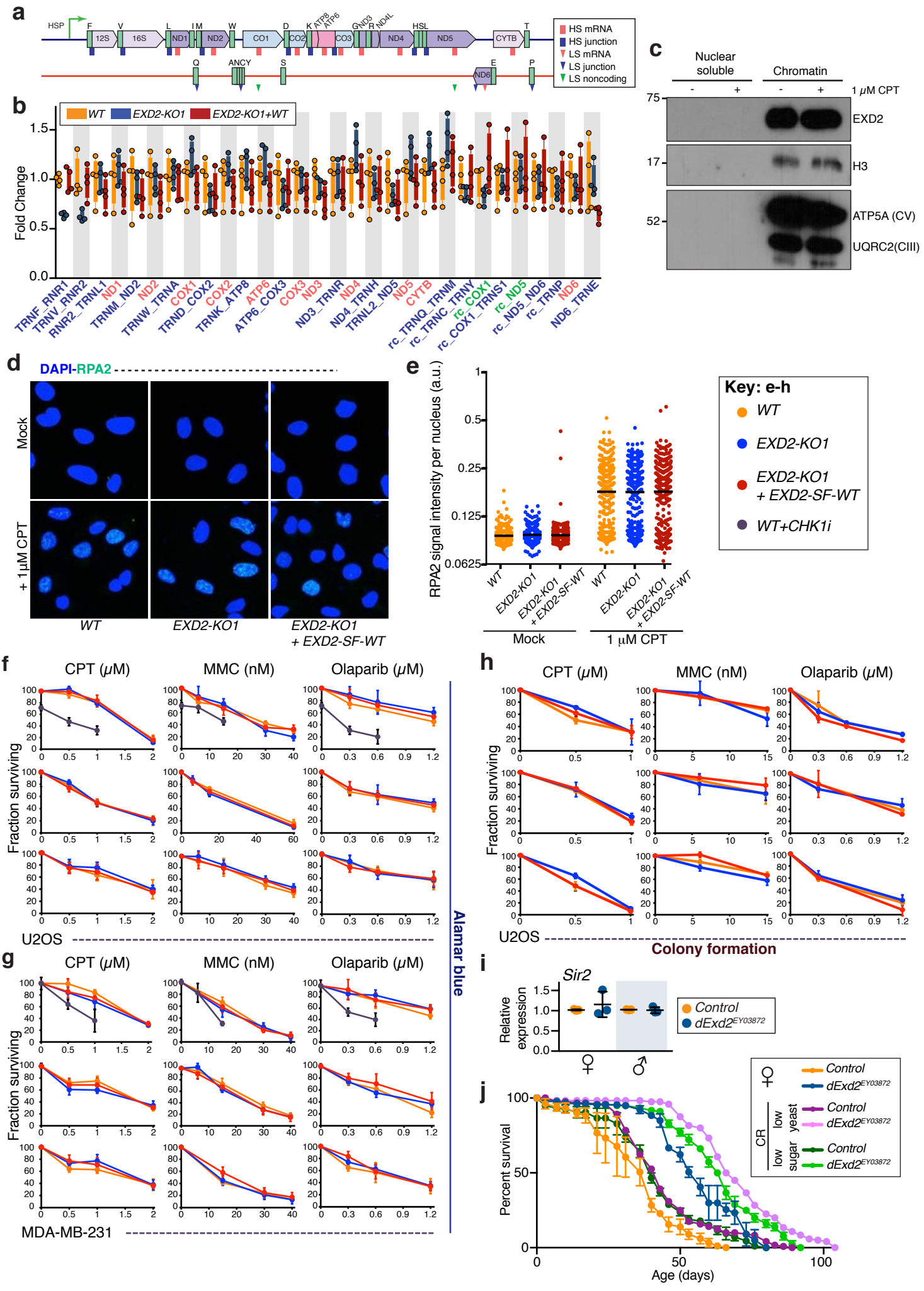

Supplementary Figure 8

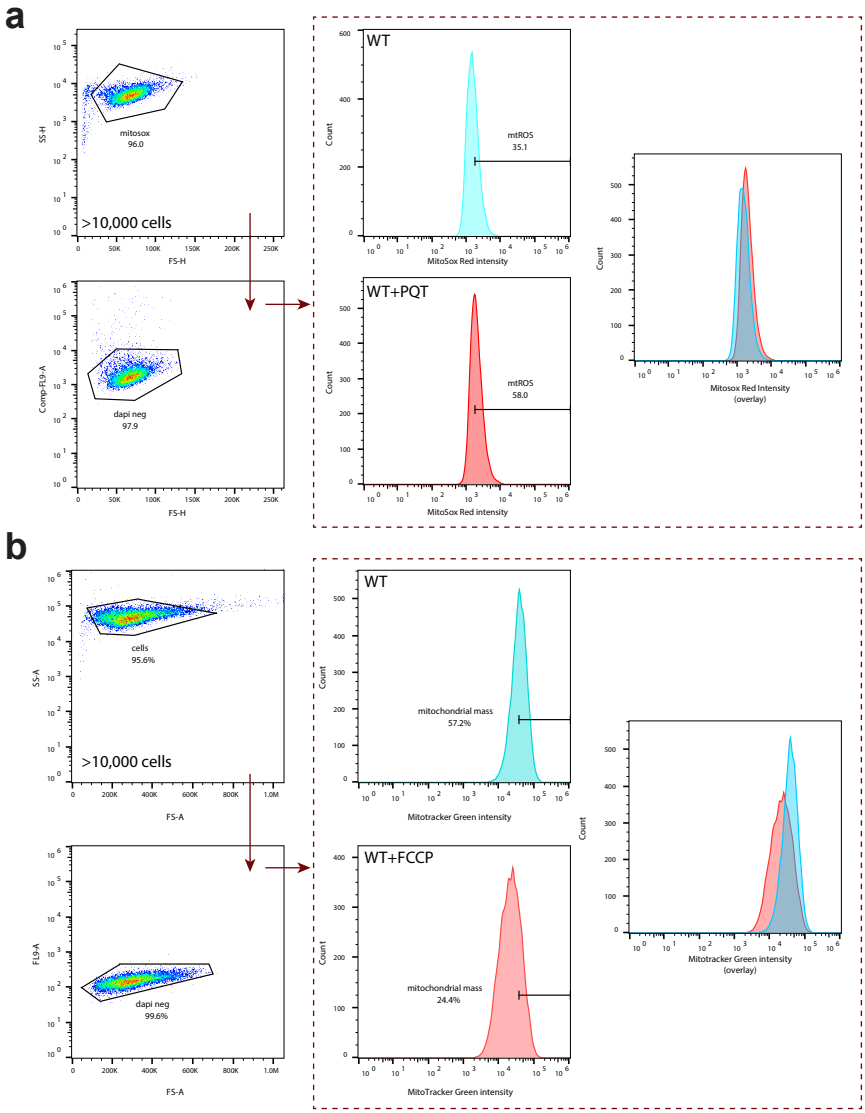

Supplementary Figure 9

Figure 1c

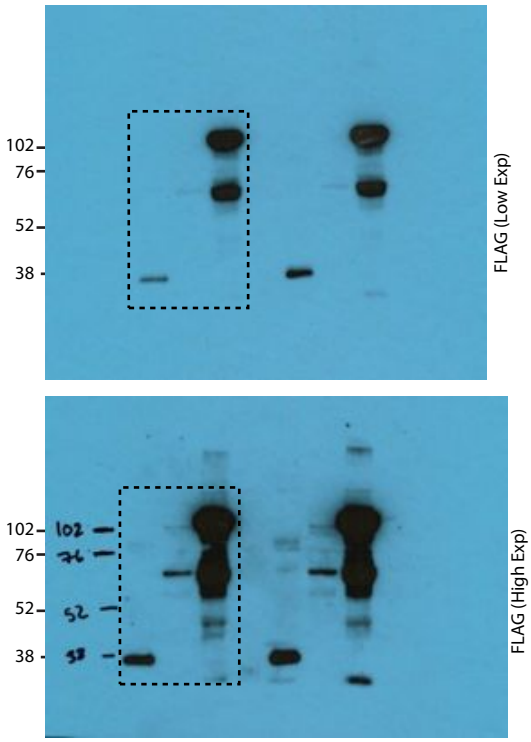

Figure 1f

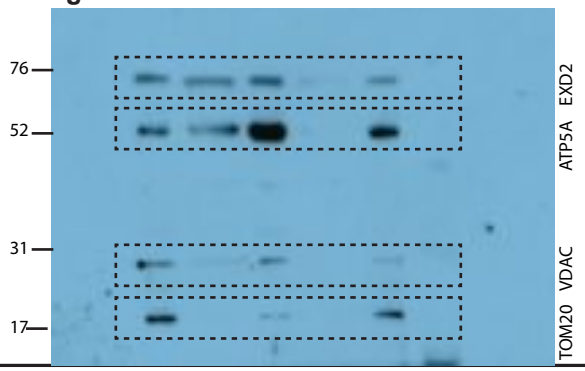

Figure 2b

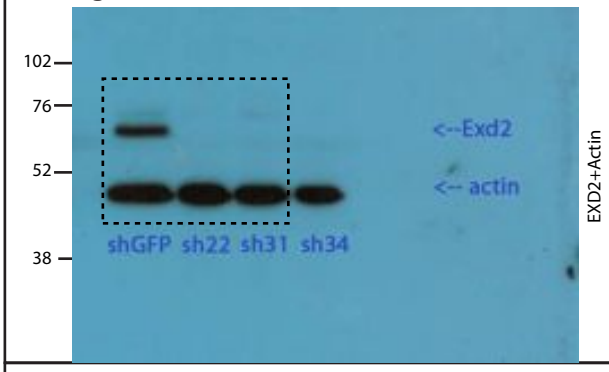

Figure 3e

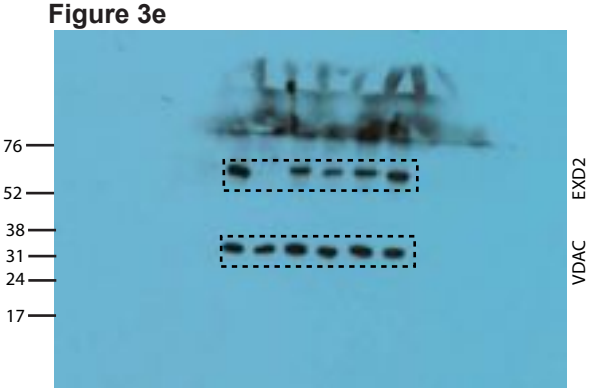

Figure 1d

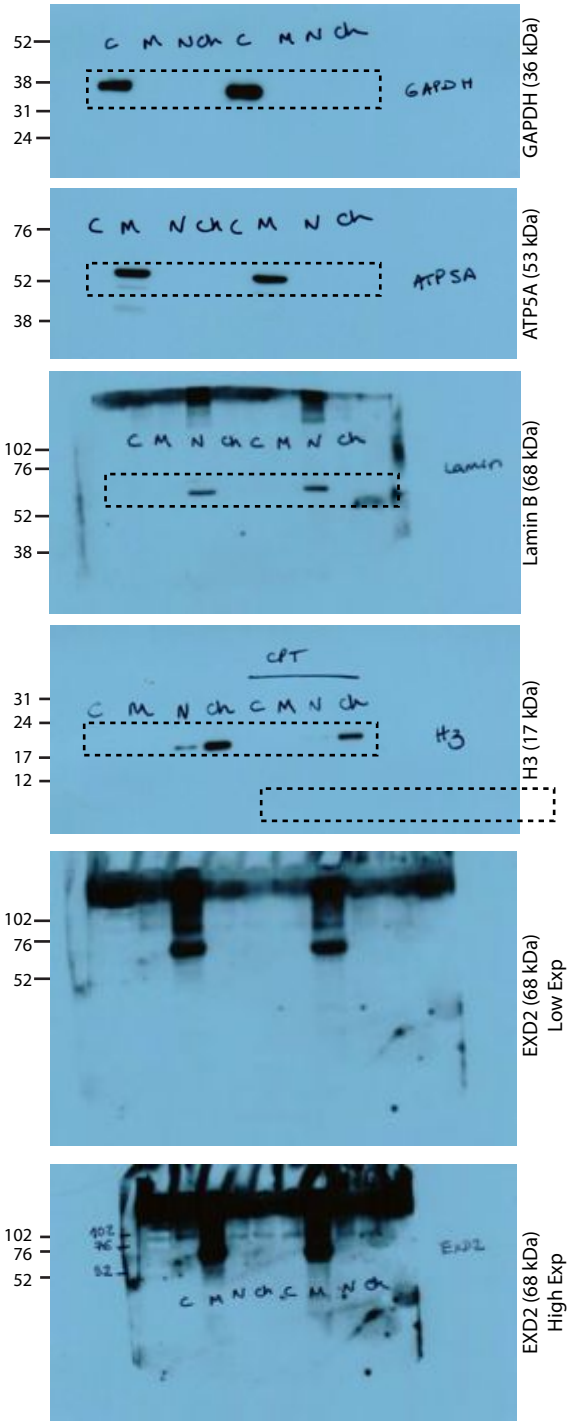

Supplementary Figure 9 (continued)

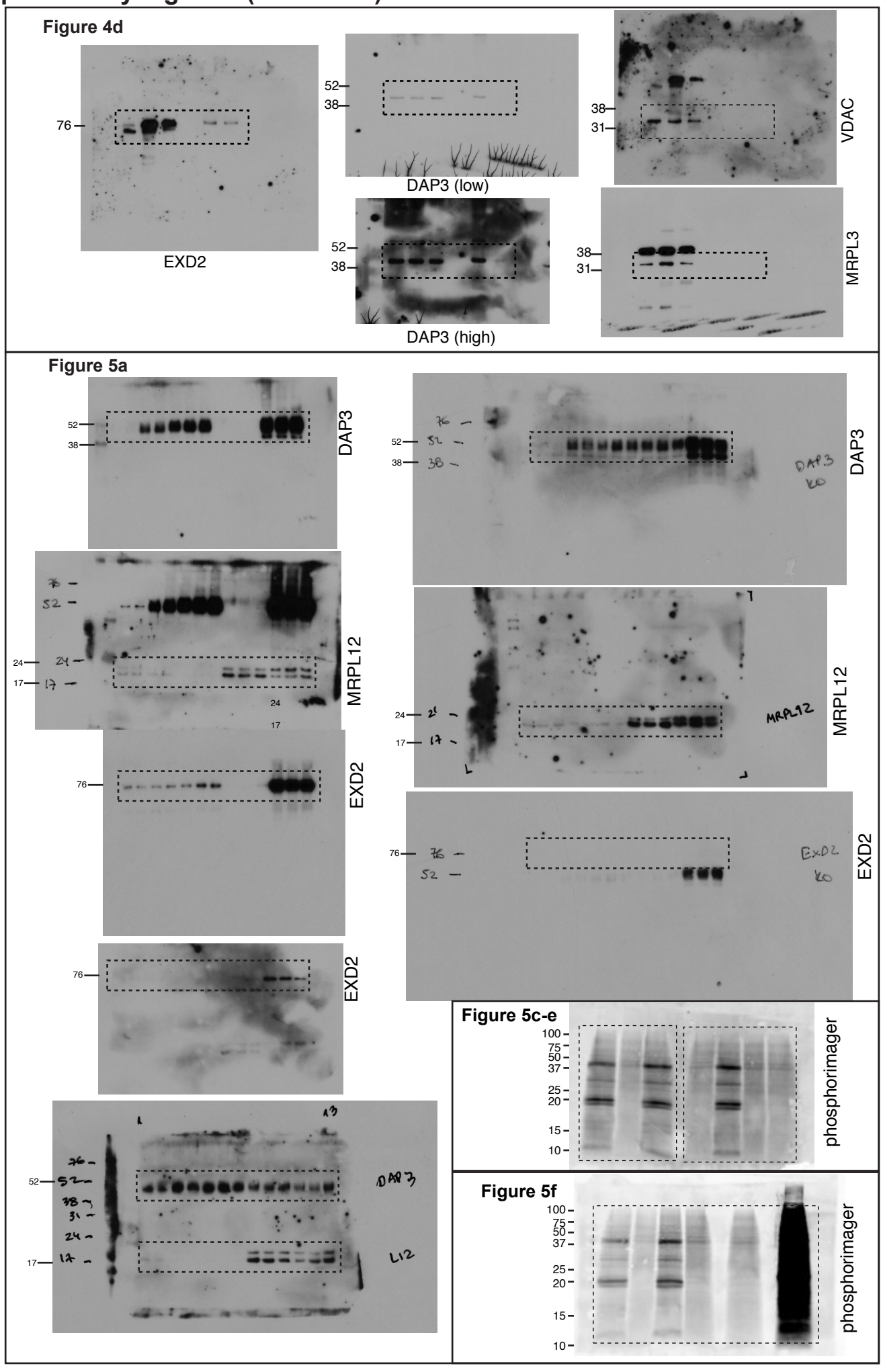

Supplementary Figure 9 (continued)

Figure 5c, e, f

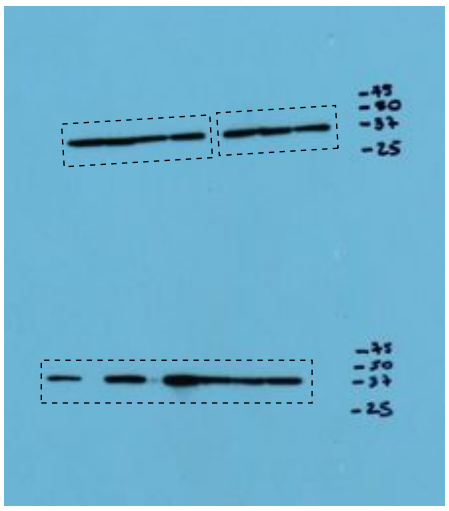

Figure 7c

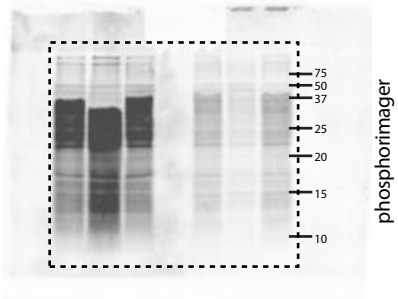

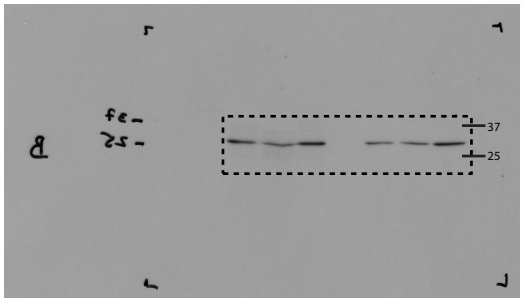

Figure 6b-i

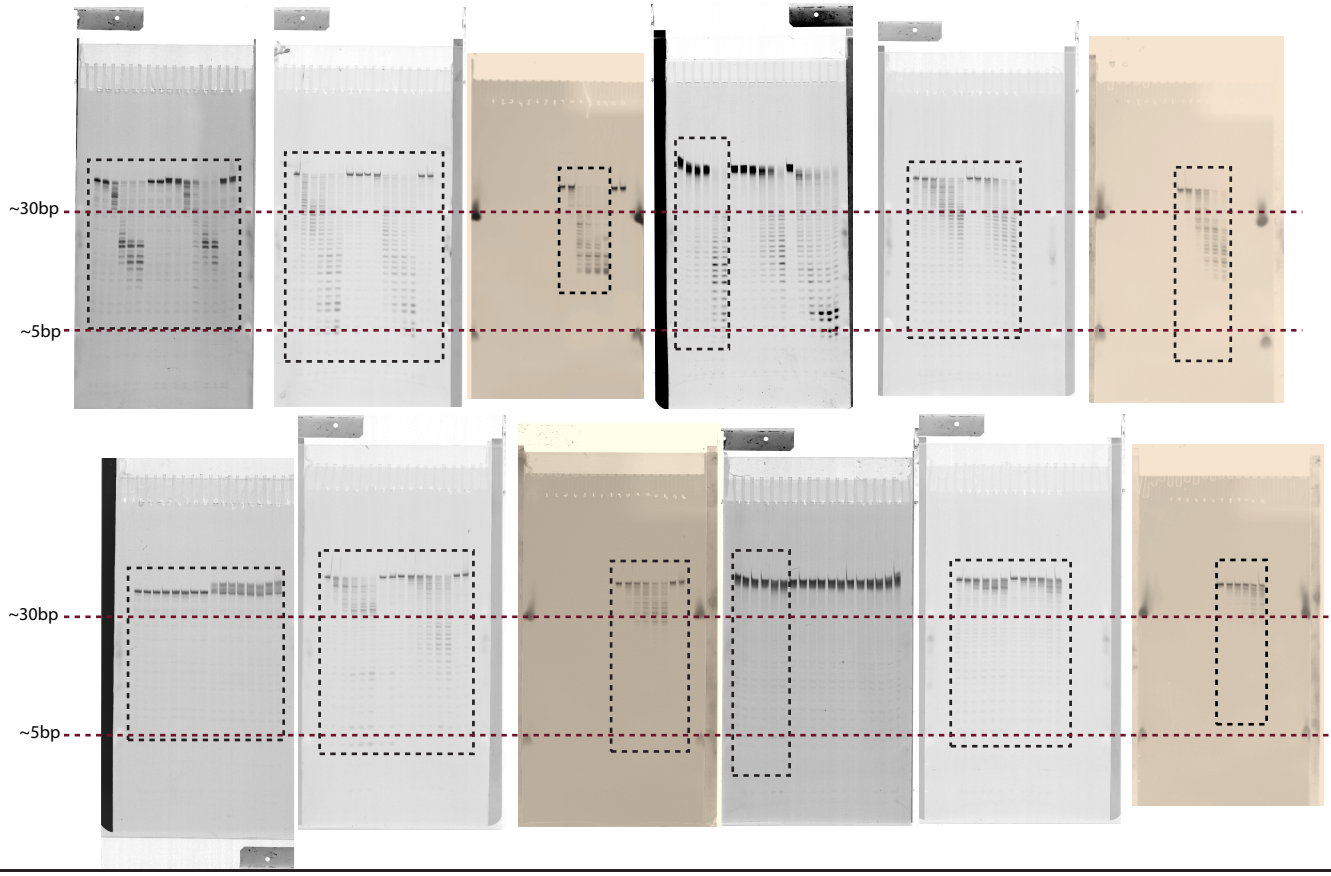

Figure 6k-m

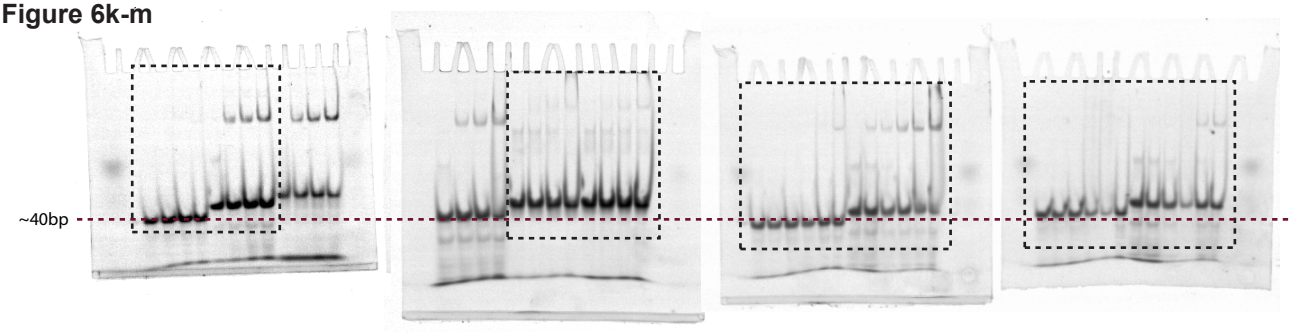

Supplementary Figure 9 (continued)

Supplementary Figure 1h

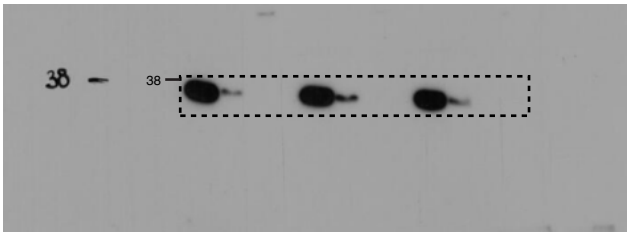

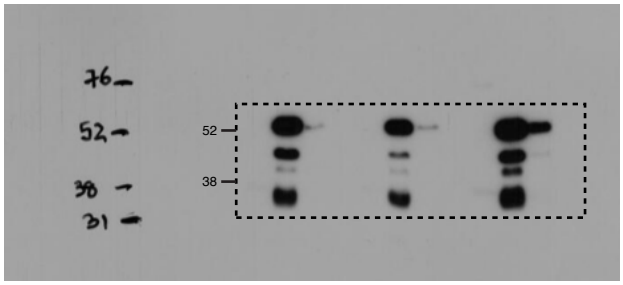

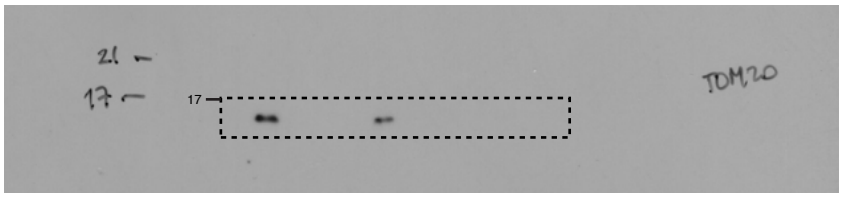

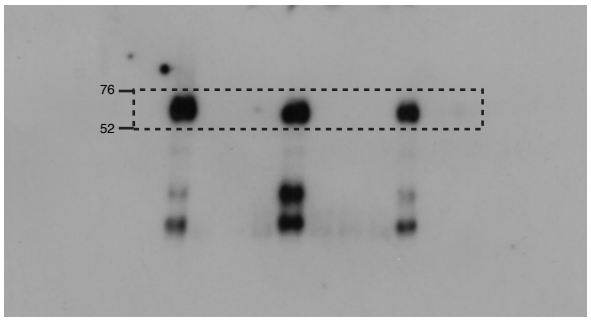

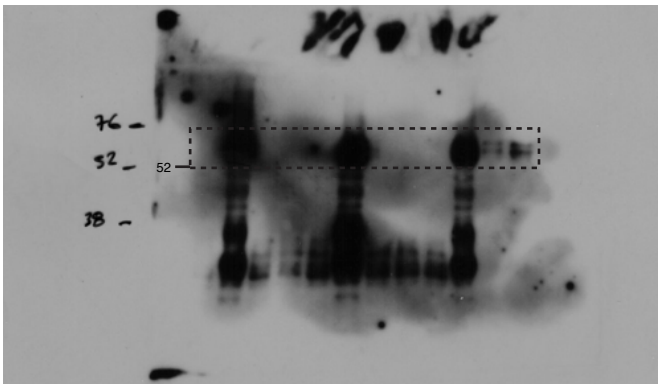

Supplementary Fig. 2a

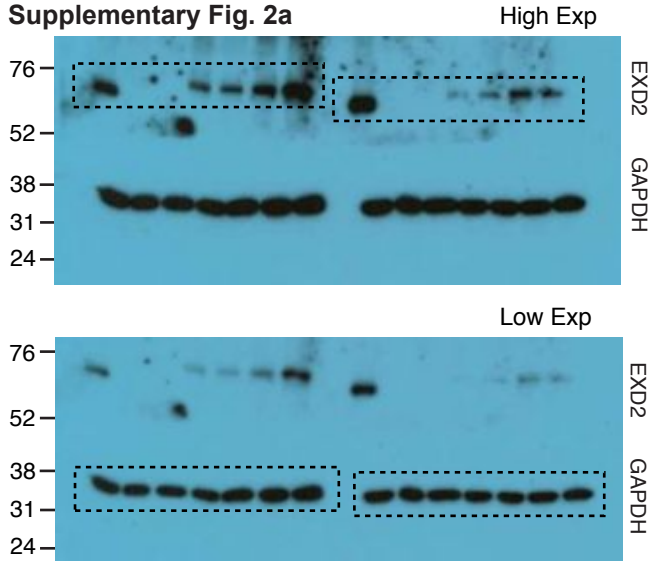

Supplementary Figure 2f

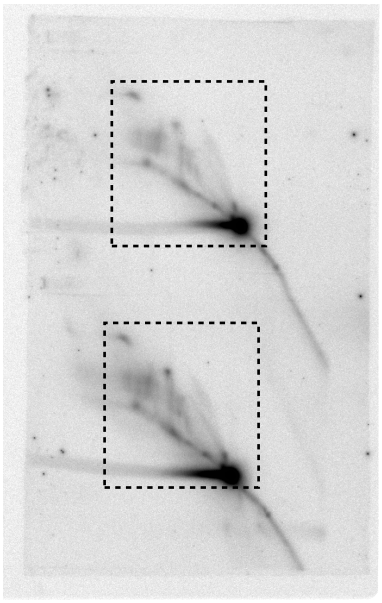

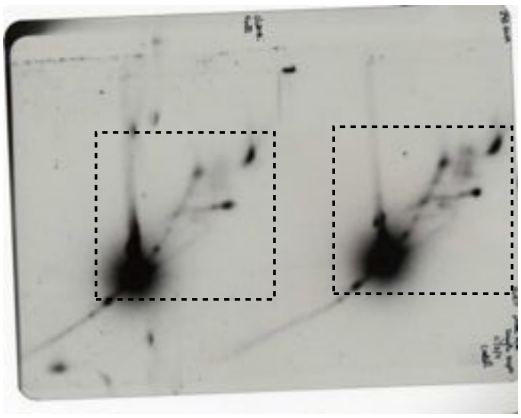

Supplementary Figure 9 (continued)

Supplementary Figure 3a

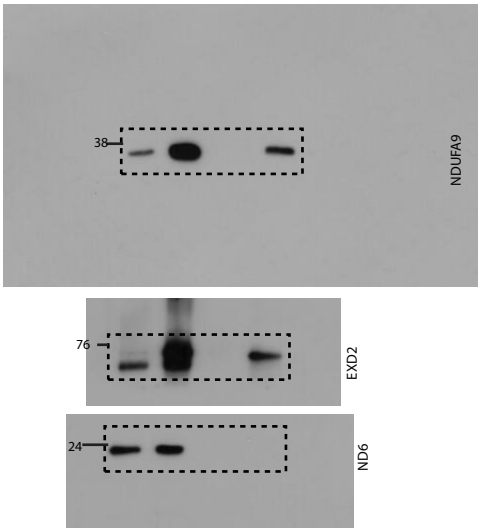

Supplementary Figure 4a

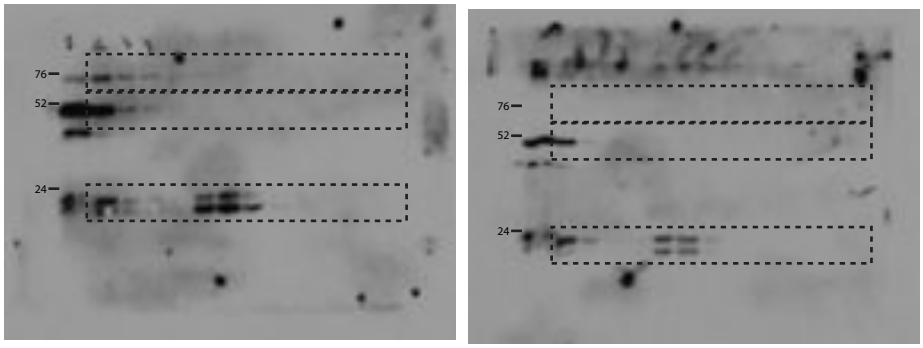

Supplementary Fig. 4b

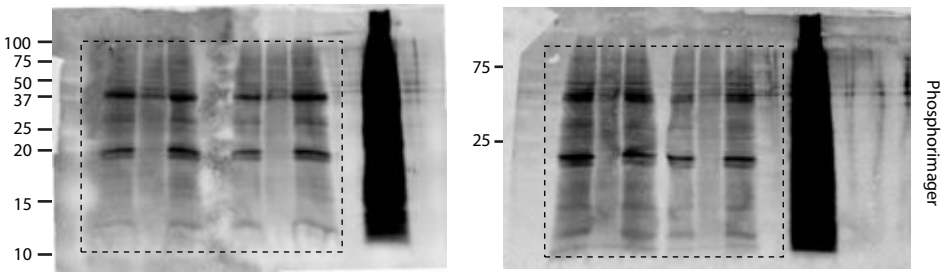

Supplementary Fig. 4c

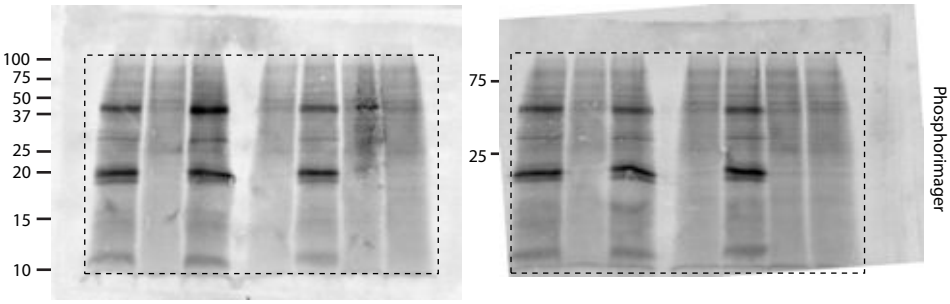

Supplementary Fig. 4d

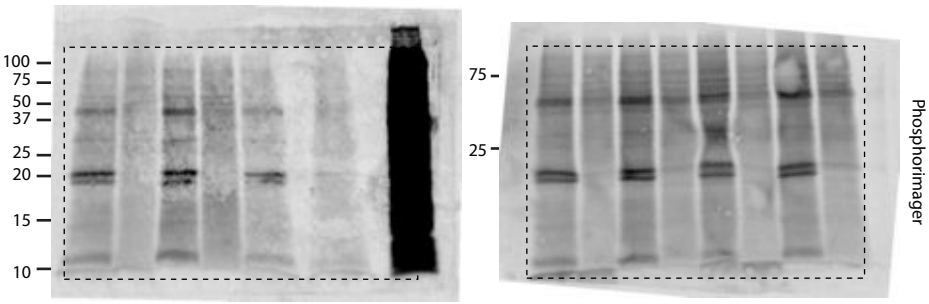

Supplementary Fig. 4e

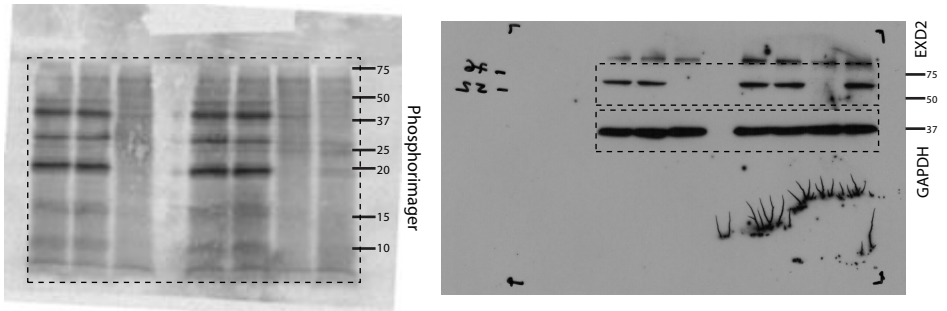

Supplementary Figure 9 (continued)

Supplementary Figure 5a

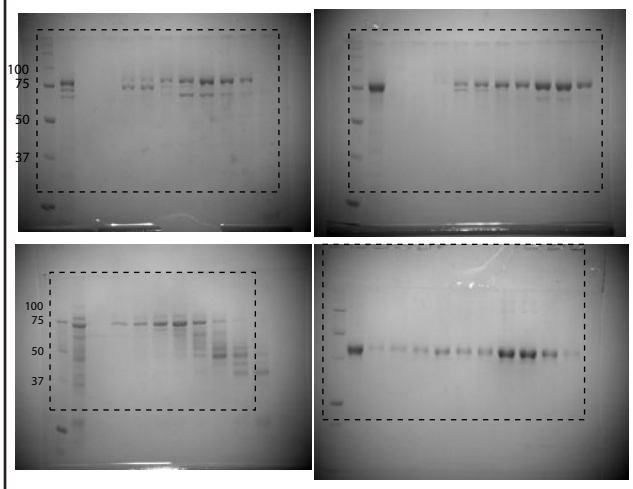

Supplementary Figure 5b-c

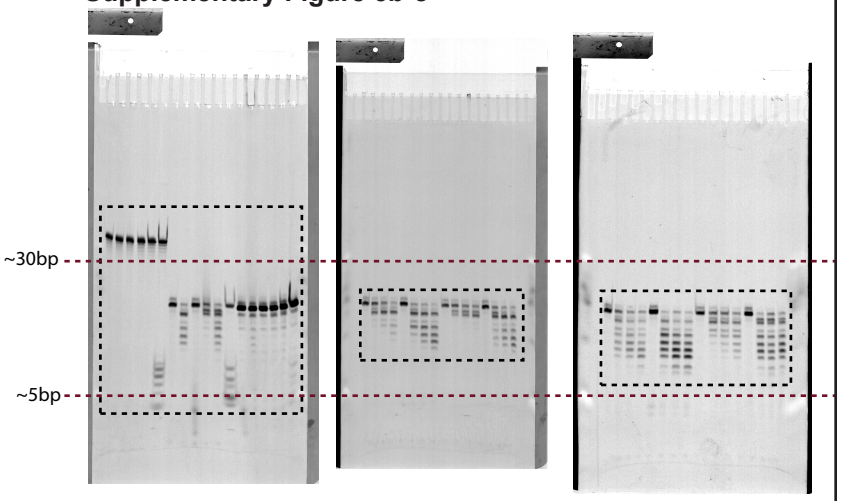

Supplementary Figure 5d-g

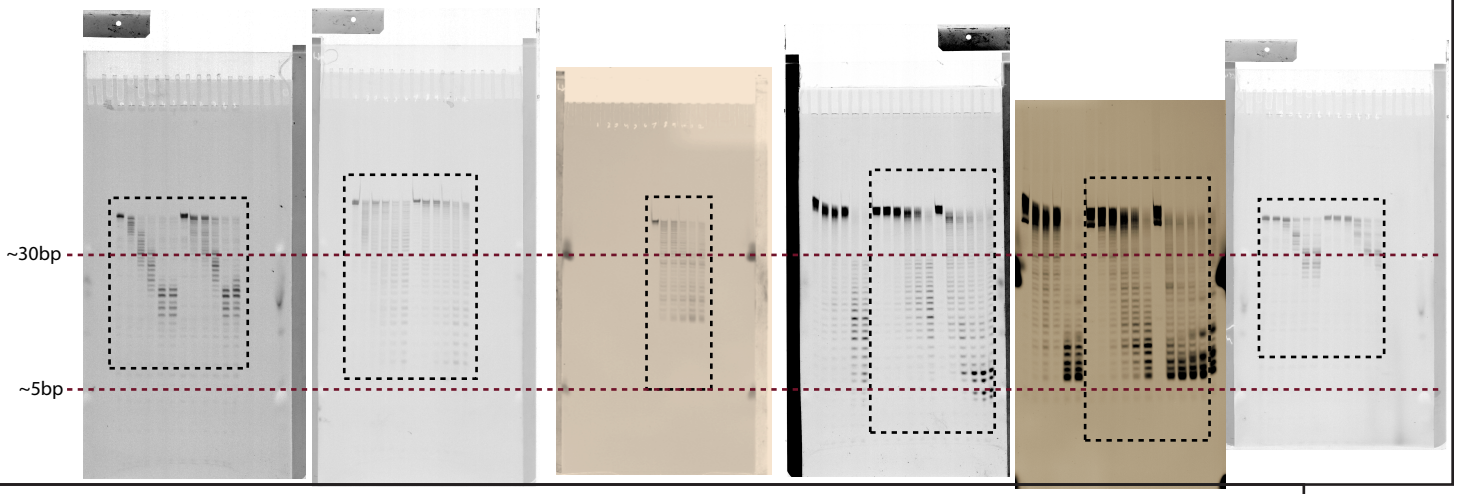

Supplementary Figure 5h-k

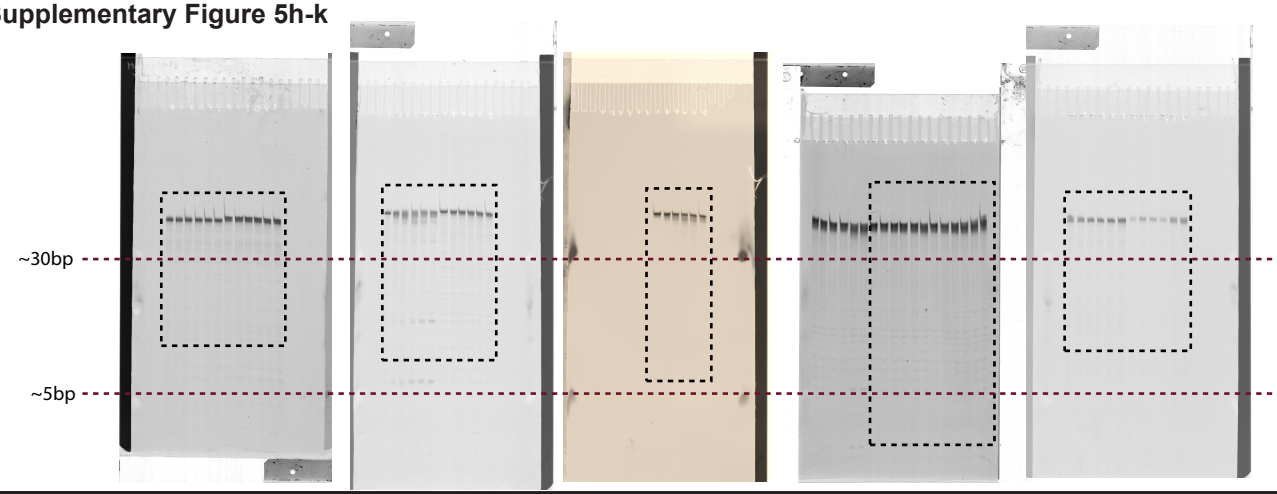

Supplementary Figure 5m

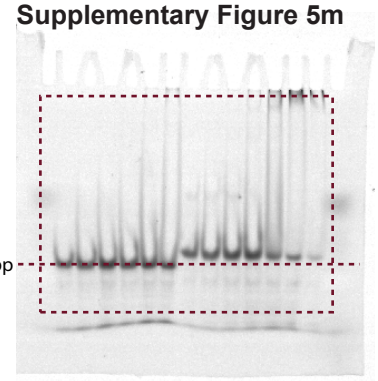

Supplementary Figure 7c

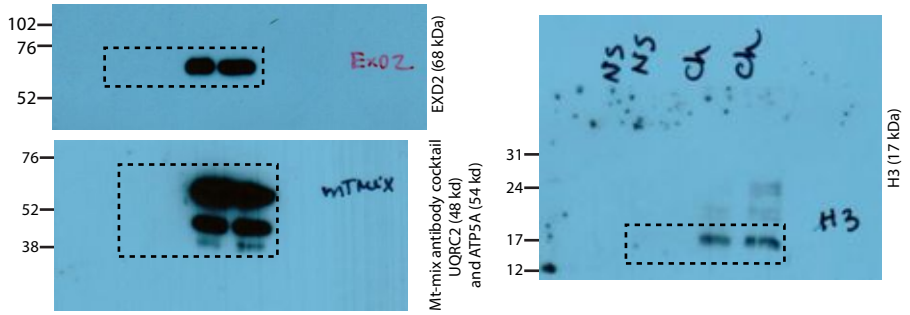

EXD2 governs germ stem cell homeostasis and lifespan by promoting mitoribosome integrity and translation

Supplementary Legends

Supplementary Figure 1: EXD2 is a conserved mitochondrial exonuclease with an HNH-like domain. (**a**) Pairwise sequence alignments of 3'-5' exonuclease domains of human EXD2 (aa 89-261) and WRN (aa 60-228). 3 conserved exonuclease signature motifs of DNAQ family highlighted in light blue boxes and metal binding residues indicated with asterisks. Nuclease dead mutations (*EXD2-NUC*) shown in red. (**b**) Unrooted Bayesian phylogenetic tree based on multiple sequence alignment of the EXO domain (PFAM: DNA_pol_A_exo1) from 44 representative sequences (domain codes indicated in key at top). Red balls indicate probability support for clades when they are >0.9%. Eukaryotic phyla indicated by text color: animals (blue), plants (dark green), algae (light green) and fungi (pink). Protein domain architectures annotated with hmmscan and hidden Markov models (see methods) for each protein. (**c**) Multiple sequence alignment of HNH-like domains (human aa 411-469) of representative EXD2 sequences. The HNH-like domain mutations in the *EXD2-C1* or *C2* alleles indicated in red. (**d**) Alignment of human EXD2 with HNH domains in non-EXD2 proteins. Superimposition of modeled EXD2 HNH-like domain with 5H0M: deep-sea thermophilic bacteriophage GVE2 HNH endonuclease. EXD2 in cyan and the Cys residues of the CxxC dyads in red coordinating a zinc ion. Catalytic DH residues characteristic of HNH endonuclease activity are not present in EXD2 (red box). (**e**) Alignment of EXD2 mitochondrial targeting sequences (MTS) from indicated species with hydrophobicity and predicted mitochondrial targeting probability. (**f**) Overexpressed EXD2-SF imaged by TEM in HEK293 cells using gold nano-particles conjugated to anti-rabbit antibodies to

recognize the FLAG antibody. Particles in the nucleus (blue), cytoplasm (black) and mitochondria (red) indicated by arrows. 1 experiment was performed. Semi-quantitative analysis of localization normalized by area is graphed (65 and 49 fields per condition, respectively) and percentage of particles graphed. (**g**) Relative localization of EXD2 in the cytoplasm or mitochondria. Percentage of particles in the mitochondria or cytoplasm in 25 fields graphed and example image shown (2 experiments). Scale bar=1μM. (**h**) EXD2 is mitochondrial and resistant to 25μM FCCP treatment relative to outer membrane TOM20. U2OS cells were treated with FCCP for indicated time and fractionated (C=cytoplasm, M=mitochondria, N=nucleus, Ch=chromatin) for western blotting for GAPDH (cytoplasm), OXPHOS components ATP5A, URQC2, CO1 and SDHB (inner membrane/matrix), TOM20 (outer membrane) and EXD2. The experiment was performed once.

Supplementary Figure 2: Cellular phenotypes of EXD2 deficient cells. (**a**) EXD2 –deficient MDA-MB-231 and U2OS cells generated by CRISPR/CAS9 targeting and complemented with *wild type* (*WT*) EXD2 or indicated mutants. One representative western blot out of 3 of EXD2 and GAPDH (loading control) is shown. (**b**) Liquid chromatography-mass spectrometry (LC-MS) analysis of glutathione (GSH/GSSG) with parallel samples treated with NAC. Color key of cell line or treatment with CAP or FCCP applies to all of figure. Averages of n=3 (*WT, EXD2-KO1, EXD2-KO1+WT w/ NAC*) or n=4 (all other samples) independent cultures shown with mean(SD). (**c**) MtDNA levels of indicated cell lines with indicated stable shRNAs. Mean (SD) of n=3 independent experiments. (**d**) MtDNA levels of indicated MDA-MB-231 cells. Parallel cultures were treated with NAC to reduce ROS levels. Mean (SD) of n=3 independent experiments *p<0.05, **p<0.01, ***p<0.0001 one way ANOVA with Dunnet's test for (c) and (d). (**e**) Mitochondrial mass measured with MitoTracker Green FM or

MitoTracker Deep Red staining. Parallel samples were treated with FCCP. Untreated MitoTracker Green samples also shown in Fig. 3d. Mean(SD) of n=3 independent experiments. (**f**) 2D-AGE analysis of mitochondrial replication intermediates in U2OS or HEK293T cells stably expressing shCont or shEXD2-22. Schematic of replication intermediates (top right panel) and location of probe and restriction sites (bottom right panel) shown. 2 experiments are shown. (**g**) Reduced colony formation of cells with stable shRNA against EXD2 in glutamine free media relative to cells in DMEM with glucose and glutamine. Mean (SD) of n=3 independent experiments. **p=0.0014 and *p=0.0202, unpaired t-test, two tailed. (**h**) OCR (mitochondrial stress test: Oligomycin, FCCP and Antimycin and Rotenone) and (**i**) ECAR (glycolysis stress test: Glucose, Oligomycin and 2-DG) in MDA-MB-231 cells. All time course values of 1 experiment with quadruplicate cultures per genotype plotted with mean. (**j**) OCR measurements from 5mM NAC treated MDA-MB-231 cells. Mean and individual values from 1 experiment with quadruplicate cultures. (**k**) ATP levels measured in MDA-MB-231 cells treated with 5mM NAC (as in Fig. 3n). Values from n=3 independent duplicate cultures shown with mean(SD). (**l**) ATP levels measured in U2OS cells by targeted mass spectrometry. Results of 8 (*WT*, *EXD2-KO1*) or 9 (*EXD2-KO1+WT*) independent cultures shown with mean(SD) (p=0.0155*, unpaired t-test, two tailed).

Supplementary Figure 3: Protein interactions, OXPHOS complexes and respiration. (**a**) EXD2 pulls down NDUFA9 but not ND6 in immunoprecipitation-western blotting of U2OS cell extracts. (**b**) Separation of digitonin-solubilized mitochondrial complexes in BlueNative-PAGE (BNP) gels; oxoglutarate dehydrogenase complex (O), pyruvate dehydrogenase (P) supercomplex I+III (CI/CIII), complexes I, V and IV (CI, CV and CIV), non-specific band (NS). Individual results from n=3 independent experiments are shown. Western blotting of one gel

(right panel) shows equal loading and that EXD2 is not likely present in the fully assembled Complex I. (**c**) Quantification of reduced OXPHOS complex levels in EXD2 deficient cells (n=3, see (b)). The relative band intensity of the *EXD2-KO1* sample compared to WT (set to 1.0) was normalized to the background (*p=0.473 (CI/CIII), ***p=.0002 (CI) and *p=0.37 (CV), t-test, two tailed). Values with mean(SD) are shown. (**d**) Complex I activity is reduced in cells lacking EXD2. Analysis of OCR to assess the activity of individual OXPHOS complexes by consecutive administration of malate and pyruvate (Complex I substrate), rotenone, succinate (Complex II substrate) and antimycin. The impairment in OCR was more apparent for Complex I activity, as Complex II was relatively unaffected. Individual measurements from n=2 independent experiments in quadruplicate are shown with mean.

Supplementary Figure 4: Mitoribosome fractionation and translation. (**a**) Sucrose gradient fractionation followed by 600 U/ml RNAseA treatment for 30 minutes. Note that profiles are similar regardless of EXD2 and aberrant fractions are lost, indicating RNA dependence. The experiment was performed once. (**b**) Examples of 7 independent experiments used in the quantification of COX3/2 translation (Fig. 5d) or shown as representative in Fig. 5c. Membranes from 2 independent experiments performed in duplicate are shown. Color key applies to all panels. (**c**) Membranes from 2 independent experiments in addition to those shown in Fig. 5c and 5d. (**d**) Technical replicate of the experiment in Fig. 5f (top panel) and independent experiment in duplicate (bottom panel). (**e**) 2 independent translation experiments in RPE1 cells and quantification of the translation defect from n=3 independent experiments with mean(SD) (**p=0.0025, unpaired t-test two tailed). Western blotting for EXD2 and GAPDH as a loading control are shown. Source data

and statistical information are shown in Supplementary Table 1 and uncropped blots in Supplementary Fig. 9.

Supplementary Figure 5: Protein purification, biochemical analysis and mtRNA processing. (**a**) Coomassie stained gel with protein eluted from an S200 gel filtration column shown for all proteins used. Red arrow highlights fractions used.(**b**) EXD2 has a 3'-5' polarity. 20nM of the indicated protein or 0.5U of ExoI were incubated with 20nM ssDNA with 3' TAMRA, no modification or 3' phosphate in the presence of 10mM $MnCl_2$. Black arrowhead;30 bp. (**c**) EXD2-WT or WRN-Exo (10-40nM) were incubated with 20nM fluorescently labelled dsDNA with a nick, a 1 nt gap, a recessed 3' end or the labelled ssDNA oligo alone in the presence of $MnCl_2$. Black arrowhead ;16 bp. (**d**) WRN-Exo (5-80nM) was incubated with fluorescently labelled ssDNA or dsDNA or (**e**) 20nM fluorescently labelled ssRNA or RNA/DNA hybrid in the presence of $MnCl_2$. Bold font;labelled molecule. Sepia panel;same gel scanned with a second laser to visualize the Cy5 labeled DNA strand. (**f**) WRN-Exo (5-80nM) and EXD2-C1/2 (5-80nM) were incubated with a dsRNA substrate labelled with FAM (forward) or Cy5 (reverse) in the presence of $MnCl_2$. Sepia panel; same gel scanned with a second laser to visualize the Cy5 labeled DNA strand. (**g**) EXD2-C1/2 (5-80nM) was incubated with fluorescently labelled ssDNA or dsDNA in the presence of $MnCl_2$. (**h**) WRN-Exo (5-80nM) was incubated with fluorescently labelled ssDNA or dsDNA or (**i**) 20nM fluorescently labelled ssRNA or RNA/DNA hybrid in the presence of $MgCl_2$. Bold font ;labelled molecule. (**j**) WRN-Exo (5-80nM) and EXD2-C1/2 (5-80nM) were incubated with a dsRNA substrate labelled with FAM (forward) or Cy5 (reverse) in the presence of $MgCl_2$. (**k**) EXD2-C1/2 (5-80nM) was incubated with fluorescently labelled ssDNA or dsDNA in the presence of $MgCl_2$. All reactions in panels b-k were carried out for 30 min at 37°C before being separated on an 18%

polyacrylamide urea TBE gel. Black arrowhead; 30 bp (d-k). (**l**) Specific activity (nM substrate cleavage/nM protein per minute) of the indicated protein measured from scanned gels.. Duplicate measurements from n=3 experiments (EXD2-WT and WRN-Exo) or n=2 experiments (EXD2-C1/2) are plotted with mean indicated. (**m**) WRN-Exo (80-310nM) was incubated with fluorescently labelled ssDNA or ssRNA, RNA/DNA hybrid or dsDNA for 30 min on ice. Complexes were separated on a 0.5x TBE 8% polyacrylamide gel. ,Data in b-e, g-i, and k: representative of 3 experiments; Data in f, j, m, f: representative of 2 experiments. Source data in Supplementary Table 1 and uncropped gels in Supplementary Fig. 9.

Supplementary Figure 6: EXD2 is conserved in *Drosophila melanogaster*. (**a**) Protein sequence alignment of human EXD2 and dEXD2 (CG6744). MTS is shaded in yellow, nuclease domains in blue and HNH-like domain in green for reference. (**b**) QRT-PCR analysis for *dEXD2* at the indicated developmental stages of *D. melanogaster*. Individual values from n=2 experiments with mean indicated. (**c**) Heatmap of ModENCODE/FlyBase *dExd2* expression data in Reads Per Kilobase of transcript per Million mapped reads (RPKM) during different developmental stages. L1-L3 = larval stages 1-3 and WPP = white prepupae. Data represent one out of 2 experiments. (**d**) Analysis of maternal contribution to larvae size. Heterozygous *dExd2* mutant females were bred with homozygous males so that all progeny receive functional mitochondria from *dExd2* heterozygous mothers. Roughly 50% of the progeny (green) are runted to a similar extent as those from breedings with homozygous parents (blue), indicating that growth defects are not strictly due to maternal inheritance of defective mitochondria. Flies were genotyped by eye color (example pictures shown on right) and the size distribution of larvae from Control flies or breedings of homozygous mutants are shown for reference. Volumes of n=50 flies

per genotype are shown with mean(SD). (**e**) Schematic model of the proposed role of EXD2 in facilitating mitochondrial translation and homeostasis, see main text for details.

Supplementary Figure 7: MitoString, subcellular fractionation, influence of EXD2 on DNA damage responses and lifespan. (**a**) Location of MitoString[1] probes. rRNAs, mRNAs and tRNAs encoded by the mtDNA are labeled in black text (tRNAs annotated by their one letter symbols). Location of mRNA probes noted in red, junction probes in blue and non-coding probes in green. Rectangles indicate probes targeting the heavy strand, while triangles indicate probes targeting the light strand. (**b**) Graphical depiction of the relative change of each of the MitoString probes compared to *WT*. Individual normalized values from quadruplicate samples shown as a box and whiskers plot. The box represents the interquartile range and the whiskers the minimum to maximum value. All 4 individual values are plotted as circles. (**c**) Subcellular fractionation using previously reported[2] methods in the presence or absence of DNA damage induced by 1μM CPT. Representative image of 2 experiments is shown. (**d**) Examples of U2OS cells immunostained for RPA2 (green) with and without 1μM CPT treatment. DNA is stained with DAPI (blue). (**e**) Quantification of the RPA2 signal intensity per nucleus. A minimum of 390 cells were quantified for each condition and mean is indicated and data represent one out of 2 experiments. (**f-h**) Cellular sensitivities of indicated cell lines in either U2OS or MDA-MB-231 background to the indicated agents determined using Alamar Blue (f,g) or colony forming assays (h). For (f,g) n=3 independent experiments plotted with the mean(SD) and for (h) n=3 independent experiments with the mean and range indicated. 50nM of a small molecule inhibitor for CHK1 (PF477736) was used in some experiments as a control to induce DNA damage sensitivity. (**i**) QRT-PCR

analysis of *Sir2* mRNA levels between *Control* and *dExd2* deficient flies. Values of n=3 independent experiments shown with mean(SD). (**j**) Calorie restriction (CR) using low sugar or low yeast diets extends lifespan regardless of *dExd2* status. n=3 independent experiments with 60 flies for each lifespan condition with the mean(SD) indicated with the exception of low yeast where n=2 independent experiments were performed and mean is indicated.

Supplementary Figure 8: Flow cytometry gating examples. (a) Examples of MitoSox Red (top) and (**b**) MitoTracker Green FM (bottom) flow cytometry gating strategies. More than 10,000 cells were collected per sample and dead cells excluded with DAPI staining. Control treatments with 75µM paraquat (PQT) or 25µM FCCP were used to induce ROS or reduce mass, respectively.

Supplementary Figure 9: Uncropped gels and membranes. Uncropped scans of membranes and gels used in the main and supplementary figures.

Supplementary Table 1: Source data and statistical information. Source data used for each plot in the paper and accompanying statistical information is provided in a separate tab for each figure.

Supplementary Table 2: Annotated summary of BioID data. Summarized data from the BioID experiments used to generate the graph and schematics in Figure 4b and 4c. Raw data is available in the MassIVE repository (ID: MSV000081337).

Supplementary Table 3: Oligonucleotides used in this study. A list of primer sequences used in the study.

Supplementary Table 4: Antibodies. A list of antibodies used in this study and their providers.

Supplementary references

1. Wolf, A.R. & Mootha, V.K. Functional genomic analysis of human mitochondrial RNA processing. *Cell Rep* **7**, 918-931 (2014).
2. Broderick, R. *et al.* EXD2 promotes homologous recombination by facilitating DNA end resection. *Nat Cell Biol* **18**, 271-280 (2016).